

A New Approach To The Treatment Of Separatrix Chaos And Its Applications

S.M. Soskin, R. Mannella, O.M. Yevtushenko, I.A. Khovanov, P.V.E. McClintock

Abstract We consider time-periodically perturbed 1D Hamiltonian systems possessing one or more separatrices. If the perturbation is weak, then the separatrix chaos is most developed when the perturbation frequency lies in the logarithmically small or moderate ranges: this corresponds to the involvement of resonance dynamics into the separatrix chaos. We develop a method matching the discrete chaotic dynamics of the separatrix map and the continuous regular dynamics of the resonance Hamiltonian. The method has allowed us to solve the long-standing problem of an accurate description of the maximum of the separatrix chaotic layer width as a function of the perturbation frequency. It has also allowed us to predict and describe new phenomena including, in particular: (i) a drastic facilitation of the onset of global chaos between neighbouring separatrices, and (ii) a huge increase in the size of the low-dimensional stochastic web.

S.M. Soskin
Institute of Semiconductor Physics, 03028 Kiev, Ukraine,
e-mail: ssoskin@ictp.it

R. Mannella
Dipartimento di Fisica, Università di Pisa, 56127 Pisa, Italy,
e-mail: mannela@df.unipi.it

O.M. Yevtushenko
Physics Department, Ludwig-Maximilians-Universität München, D-80333 München, Germany,
e-mail: bom@ictp.it

I.A. Khovanov
School of Engineering, University of Warwick, Coventry CV4 7AL, UK,
e-mail: i.khovanov@warwick.ac.uk

P.V.E. McClintock
Physics Department, Lancaster University, Lancaster LA1 4YB, UK,
e-mail: p.v.e.mcclintock@lancaster.ac.uk

1 Introduction

Separatrix chaos is the germ of Hamiltonian chaos [51]. Consider an integrable Hamiltonian system possessing a saddle, i.e. a hyperbolic point in the one-dimensional case, or a hyperbolic invariant torus, in higher-dimensional cases. The stable (incoming) and unstable (outgoing) manifolds of the saddle are called *separatrices* [18]: they separate trajectories that have different phase space topologies. If a weak time-periodic perturbation is added, then the separatrix is destroyed; it is replaced by a *separatrix chaotic layer* (SCL) [51, 18, 23, 29]. Even if the unperturbed system does not possess a separatrix, the resonant part of the perturbation generates a separatrix in the auxiliary resonance phase space while the non-resonant part of the perturbation destroys this separatrix, replacing it with a chaotic layer [51, 18, 23, 10]. Thus separatrix chaos is of a fundamental importance for Hamiltonian chaos.

One of the most important characteristics of SCL is its width in energy (or expressed in related quantities). It can be easily found *numerically* by integration of the Hamiltonian equations with a set of initial conditions in the vicinity of the separatrix: the space occupied by the chaotic trajectory in the Poincaré section has a higher dimension than that for a regular trajectory, e.g. in the 3/2D case the regular trajectories lie on lines i.e. 1D objects while the chaotic trajectory lies within the SCL i.e. the object outer boundaries of which limit a 2D area.

On the other hand, it is important to be able to describe *theoretically* both the outer boundaries of the SCL and its width. There is a long and rich history of the such studies. The results may be classified as follows.

1.1 Heuristic results

Consider a 1D Hamiltonian system perturbed by a weak time-periodic perturbation:

$$\begin{aligned} H &= H_0(p, q) + hV(p, q, t), \\ V(p, q, t + 2\pi/\omega_f) &= V(p, q, t), \quad h \ll 1, \end{aligned} \tag{1}$$

where $H_0(p, q)$ possesses a separatrix and, for the sake of notational compactness, all relevant parameters of H_0 and V , except possibly for ω_f , are assumed to be ~ 1 .

Physicists proposed a number of different heuristic criteria [53, 10, 23, 55, 51, 52] for the SCL width ΔE in terms of energy $E \equiv H_0(p, q)$ which gave qualitatively similar results:

$$\begin{aligned} \Delta E &\equiv \Delta E(\omega_f) \sim \omega_f \delta, \\ \delta &\equiv h|\varepsilon|, \\ |\varepsilon| &\lesssim 1 && \text{for } \omega_f \lesssim 1, \\ |\varepsilon| &\propto \exp(-a\omega_f) \ll 1 && (a \sim 1) \quad \text{for } \omega_f \gg 1. \end{aligned} \tag{2}$$

The quantity $\delta \equiv h|\varepsilon|$ is called the *separatrix split* [51] (see also Eq. (4) below): it determines the maximum distance between the perturbed incoming and outgoing separatrices [53, 10, 23, 55, 51, 52, 1, 18, 29].

It follows from (2) that the maximum of ΔE should lie in the frequency range $\omega_f \sim 1$ while the maximum itself should be $\sim h$:

$$\Delta E_{\max} \equiv \max_{\omega_f} \{\Delta E(\omega_f)\} \sim h, \quad \omega_f^{(\max)} \sim 1. \quad (3)$$

1.2 Mathematical and accurate physical results

Many papers studied the SCL by mathematical or accurate physical methods.

For the range $\omega_f \gg 1$, many works studied the separatrix splitting (see the review [18] and references therein) and the SCL width in terms of normal coordinates (see the review [29] and references therein). Though quantities studied in these works differ from those typically studied by physicists [53, 10, 23, 55, 51, 52], they implicitly confirm the main qualitative conclusion from the heuristic formula (2) in the high frequency range: provided that $\omega_f \gg 1$ the SCL width is exponentially small.

There were also several works studying the SCL in the opposite (i.e. adiabatic) limit $\omega_f \rightarrow 0$: see e.g. [27, 14, 28, 42, 45] and references therein. In the context of the SCL width, it is most important that $\Delta E(\omega_f \rightarrow 0) \sim h$ for most of the systems [27, 14, 28]. For a particular class of systems, namely for ac-driven spatially periodic systems (e.g. the ac-driven pendulum), the width of the SCL part above the separatrix diverges in the adiabatic limit [42, 45]: the divergence develops for $\omega_f \ll 1/\ln(1/h)$.

Finally, there is a qualitative estimation of the SCL width for the range $\omega_f \sim 1$ within the Kolmogorov-Arnold-Moser (KAM) theory [29]. The quantitative estimate within the KAM theory is lacking, apparently being very difficult for this frequency range [17]. It follows from the results in [29] that the width in this range is of the order of the separatrix split, which itself is of the order of h .

Thus it could seem to follow that, for all systems except ac-driven spatially periodic systems, the maximum in the SCL width is $\sim h$ and occurs in the range $\omega_f \sim 1$, very much in agreement with the heuristic result (3). Even for ac-driven spatially periodic systems, this conclusion could seem to apply to the width of the SCL part below the separatrix over the whole frequency range, and to the width of the SCL part above the separatrix for $\omega_f \gtrsim 1/\ln(1/h)$.

1.3 Numerical evidence for high peaks in $\Delta E(\omega_f)$ and their rough estimation

The above conclusion disagrees with several numerical studies carried out during the last decade (see e.g. [42, 45, 34, 25, 40, 24, 47, 35]) which have revealed the existence of sharp peaks in $\Delta E(\omega_f)$ in the frequency range $1/\ln(1/h) \lesssim \omega_f \lesssim 1$ the heights of which greatly exceed h (see also Figs. 2, 3, 5, 6 below). Thus, the peaks represent the general *dominant feature* of the function $\Delta E(\omega_f)$. They were related by the authors of [34, 25, 40, 24, 47, 35] to the absorption of nonlinear resonances by the SCL. For some partial case, rough heuristic estimates for the position and magnitude of the peaks were made in [34, 35].

1.4 Accurate description of the peaks and of the related phenomena

Until recently, accurate analytic estimates for the peaks were lacking. It is explicitly stated in [24] that the search for the mechanism through which resonances are involved in separatrix chaos, and for an accurate analytic description of the peaks in the SCL width as function of the perturbation frequency, are being among the most important and challenging tasks in the study of separatrix chaos. The first step towards accomplishing them was taken through the proposal [43, 44] of a new approach to the theoretical treatment of the separatrix chaos in the relevant frequency range. It was developed and applied to the onset of global chaos between two close separatrices. The application of the approach [43, 44] to the commoner single-separatrix case was also discussed. The approach has been further developed [38, 39], including an explicit theory for the single-separatrix case [39].

The present paper reviews the new approach [43, 44, 38, 39] and its applications to the single-separatrix [39] and double-separatrix [43, 44] cases. We also briefly review application to the enlargement of the low-dimensional stochastic web [46] and discuss other promising applications.

Though the form of our treatment differs from typical forms of mathematical theorems in this subject (cf. [18, 29]), it yields the *exact* expressions for the leading term in the relevant asymptotic expansions (the parameter of smallness is $\alpha \equiv 1/\ln(1/h)$) and, in some case, even for the next-order term. Our theory is in excellent agreement with results obtained by numerical integration of the equations of motion.

Sec. 2 describes the basic ideas underlying the approach. Sec. 3 is devoted to the leading-order asymptotic description of the single-separatrix chaotic layers. Sec. 4 presents an asymptotic description of the onset of global chaos in between two close separatrices. Sec. 5 describes the increase in sizes of a stochastic web. Conclusions are drawn in Sec. 6. Sec. 7 presents the Appendix, which explicitly matches the separatrix map and the resonance Hamiltonian descriptions for the double-separatrix case.

2 Basic ideas of the approach

The new approach [43, 44, 38, 39] may be formulated briefly as a matching between the discrete chaotic dynamics of the separatrix map in the immediate vicinity of the separatrix and the continuous regular dynamics of the resonance Hamiltonian beyond that region. The present section describes the general features of the approach in more detail.

Motion near the separatrix may be approximated by the *separatrix map* (SM) [53, 10, 23, 55, 51, 52, 1, 29, 34, 35, 43, 44, 31]. This was introduced in [53] and its various modifications were subsequently used in many studies. It is sometimes known as the *whisker map*. It was re-derived rigorously in [31] as the leading-order approximation of motion near the separatrix in the asymptotic limit $h \rightarrow 0$, and an estimate of the error was also carried out in [31] (see also the review [29] and references therein).

The main ideas that allow one to introduce the SM [53, 10, 23, 55, 51, 52, 1, 29, 43, 44, 31] are as follows. For the sake of simplicity, let us consider a perturbation V that does not depend on the momentum: $V \equiv V(q, t)$. A system with energy close to the separatrix value spends most of its time in the vicinity of the saddle(s), where the velocity \dot{q} is exponentially small. Differentiating $E \equiv H_0(p, q)$ with respect to time and allowing for the equations of motion of the system (1), we can show that $dE/dt \equiv \partial V / \partial q \dot{q} \propto \dot{q}$. Thus, the perturbation can significantly change the energy only when the velocity is not small i.e. during the relatively short intervals while the system is away from the saddle(s): these intervals correspond to *pulses* of velocity as a function of time (cf. Fig. 20 in the Appendix below). Consequently, it is possible to approximate the continuous Hamiltonian dynamics by a discrete dynamics which maps the energy E , the perturbation angle $\varphi \equiv \omega_f t$, and the velocity sign $\sigma \equiv \text{sgn}(\dot{q})$, from pulse to pulse.

The actual form of the SM may vary, depending on the system under study, but its features relevant in the present context are similar for all systems. For the sake of clarity, consider the explicit case when the separatrix of $H_0(p, q)$ possesses a single saddle and two symmetric loops while $V = q \cos(\omega_f t)$. Then the SM reads [43] (cf. Appendix):

$$\begin{aligned}
 E_{i+1} &= E_i + \sigma_i h \varepsilon \sin(\varphi_i), \\
 \varphi_{i+1} &= \varphi_i + \frac{\omega_f \pi (3 - \text{sgn}(E_{i+1} - E_s))}{2\omega(E_{i+1})}, \\
 \sigma_{i+1} &= \sigma_i \text{sgn}(E_s - E_{i+1}), \quad |\sigma_i| = 1, \\
 \varepsilon &\equiv \varepsilon(\omega_f) = \text{sgn} \left(\left. \frac{\partial H_0}{\partial p} \right|_{t \rightarrow -\infty} \right) \int_{-\infty}^{\infty} dt \left. \frac{\partial H_0}{\partial p} \right|_{E_s} \sin(\omega_f t), \\
 E_i &\equiv H_0(p, q)|_{t_i - \Delta}, \quad \varphi_i \equiv \omega_f t_i, \quad \sigma_i \equiv \text{sgn} \left(\left. \frac{\partial H_0}{\partial p} \right|_{t_i} \right),
 \end{aligned} \tag{4}$$

where E_s is the separatrix energy, $\omega(E)$ is the frequency of oscillation with energy E in the unperturbed case (i.e. for $h = 0$), t_i is the instant corresponding to the i -th turning point in the trajectory $q(t)$ (cf. Fig. 20 in the Appendix below), and Δ is an arbitrary value from the range of time intervals which greatly exceed the characteristic duration of the velocity pulse while being much smaller than the interval between the subsequent pulses [53, 10, 23, 55, 51, 52, 1, 29, 31]. Consider the two most general ideas of our approach.

1. If a trajectory of the SM includes a state with $E = E_s$ and an arbitrary φ and σ , then this trajectory is chaotic. Indeed, the angle φ of such a state is not correlated with the angle of the state at the previous step of the SM, due to the divergence of $\omega^{-1}(E \rightarrow E_s)$. Therefore, the angle at the previous step may deviate from a multiple of 2π by an arbitrary value. Hence the energy of the state at the previous step may deviate from E_s by an arbitrary value within the interval $[-h|\varepsilon|, h|\varepsilon|]$. The velocity sign σ is not correlated with that at the previous step either¹. Given that a regular trajectory of the SM cannot include a step where all three variables change random-like, we conclude that such a trajectory must be chaotic. Though the above arguments may appear to be obvious, they cannot be considered a mathematically rigorous proof, so that the statement about the chaotic nature of the SM trajectory which includes any state with $E = E_s$ should be considered as a conjecture supported by the above arguments and by numerical iteration of the SM. Possibly, a mathematically rigorous proof should involve an analysis of the Lyapunov exponents for the SM (cf. [23]) but this appears to be a technically difficult problem. We emphasize however that a rigorous proof of the conjecture is not crucial for the validity of the main results of the present paper, namely for the *leading* terms in the asymptotic expressions describing (i) the peaks of the SCL width as a function of the perturbation frequency in the single-separatrix case, and (ii) the related quantities for the double-separatrix case. It will become obvious from the next item that, to derive the leading term, it is sufficient to know that the chaotic trajectory does visit areas of the phase space where the energy deviates from the separatrix by values of the order of the separatrix split $\delta \equiv h|\varepsilon|$, which is a widely accepted fact [53, 10, 23, 55, 51, 52, 1, 18, 29].
2. It is well known [53, 10, 23, 55, 51, 52, 1, 18, 29, 34, 35, 43, 44], that, at the leading-order approximation, the frequency of eigenoscillation as function of the energy near the separatrix is proportional to the reciprocal of the logarithmic factor

$$\omega(E) = \frac{b\pi\omega_0}{\ln\left(\frac{\Delta H}{|E-E_s|}\right)}, \quad b = \frac{3 - \text{sgn}(E - E_s)}{2}, \quad (5)$$

$$|E - E_s| \ll \Delta H \equiv E_s - E_{st},$$

¹ Formally, $\text{sgn}(E - E_s)$ is not defined for $E = E_s$ but, if to shift E from E_s for an infinitesimal value, $\text{sgn}(E - E_s)$ acquires a value equal to either +1 or -1, depending on the sign of the shift. Given that σ_{i+1} is proportional to $\text{sgn}(E_s - E_{i+1})$ while the latter is random-like (as it has been shown above), σ_{i+1} is not correlated with σ_i if $E_{i+1} = E_s \pm 0$.

where E_{st} is the energy of the stable states.

Given that the argument of the logarithm is large in the relevant range of E , the function $\omega(E)$ is nearly constant for a substantial variation of the argument. Therefore, as the SM maps the state $(E_0 = E_s, \varphi_0, \sigma_0)$ onto the state with $E = E_1 \equiv E_s + \sigma_0 h \varepsilon \sin(\varphi_0)$, the value of $\omega(E)$ for the given $\text{sgn}(\sigma_0 \varepsilon \sin(\varphi_0))$ is nearly the same for most of the angles φ_0 (except in the vicinity of multiples of π),

$$\begin{aligned} \omega(E) &\approx \omega_r^{(\pm)}, \\ \omega_r^{(\pm)} &\equiv \omega(E_s \pm h), \quad \text{sgn}(\sigma_0 \varepsilon \sin(\varphi_0)) = \pm 1. \end{aligned} \quad (6)$$

Moreover, if the deviation of the SM trajectory from the separatrix increases further, $\omega(E)$ remains close to $\omega_r^{(\pm)}$ provided the deviation is not too large, namely if $\ln(|E - E_s|/h) \ll \ln(\Delta H/h)$. If $\omega_f \lesssim \omega_r^{(\pm)}$, then the evolution of the SM (4) may be regular-like for a long time until the energy returns to the close vicinity of the separatrix, where the trajectory becomes chaotic. Such behavior is especially pronounced if the perturbation frequency is close to $\omega_r^{(+)}$ or $\omega_r^{(-)}$ or to one of their multiples of relatively low order: the resonance between the perturbation and the eigenoscillation gives rise to an accumulation of energy changes for many steps of the SM, which results in a deviation of E from E_s that greatly exceeds the separatrix split $h|\varepsilon|$. Consider a state at the boundary of the SCL. The deviation of energy of such a state from E_s depends on its position at the boundary. In turn, the maximum deviation is a function of ω_f . The latter function possesses the absolute maximum at ω_f close to $\omega_r^{(+)}$ or $\omega_r^{(-)}$ typically², for the upper or lower boundary of the SCL respectively. This corresponds to the absorption of the, respectively upper and lower, 1st-order nonlinear resonance by the SCL.

The second of these intuitive ideas has been explicitly confirmed [43] (see Appendix): in the relevant range of energies, the separatrix map has been shown to reduce to two differential equations which are identical to the equations of motion of the auxiliary resonance Hamiltonian describing the resonance dynamics in terms of the conventional canonically conjugate slow variables, action I and slow angle $\tilde{\psi} \equiv n\psi - \omega_f t$ where ψ is the angle variable [10, 23, 55, 51, 52, 1] (see Eq. (16) below) and n is the relevant resonance number i.e. the integer closest to the ratio $\omega_f/\omega_r^{(\pm)}$.

Thus the matching between the discrete chaotic dynamics of the SM and the continuous regular-like dynamics of the resonance Hamiltonian arises in the following

² For the SM relating to ac-driven spatially periodic systems, the time during which the SM undergoes a regular-like evolution above the separatrix diverges in the adiabatic limit $\omega_f \rightarrow 0$ [45], and the width of the part of the SM layer above the separatrix diverges too. However, we do not consider this case here since it is irrelevant to the main subject of the present paper i.e. to the involvement of the resonance dynamics into the separatrix chaotic motion.

way [43]. After the chaotic trajectory of the SM visits any state on the separatrix, the system transits in one step of the SM to a given upper or lower curve in the $I - \tilde{\psi}$ plane which has been called [43] the upper or lower *generalized separatrix split* (GSS) curve³ respectively:

$$E = E_{GSS}^{(\pm)}(\tilde{\psi}) \equiv E_s \pm \delta |\sin(\tilde{\psi})|, \quad \delta \equiv h|\varepsilon|, \quad (7)$$

where δ is the conventional separatrix split [51], ε is the amplitude of the Melnikov-like integral defined in Eq. (4) above (cf. [53, 10, 23, 55, 51, 52, 1, 18, 29, 34, 47, 35, 43, 44]), and the angle $\tilde{\psi}$ may take any value either from the range $[0, \pi]$ or from the range $[\pi, 2\pi]$ ⁴.

After that, because of the closeness of ω_f to the n -th harmonic of $\omega(E)$ in the relevant range of E ⁵, for a relatively long time the system follows the *nonlinear resonance* (NR) dynamics (see Eq. (16) below), during which the deviation of the energy from the separatrix value grows, greatly exceeding δ for most of the trajectory. As time passes, $\tilde{\psi}$ is moving and, at some point, the growth of the deviation changes for the decrease. This decrease lasts until the system hits the GSS curve, after which it returns to the separatrix just for one step of the separatrix map. At the separatrix, the slow angle $\tilde{\psi}$ changes random-like, so that a new stage of evolution similar to the one just described occurs, i.e. the nonlinear resonance dynamics starting from the GSS curve with a new (random) value of $\tilde{\psi}$.

Of course, the SM cannot describe the variation of the energy during the velocity pulses (i.e. in between instants relevant to the SM): in some cases this variation can be comparable to the change within the SM dynamics. This additional variation will be taken into account below, where relevant.

One might argue that, even for the instants relevant to the SM, the SM describes the original Hamiltonian dynamics only approximately [31] and may therefore miss some fine details of the motion: for example, the above picture does not include small windows of stability on the separatrix itself. However these fine details are irrelevant in the present context, in particular the relative portion of the windows of stability on the separatrix apparently vanishes in the asymptotic limit $h \rightarrow 0$.

The boundary of the SM chaotic layer is formed by those parts of the SM chaotic trajectory which deviate from the separatrix more than others. It follows from the structure of the chaotic trajectory described above that the upper/lower boundary of the SM chaotic layer is formed in one of the two following ways [43, 44]: (i) if there exists a *self-intersecting* resonance trajectory (in other words, the resonance separatrix) the lower/upper part of which (i.e. the part situated below/above the

³ The GSS curve corresponds to the step of the SM which follows the state with $E = E_s$, as described above.

⁴ Of these two intervals, the relevant one is that in which the derivative dE/dt in the nonlinear resonance equations (see Eq. (16) below) is positive or negative, for the case of the upper or lower GSS curve respectively.

⁵ I.e. E determined by Eq. (7) for any $\tilde{\psi}$ except from the vicinity of multiples of π . As shown in [43], Eq. (7) is irrelevant to the boundary of the chaotic layer in the range of $\tilde{\psi}$ close to multiples of π while the boundary in this range of $\tilde{\psi}$ still lies in the resonance range of energies, where $\omega(E) \approx \omega^{(\pm)}$.

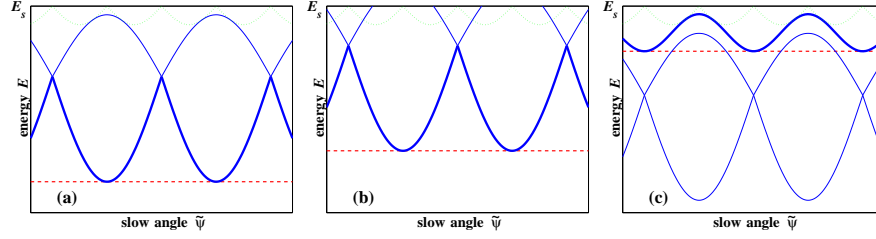


Fig. 1 Schematic figure illustrating the formation of the peak of the function $\Delta E_{sm}^{(-)}(\omega_f)$: (a) $\omega_f = \omega_{\max}$; (b) $\omega_f < \omega_{\max}$; (c) $\omega_f > \omega_{\max}$. The relevant (lower) GSS curve is shown by the dotted line. The relevant trajectories of the resonance Hamiltonian are shown by solid lines. The lower boundary of the layer is marked by a thick solid line: in (a) and (b) the lower boundary is formed by the lower part of the resonance separatrix while, in (c) it is formed by the resonance trajectory tangent to the GSS curve. The dashed line marks, for a given ω_f , the maximal deviation of the lower boundary from the separatrix energy E_s .

self-intersection) touches or intersects the upper/lower GSS curve while the upper/lower part does not, then the upper/lower boundary of the layer is formed by the upper/lower part of this self-intersecting trajectory (Figs. 1(a) and 1(b)); (ii) otherwise the boundary is formed by the resonance trajectory *tangent* to the GSS curve (Fig. 1(c)). It is shown below that, in both cases, the variation of the energy along the resonance trajectory is larger than the separatrix split δ by a logarithmically large factor $\propto \ln(1/h)$. Therefore, over the boundary of the SM chaotic layer the largest deviation of the energy from the separatrix value, $\Delta E_{sm}^{(\pm)}$, may be taken, in the leading-order approximation, to be equal to the largest variation of the energy along the resonance trajectory forming the boundary, while the latter trajectory can be entirely described within the resonance Hamiltonian formalism.

Finally, we mention that, as is obvious from the above description of the boundary, $\Delta E_{sm}^{(\pm)} \equiv \Delta E_{sm}^{(\pm)}(\omega_f)$ possesses a local maximum $\Delta E_{\max,sm}^{(\pm)}$ at ω_f for which the resonance separatrix just *touches* the corresponding GSS curve (see Fig. 1(a)).

3 Single-Separatrix Chaotic Layer

It is clear from Sec. 2 above that $\Delta E_{\max,sm}^{(\pm)}$ is equal in leading order to the width ΔE_{NR} of the nonlinear resonance which touches the separatrix. In Sec. 3.1 below, we *roughly* estimate ΔE_{NR} in order to classify two different types of systems. Secs. 3.2 and 3.3 present the *accurate* leading-order asymptotic theory for the two types of systems. The *next-order* correction is estimated in Sec. 3.4, while a *discussion* is presented in Sec. 3.5.

3.1 Rough estimates. Classification of systems.

Let us roughly estimate ΔE_{NR} : it will turn out that it is thus possible to classify all systems into two different types. With this aim, we expand the perturbation V into two Fourier series in t and in ψ respectively:

$$V \equiv \frac{1}{2} \sum_l V^{(l)}(E, \psi) e^{-il\omega_f t} + \text{c.c.} \equiv \frac{1}{2} \sum_{l,k} V_k^{(l)}(E) e^{i(k\psi - l\omega_f t)} + \text{c.c.} \quad (8)$$

As in standard nonlinear resonance theory [10, 23, 55, 51, 52], we single out the relevant (for a given peak) numbers K and L for the blind indices k and l respectively, and denote the absolute value of $V_K^{(L)}$ as V_0 :

$$V_0(E) \equiv |V_K^{(L)}(E)|. \quad (9)$$

To estimate the width of the resonance roughly, we use the pendulum approximation of resonance dynamics [10, 23, 55, 51, 52, 1]:

$$\Delta E_{NR} \sim \sqrt{8hV_0\omega_f/|d\omega/dE|}. \quad (10)$$

This approximation assumes constancy of $d\omega/dE$ in the resonance range of energies, which is not the case here: in reality, $\omega(E) \propto 1/\ln(1/|E - E_s|)$ in the vicinity of the separatrix [53, 10, 23, 55, 51, 52, 1, 29, 34, 47, 35, 43, 44], so that the relevant derivative $|d\omega/dE| \sim (\omega_r^{(\pm)})^2/(\omega_0|E - E_s|)$ varies strongly within the resonance range. However, for our rough estimate we may use the maximal value of $|E - E_s|$, which is approximately equal to ΔE_{NR} . If ω_f is of the order of $\omega_r^{(\pm)} \sim \omega_0/\ln(1/h)$, then Eq. (10) reduces to the following approximate asymptotic equation for ΔE_{NR} :

$$\Delta E_{NR} \sim V_0(E = E_s \pm \Delta E_{NR})h \ln(1/h), \quad h \rightarrow 0. \quad (11)$$

The asymptotic solution of Eq. (11) depends on $V_0(E_s \pm \Delta E_{NR})$ as a function of ΔE_{NR} . In this context, all systems can be divided in two types.

I The separatrix of the unperturbed system has *two or more* saddles while the relevant Fourier coefficient $V^{(L)} \equiv V^{(L)}(E, \psi)$ possesses *different* values on adjacent saddles. Given that, for $E \rightarrow E_s$, the system stays most of time near one of the saddles, the coefficient $V^{(L)}(E \rightarrow E_s, \psi)$ as a function of ψ is nearly a ‘‘square wave’’: it oscillates between the values at the different saddles. The relevant K is typically odd and, therefore, $V_0(E \rightarrow E_s)$ approaches a well defined non-zero value. Thus, the quantity $V_0(E = E_s \pm \Delta E_{NR})$ in Eq. (11) may be approximated by this non-zero limit, and we conclude therefore that

$$\Delta E_{NR} \propto h \ln(1/h), \quad h \rightarrow 0. \quad (12)$$

II Either (i) the separatrix of the unperturbed system has a *single saddle*, or (ii) it has more than one saddle but the perturbation coefficient $V^{(L)}$ is *identical* for all saddles. Then $V^{(L)}(E \rightarrow E_s, \psi)$, as a periodic function of ψ , significantly differs

from its value at the saddle(s) only during a small part of the period in ψ : this part is $\sim \omega(E)/\omega_0 \sim 1/\ln(1/|E_s - E|)$. Hence, $V_0(E_s \pm \Delta E_{NR}) \propto 1/\ln(1/\Delta E_{NR})$. Substituting this value in Eq. (11), we conclude that

$$\Delta E_{NR} \propto h, \quad h \rightarrow 0. \quad (13)$$

Thus, for systems of type I, the maximum width of the SM chaotic layer is proportional to h times a logarithmically large factor $\propto \ln(1/h)$ while, for systems of type II, it is proportional to h times a numerical factor.

As shown below, the variation of energy in between the instants relevant to the SM is $\sim h$, i.e. much less than ΔE_{NR} (12) for systems of the type I, and of the same order as ΔE_{NR} (13) for systems of type II. Therefore, one may expect that the maximum width of the layer for the original Hamiltonian system (1), $\Delta E^{(\pm)}$, is at least roughly approximated by that for the SM, $\Delta E_{sm}^{(\pm)}$, so that the above classification of systems is relevant to $\Delta E^{(\pm)}$ too. This is confirmed both by numerical integration of the equations of motion of the original Hamiltonian system and by the accurate theory presented in the next two sub-sections.

3.2 Asymptotic theory for systems of type I.

For the sake of clarity, we consider a particular example of a type I system; its generalization is straightforward.

We choose an archetypal example: the ac-driven pendulum (sometimes referred to as a pendulum subject to a dipole time-periodic perturbation) [55, 42, 45]:

$$\begin{aligned} H &= H_0 + hV, \\ H_0 &= \frac{p^2}{2} - \cos(q), \quad V = -q \cos(\omega_f t), \quad h \ll 1. \end{aligned} \quad (14)$$

Fig. 2 presents the results of numerical simulations for a few values of h and several values of ω_f . It shows that: (i) that the function $\Delta E^{(-)}(\omega_f)$ indeed possesses sharp peaks whose heights greatly exceed the estimates by the heuristic [55], adiabatic [14] and moderate-frequency [29] theories (see inset); (ii) as predicted by our rough estimates of Sec. 3.1, the 1st peak of $\Delta E^{(-)}(\omega_f)$ shifts to smaller values of ω_f while its magnitude grows, as h decreases. Below, we develop a leading-order asymptotic theory, in which the parameter of smallness is $1/\ln(1/h)$, and compare it with results of the simulations.

Before moving on, we note that the SM (approximated in the relevant case by nonlinear resonance dynamics) considers states of the system only at discrete instants. Apart from the variation of energy within the SM dynamics, a variation of energy in the Hamiltonian system also occurs in between the instants relevant to the SM. Given that $\omega_f \ll 1$, this latter variation may be considered in adiabatic approximation and it is of the order of h [14, 35]. It follows from the above rough estimates,

and from the more accurate consideration below, that the variation of energy within the SM dynamics for systems of type I is logarithmically larger i.e. larger by the factor $\ln(1/h)$. The variation of energy in between the instants relevant to the SM may therefore be neglected to leading-order for systems of type I: $\Delta E^{(-)} \simeq \Delta E_{sm}^{(-)}$. For the sake of notational compactness, we shall henceforth omit the subscript “*sm*” in this subsection.

For the system (14), the separatrix energy is equal to 1, while the asymptotic (for $E \rightarrow E_s$) dependence $\omega(E)$ is [55]:

$$\omega(E) \simeq \frac{\pi}{\ln(32/|E_s - E|)}, \quad (15)$$

$$E_s = 1, \quad |E_s - E| \ll 1.$$

Let us consider the range of energies below E_s (the range above E_s may be considered in an analogous way) and assume that ω_f is close to an odd multiple of $\omega_f^{(-)}$. The nonlinear resonance dynamics of the slow variables in the range of

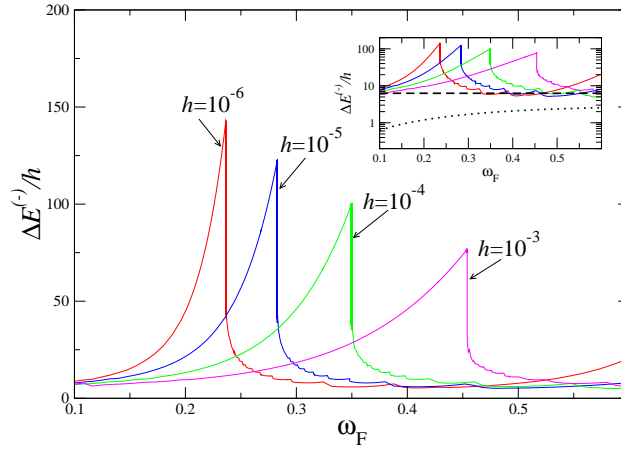


Fig. 2 Computer simulations for the ac driven pendulum (14) (an archetypal example of type I): the deviation $\Delta E^{(-)}$ of the lower boundary of the chaotic layer from the separatrix, normalized by the perturbation amplitude h , is plotted as a function of the perturbation frequency ω_f , for various h . The inset presents the same data but with a logarithmic ordinate and with the estimates by the heuristic [55], adiabatic [14] and moderate-frequency [29] theories. The heuristic estimate is shown by the dotted line: as an example of the heuristic estimate, we use the formula from [55]: $\Delta E^{(-)}/h = 2\pi\omega_f/\cosh(\pi\omega_f/2)$. The adiabatic and moderate-frequency estimates are shown by the dashed line: the adiabatic estimate for $\Delta E^{(-)}(\omega_f)$ is equal approximately to 2π ; the estimate following from the results of the work [29] for $\omega_f \sim 1$ is of the same order, so that it is schematically represented in the inset in Fig. 2 by the same line as for the adiabatic estimate (dashed line). The inset shows explicitly that the simulation results exceed the estimates of the former theories by 1 or 2 orders of magnitude, over a wide range of frequencies.

approximately resonant energies may be described as follows [43, 41] (cf. also [10, 23, 55, 51, 52, 1]):

$$\begin{aligned}
\frac{dI}{dt} &= -\frac{\partial \tilde{H}(I, \tilde{\psi})}{\partial \tilde{\psi}}, & \frac{d\tilde{\psi}}{dt} &= \frac{\partial \tilde{H}(I, \tilde{\psi})}{\partial I}, & (16) \\
\tilde{H}(I, \tilde{\psi}) &= \int_{I(E_s)}^I d\tilde{I} (n\omega - \omega_f) - nhq_n \cos(\tilde{\psi}) \\
&\equiv n(E - E_s) - \omega_f(I - I(E_s)) - nhq_n \cos(\tilde{\psi}), \\
I \equiv I(E) &= \int_{E_{\min}}^E \frac{d\tilde{E}}{\omega(\tilde{E})}, & E &\equiv H_0(p, q), \\
\tilde{\psi} &= n\psi - \omega_f t, \\
\psi &= \pi + \text{sign}(p)\omega(E) \int_{q_{\min}(E)}^q \frac{d\tilde{q}}{\sqrt{2(E - U(\tilde{q}))}} + 2\pi l, \\
q_n \equiv q_n(E) &= \frac{1}{2\pi} \int_0^{2\pi} d\psi q(E, \psi) \cos(n\psi), \\
|n\omega - \omega_f| &\ll \omega, & n &\equiv 2j - 1, & j = 1, 2, 3, \dots,
\end{aligned}$$

where I and ψ are the canonical variables action and angle respectively [10, 23, 55, 51, 52, 1]; E_{\min} is the minimal energy over all q, p , $E \equiv H_0(p, q)$; $q_{\min}(E)$ is the minimum coordinate of the conservative motion with a given value of energy E ; l is the number of right turning points in the trajectory $[q(\tau)]$ of the conservative motion with energy E and given initial state (q_0, p_0) .

The resonance Hamiltonian $\tilde{H}(I, \tilde{\psi})$ is obtained in the following way. First, the original Hamiltonian H is transformed to action-angle variables $I - \psi$. Then it is multiplied by n and the term $\omega_f I$ is extracted (the latter two operations correspond to the transformation $\psi \rightarrow \tilde{\psi} \equiv n\psi - \omega_f t$). Finally, the result is being averaged over time i.e. only the resonance term in the double Fourier expansion of the perturbation is kept (it may be done since the effect of the fast-oscillating terms on the dynamics of slow variables is small: see the estimate of the corrections in Sec. 3.4 below).

Let us derive asymptotic expression for $I(E)$, substituting the asymptotic expression (15) for $\omega(E)$ into the definition of $I(E)$ (16) and carrying out the integration:

$$I(E) \simeq I(E_s) - \frac{E_s - E}{\pi} \left(\ln \left(\frac{32}{E_s - E} \right) + 1 \right). \quad (17)$$

As for the asymptotic value $q_n(E \rightarrow E_s)$, it can be seen that $q(E \rightarrow E_s, \psi)$, as a function of ψ , asymptotically approaches a ‘‘square wave’’, oscillating between $-\pi$ and π , so that, for sufficiently small j ,

$$\begin{aligned}
q_{2j-1}(E \rightarrow E_s) &\simeq (-1)^{j+1} \frac{2}{2j-1}, & (18) \\
q_{2j} &= 0,
\end{aligned}$$

$$j = 1, 2, \dots \ll \frac{\pi}{2\omega(E)}.$$

The next issue is the analysis of the phase space of the resonant Hamiltonian (16). Substituting \tilde{H} (16) into the equations of motion (16), it can be seen that their stationary points have the following values of the slow angle

$$\tilde{\psi}_+ = \pi, \quad \tilde{\psi}_- = 0, \quad (19)$$

while the corresponding action is determined by the equation

$$n\omega - \omega_f \mp nh \frac{dq_n}{dI} = 0, \quad n \equiv 2j - 1, \quad (20)$$

where the sign “ \mp ” corresponds to $\tilde{\psi}_\mp$ (19).

The term $\propto h$ in (20) may be neglected to leading-order (cf. [10, 23, 55, 51, 52, 1, 43, 41]), and Eq. (20) reduces to the resonance condition

$$(2j - 1)\omega(E_r^{(j)}) = \omega_f, \quad (21)$$

the lowest-order solution of which is

$$E_s - E_r^{(j)} \simeq 32 \exp\left(-\frac{(2j-1)\pi}{\omega_f}\right). \quad (22)$$

Eqs. (19) and (22) together with (17) explicitly determine the elliptic and hyperbolic points of the Hamiltonian (16). The hyperbolic point is often referred to as a “saddle” and corresponds to $\tilde{\psi}_+$ or $\tilde{\psi}_-$ in (19) for even or odd j respectively. The saddle point generates the resonance separatrix. Using the asymptotic relations (17) and (18), we find that the resonance Hamiltonian (16) takes the following asymptotic value in the saddle:

$$\begin{aligned} \tilde{H}_{saddle} &\simeq \frac{E_s - E_r^{(j)}}{\pi} \omega_f - 2h \\ &\simeq \frac{\omega_f}{\pi} 32 \exp\left(-\frac{\pi(2j-1)}{\omega_f}\right) - 2h. \end{aligned} \quad (23)$$

The second asymptotic equality in (23) takes into account the relation (22).

As explained in Sec. 2 above, $\Delta E^{(-)}(\omega_f)$ possesses a local maximum at ω_f for which the resonance separatrix is tangent to the lower GSS curve (Fig. 1(a)). For the relevant frequency range $\omega_f \rightarrow 0$, the separatrix split (which represents the maximum deviation of the energy along the GSS curve from E_s) approaches the following value [55] in the asymptotic limit $h \rightarrow 0$

$$\delta \simeq 2\pi h, \quad \omega_f \ll 1. \quad (24)$$

As shown below, the variation of energy along the relevant resonance trajectories is much larger. Therefore, in the leading-order approximation, the GSS curve may

simply be replaced by the separatrix of the unperturbed system i.e. by the horizontal line $E = E_s$ or, equivalently, $I = I(E_s)$. Then the tangency occurs at $\tilde{\psi}$, shifted from the saddle by π , so that the condition of tangency is written as

$$\tilde{H}_{saddle} = \tilde{H}(I = I(E_s), \tilde{\psi} = \tilde{\psi}_{saddle} + \pi) \equiv 2h. \quad (25)$$

Substituting here \tilde{H}_{saddle} (23), we finally obtain the following transcendental equation for $\omega_{\max}^{(j)}$:

$$x \exp(x) = \frac{8(2j-1)}{h}, \quad x \equiv \frac{(2j-1)\pi}{\omega_{\max}^{(j)}}. \quad (26)$$

Fig. 3(b) demonstrates the excellent agreement between Eq. (26) and simulations of the Hamiltonian system over a wide range of h .

In the asymptotic limit $h \rightarrow 0$, the lowest-order explicit solution of Eq. (26) is

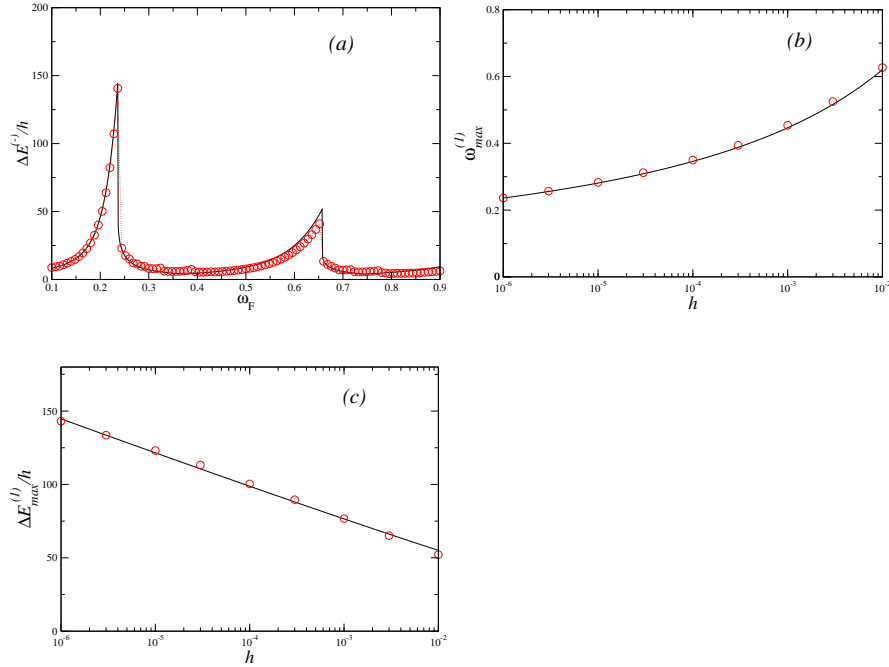


Fig. 3 An archetypal example of a type I system: the ac-driven pendulum (14). Comparison of theory (solid lines) and simulations (circles) for: (a) the deviation $\Delta E^{(-)}(\omega_f)$ of the lower boundary of the chaotic layer from the separatrix, normalized by the perturbation amplitude h , as a function of the perturbation frequency ω_f , for $h = 10^{-6}$; the theory is from Eqs. (26), (31), (32), (38), (39) and (41) (note the discontinuous drop by the factor e from the maximum to the right wing). (b) The frequency of the 1st maximum in $\Delta E^{(-)}(\omega_f)$ as a function of h ; the theory is from Eq. (26). (c) The 1st maximum in $\Delta E^{(-)}(\omega_f)/h$ as a function of h ; the theory is from Eqs. (34) and (26).

$$\omega_{\max}^{(j)} \simeq \frac{(2j-1)\pi}{\ln\left(\frac{8(2j-1)}{h}\right)}, \quad j = 1, 2, \dots \ll \ln\left(\frac{1}{h}\right). \quad (27)$$

As follows from Eq. (26), the value of $E_s - E_r^{(j)}$ (22) for $\omega_f = \omega_{\max}^{(j)}$ is

$$E_s - E_r^{(j)}(\omega_f = \omega_{\max}^{(j)}) = \frac{4\pi h}{\omega_{\max}^{(j)}}. \quad (28)$$

Its leading-order expression is:

$$E_s - E_r^{(j)}(\omega_f = \omega_{\max}^{(j)}) \simeq \frac{4h}{2j-1} \ln\left(\frac{8(2j-1)}{h}\right), \quad h \rightarrow 0. \quad (29)$$

If $\omega_f \leq \omega_{\max}^{(j)}$ then, in the chaotic layer, the largest deviation of energy from the separatrix value corresponds to the minimum energy $E_{\min}^{(j)}$ on the nonlinear resonance separatrix (Fig. 1(a,b)), which occurs at $\tilde{\psi}$ shifted by π from the saddle. The condition of equality of \tilde{H} at the saddle and at the minimum of the resonance separatrix is written as

$$\tilde{H}_{saddle} = \tilde{H}(I(E_{\min}^{(j)}), \tilde{\psi}_{saddle} + \pi). \quad (30)$$

Let us seek its asymptotic solution in the form

$$E_s - E_{\min}^{(j)} \equiv \Delta E_l^{(j)} = (1+y)(E_s - E_r^{(j)}) \simeq (1+y)32 \exp\left(-\frac{\pi(2j-1)}{\omega_f}\right),$$

$$y \gtrsim 1. \quad (31)$$

Substituting (31) and (23) into Eq. (30), we obtain for y the following transcendental equation:

$$(1+y)\ln(1+y) - y = \frac{h}{8(2j-1)} x_f \exp(x_f), \quad (32)$$

$$x_f \equiv \frac{\pi(2j-1)}{\omega_f}, \quad \omega_f \leq \omega_{\max}^{(j)}, \quad y > 0,$$

where $\omega_{\max}^{(j)}$ is given by Eq. (26).

Eqs. (31) and (32) describe the left wing of the j -th peak of $\Delta E^{(-)}(\omega_f)$. Fig. 3(a) demonstrates the good agreement between our analytic theory and simulations for the Hamiltonian system.

It follows from Eq. (26) that Eq. (32) for $\omega_f = \omega_{\max}^{(j)}$ reduces to the relation $\ln(1+y) = 1$, i.e.

$$1 + y(\omega_{\max}^{(j)}) = e. \quad (33)$$

It follows from Eqs. (33), (31) and (28) that the maximum for a given peak is:

$$\Delta E_{\max}^{(j)} \equiv E_s - E_{\min}^{(j)}(\omega_{\max}^{(j)}) = \frac{4\pi e h}{\omega_{\max}^{(j)}}. \quad (34)$$

Fig. 3(c) shows the excellent agreement of this expression with our simulations of the Hamiltonian system over a wide range of h .

The leading-order expression for $\Delta E_{\max}^{(j)}$ is:

$$\Delta E_{\max}^{(j)} \simeq \frac{4eh}{2j-1} \ln(8(2j-1)/h), \quad h \rightarrow 0, \quad (35)$$

which confirms the rough estimate (12).

As ω_f decreases, it follows from Eq. (32) that y increases exponentially sharply. In order to understand how $\Delta E_l^{(j)}$ decreases upon decreasing ω_f , it is convenient to rewrite Eq. (31) re-expressing the exponent by means of Eq. (32):

$$\Delta E_l^{(j)}(\omega_f) = \frac{4\pi h}{\omega_f(\ln(1+y) - y/(1+y))}. \quad (36)$$

It follows from Eqs. (32) and (36) that $\Delta E_l^{(j)}$ decreases *power-law-like* when ω_f is decreased. In particular, $\Delta E_l^{(j)} \propto 1/(\omega_{\max}^{(j)} - \omega_f)$ at the far part of the wing.

As for the right wing of the peak, i.e. for $\omega_f > \omega_{\max}^{(j)}$, over the chaotic layer, the largest deviation of energy from the separatrix value corresponds to the minimum of the resonance trajectory tangent to the GSS curve (Fig. 1(c)). The value of $\tilde{\psi}$ at the minimum coincides with $\tilde{\psi}_{saddle}$. In the leading-order approximation, the GSS curve may be replaced by the horizontal line $I = I(E_s)$, so that the tangency occurs at $\tilde{\psi} = \tilde{\psi}_{saddle} + \pi$. Then the energy at the minimum $E_{\min}^{(j)}$ can be found from the equation

$$\tilde{H}(I(E_s), \tilde{\psi}_{saddle} + \pi) = \tilde{H}(I(E_{\min}^{(j)}), \tilde{\psi}_{saddle}) \quad (37)$$

Let us seek its asymptotic solution in the form

$$\begin{aligned} E_s - E_{\min}^{(j)} \equiv \Delta E_r^{(j)} &= z(E_s - E_r^{(j)}) \simeq z32 \exp\left(-\frac{\pi(2j-1)}{\omega_f}\right) \\ 0 < z < 1, \quad z &\sim 1. \end{aligned} \quad (38)$$

Substituting (38) into (37), we obtain for z the following transcendental equation:

$$\begin{aligned} z(1 + \ln(1/z)) &= \frac{h}{8(2j-1)} x_f \exp(x_f) \\ x_f &\equiv \frac{\pi(2j-1)}{\omega_f}, \quad \omega_f > \omega_{\max}^{(j)}, \quad 0 < z < 1, \end{aligned} \quad (39)$$

where $\omega_{\max}^{(j)}$ is given by Eq. (26). Eqs. (38) and (39) describe the right wing of the j -th peak of $\Delta E^{(-)}(\omega_f)$. Fig. 3(a) demonstrates the good agreement between our analytic theory and simulations.

It follows from Eq. (26) that the solution of Eq. (39) for $\omega_f \rightarrow \omega_{\max}^{(j)}$ is $z \rightarrow 1$, so the right wing starts from the value given by Eq. (28) (or, approximately, by Eq. (29)). Expressing the exponent in (38) from (39), we obtain the following equation

$$\Delta E_r^{(j)}(\omega_f) = \frac{4\pi h}{\omega_f(1 + \ln(1/z))}. \quad (40)$$

It follows from Eqs. (39) and (40) that $\Delta E_r^{(j)}$ decreases *power-law-like* for increasing ω_f . In particular, $\Delta E_r^{(j)} \propto 1/(\omega_f - \omega_{\max}^{(j)})$ in the far part of the wing. Further analysis of the asymptotic shape of the peak is presented in Sec. 3.5 below.

Beyond the peaks, the function $\Delta E^{(-)}(\omega_f)$ is logarithmically small in comparison with the maxima of the peaks. The functions $\Delta E_l^{(j)}(\omega_f)$ and $\Delta E_r^{(j)}(\omega_f)$ in the ranges beyond the peaks are also logarithmically small. Hence, nearly any function of $\Delta E_r^{(j)}(\omega_f)$ and $\Delta E_l^{(j+1)}(\omega_f)$ which is close to $\Delta E_r^{(j)}(\omega_f)$ in the vicinity of $\omega_{\max}^{(j)}$ and to $\Delta E_l^{(j+1)}(\omega_f)$ in the vicinity of $\omega_{\max}^{(j+1)}$ while being sufficiently small beyond the peaks may be considered as an approximation of the function $\Delta E^{(-)}(\omega_f)$ to logarithmic accuracy with respect to the maxima of the peaks, $\Delta E_{\max}^{(j)}$ and $\Delta E_{\max}^{(j+1)}$, in the whole range $[\omega_{\max}^{(j)}, \omega_{\max}^{(j+1)}]$. One of the easiest options is the following:

$$\begin{aligned} \Delta E^{(-)}(\omega_f) &= \Delta E_l^{(1)}(\omega_f) && \text{for } \omega_f < \omega_{\max}^{(1)}, \\ \Delta E^{(-)}(\omega_f) &= \max\{\Delta E_r^{(j)}(\omega_f), \Delta E_l^{(j+1)}(\omega_f)\} && \text{for } \omega_{\max}^{(j)} < \omega_f < \omega_{\max}^{(j+1)}, \\ j = 1, 2, \dots &\ll \frac{\pi}{2\omega_{\max}^{(1)}}. && \end{aligned} \quad (41)$$

We used this function in Fig. 3(a), and the analogous one will also be used in the other cases.

In fact, the theory may be generalized in such a way that Eq. (41) would approximate $\Delta E^{(-)}(\omega_f)$ well in the ranges far beyond the peaks with logarithmic accuracy, even with respect to $\Delta E^{(-)}(\omega_f)$ itself rather than to $\Delta E_{\max}^{(j)}$ only (cf. the next section). However, we do not do this in the present case, being interested primarily in the leading-order description of the peaks.

Finally, we demonstrate in Fig. 4 that the lowest-order theory describes the boundary of the layers quite well, even in the Poincaré section rather than only in energy/action.

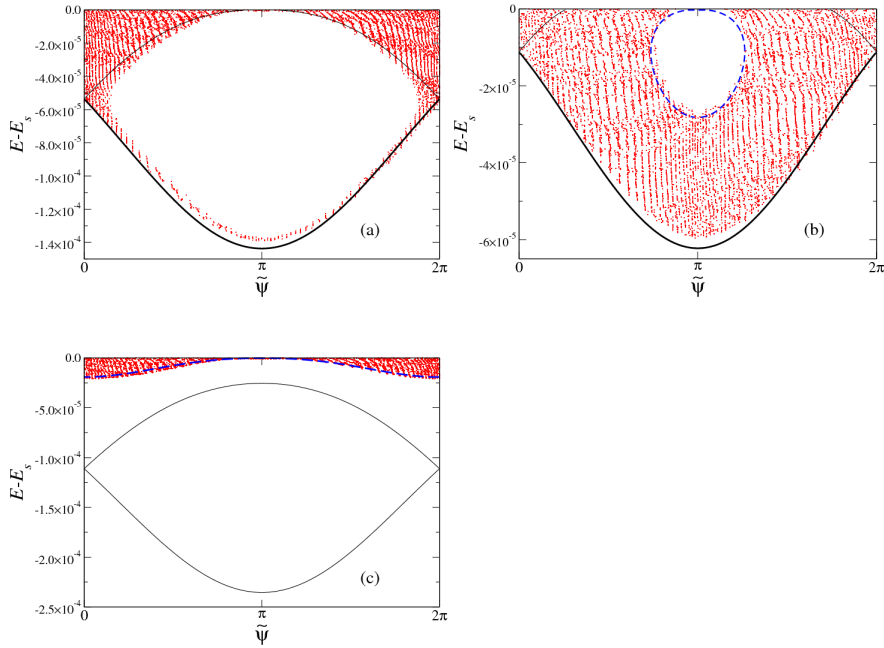


Fig. 4 Some characteristic Poincaré sections in the 2π -interval of the energy-angle plane for the system (14) with $h = 10^{-6}$ and ω_f equal to: (a) 0.236 (maximum), (b) 0.21 (left wing), (c) 0.25 (right wing). Results of the numerical integration of the equations of motion for the original Hamiltonian (14) are shown by (red) dots. The NR separatrix calculated in the leading-order approximation (i.e. by the integration of the resonant equations of motion (16) in which $\omega(E)$, $I(E)$ and $q_1(E)$ are approximated by the explicit formulæ (15), (17) and (18) respectively) is drawn by the (black) solid line. The NR trajectory (calculated in the leading-order approximation) tangent to the line $E = E_s$ is drawn by the (blue) dashed line. The outer boundary (marked by a thicker line) is approximated by: the lower part of the NR separatrix in cases (a) and (b), and by the tangent NR trajectory in case (c) The boundary of the island of stability in the cases (a) and (b) is approximated by the tangent NR trajectory (which coincides in the case (a) with the NR separatrix).

3.3 Asymptotic theory for systems of type II.

We consider two characteristic examples of type II systems, corresponding to the classification given in Sec. 3.1. As an example of a system where the separatrix of the unperturbed system possesses a single saddle, we consider an ac-driven Duffing oscillator [1, 18, 29, 40]. As an example of the system where the separatrix possesses more than one saddle, while the perturbation takes equal values at the saddles, we consider a pendulum with an oscillating suspension point [1, 18, 29, 34, 35]. The treatment of these cases is similar in many respects to that presented in Sec. 3.2 above. So, we present it in less detail, emphasizing the differences.

3.3.1 AC-driven Duffing oscillator.

Consider the following archetypal Hamiltonian [1, 18, 29, 40]:

$$\begin{aligned} H &= H_0 + hV, \\ H_0 &= \frac{p^2}{2} - \frac{q^2}{2} + \frac{q^4}{4}, \quad V = -q \cos(\omega_f t), \quad h \ll 1. \end{aligned} \quad (42)$$

The asymptotic dependence of $\omega(E)$ on E for E below the separatrix energy $E_s = 0$ is the following [1, 13]

$$\begin{aligned} \omega(E) &\simeq \frac{2\pi}{\ln(16/(E_s - E))}, \\ E_s &= 0, \quad 0 < E_s - E \ll 1. \end{aligned} \quad (43)$$

Correspondingly, the resonance values of energies (determined by the condition analogous to (21)) are

$$E_s - E_r^{(j)} = 16 \exp\left(-\frac{2\pi j}{\omega_f}\right), \quad j = 1, 2, 3, \dots \quad (44)$$

The asymptotic dependence of $I(E)$ is

$$I(E) \simeq I(E_s) - \frac{E_s - E}{2\pi} \left(\ln\left(\frac{16}{E_s - E}\right) + 1 \right). \quad (45)$$

The nonlinear resonance dynamics is described by the resonance Hamiltonian \tilde{H} which is identical in form to Eq. (16). Obviously, the actual dependences $\omega(E)$ and $I(E)$ are given by Eq. (43) and (45) respectively. The most important difference is in $q_j(E)$: instead of a non-zero value (see (18)), it approaches 0 as $E \rightarrow E_s$. Namely, it is $\propto \omega(E)$ [1, 13]:

$$q_j(E) \simeq \frac{1}{\sqrt{2}} \omega(E), \quad j = 1, 2, \dots \ll \frac{\pi}{\omega(E)}, \quad (46)$$

i.e. q_j is much smaller than in systems of type I (cf. (18)). Due to this, the resonance is “weaker”. At the same time, the separatrix split δ is also smaller, namely $\sim h\omega_f$ (cf. [43]) rather than $\sim h$ as for the systems of type I. That is why the separatrix chaotic layer is still dominated by resonance dynamics while the matching of the separatrix map and nonlinear resonance dynamics is still valid in the asymptotic limit $h \rightarrow 0$ [43].

Similarly to the previous section, we find the value of \tilde{H} in the saddle in the leading-order approximation⁶:

⁶ The only essential difference is that q_n at the saddle is described by Eq. (46) rather than by Eq. (18).

$$\tilde{H}_{saddle} \simeq \omega_f \left(\frac{E_s - E_r^{(j)}}{2\pi} - \frac{h}{\sqrt{2}} \right), \quad (47)$$

where $E_s - E_r^{(j)}$ is given in (44).

As before, the maximum width of the layer corresponds to ω_f , for which the resonance separatrix is tangent to the GSS curve (Fig. 1(a)). It can be shown [43] that the angle of tangency asymptotically approaches $\tilde{\psi}_{saddle} + \pi = \pi$ while the energy still lies in the resonance range. Here $\omega(E) \approx \omega_r^{(-)} \approx \omega_f/j$. Using the expressions for $\tilde{H}(E, \tilde{\psi})$ (cf. (16)), $I(E)$ (45), $q_j(E)$ (46), and taking into account that in the tangency $E < \delta \sim h\omega_f \ll h$, to leading-order the value of \tilde{H} at the tangency reads

$$\tilde{H}_{tangency} \simeq \omega_f \frac{h}{\sqrt{2}}. \quad (48)$$

Allowing for Eqs. (47) and (48), the condition for the maximum, $\tilde{H}_{saddle} = \tilde{H}_{tangency}$, reduces to

$$E_s - E_r^{(j)}(\omega_{\max}^{(j)}) \simeq 2\pi\sqrt{2}h. \quad (49)$$

Thus these values $E_s - E_r^{(j)}$ are logarithmically smaller than the corresponding values (28) for systems of type I.

The values of ω_f corresponding to the maxima of the peaks in $\Delta E^{(-)}(\omega_f)$ are readily obtained from (49) and (44):

$$\omega_{\max}^{(j)} \simeq \frac{2\pi j}{\ln(4\sqrt{2}/(\pi h))}, \quad j = 1, 2, \dots \ll \ln(1/h). \quad (50)$$

The derivation to leading order of the shape of the peaks for the chaotic layer of the separatrix map, i.e. within the nonlinear resonance (NR) approximation, is similar to that for type I. So, we present only the results, marking them with the subscript “NR”.

The left wing of the j th peak of $\Delta E_{NR}^{(-)}(\omega_f)$ is described by the function

$$\Delta E_{i, NR}^{(j)}(\omega_f) = 16(1+y) \exp\left(-\frac{2\pi j}{\omega_f}\right) \equiv \frac{2\pi\sqrt{2}h}{\ln(1+y) - y/(1+y)}, \quad (51)$$

$$\omega_f \leq \omega_{\max}^{(j)},$$

where y is the positive solution of the transcendental equation

$$(1+y) \ln(1+y) - y = \frac{\pi h}{4\sqrt{2}} \exp\left(\frac{2\pi j}{\omega_f}\right), \quad y > 0. \quad (52)$$

In common with the type I case, $1 + y(\omega_{\max}^{(j)}) = e$, so that

$$\Delta E_{\max, NR}^{(j)} = e(E_s - E_f^{(j)}(\omega_{\max}^{(j)})) \simeq 2\pi\epsilon\sqrt{2}h. \quad (53)$$

Eq. (53) confirms the rough estimate (13). The right wing of the peak is described by the function

$$\Delta E_{r, NR}^{(j)}(\omega_f) = 16z \exp\left(-\frac{2\pi j}{\omega_f}\right) \equiv \frac{2\pi\sqrt{2}h}{1 + \ln(1/z)}, \quad (54)$$

$$\omega_f > \omega_{\max}^{(j)},$$

where $z < 1$ is the solution of the transcendental equation

$$z(1 + \ln(1/z)) = \frac{\pi h}{4\sqrt{2}} \exp\left(\frac{2\pi j}{\omega_f}\right), \quad 0 < z < 1. \quad (55)$$

As in the type I case, $z(\omega_f \rightarrow \omega_{\max}^{(j)}) \rightarrow 1$.

It follows from Eqs. (49) and (53) that the typical variation of energy within the nonlinear resonance dynamics (that approximates the separatrix map dynamics) is $\propto h$. For the Hamiltonian system, the variation of energy in between the discrete instants corresponding to the separatrix map [55, 51, 52, 1, 43, 31] is also $\propto h$. Therefore, unlike the type I case, one needs to take it into account even at the leading-order approximation. Let us consider the right well of the Duffing potential (the results for the left well are identical), and denote by t_k the instant at which the energy E at a given k -th step of the separatrix map is taken: it corresponds to the beginning of the k -th pulse of velocity [55, 43] i.e. the corresponding q is close to a left turning point q_{lp} in the trajectory $[q(\tau)]$. Let us also take into account that the relevant frequencies are small so that the adiabatic approximation may be used. Thus, the change of energy from t_k up to a given instant t during the following pulse of velocity ($t - t_k \sim 1$) may be calculated as

$$\begin{aligned} \Delta E &= \int_{t_k}^t d\tau \dot{q} h \cos(\omega_f \tau) \simeq h \cos(\omega_f t_k) \int_{t_k}^t d\tau \dot{q} \\ &= h \cos(\omega_f t_k) (q(t) - q_{lp}) \end{aligned} \quad (56)$$

For the motion near the separatrix, the velocity pulse corresponds approximately to $\psi = 0$ (see the definition of ψ (16)). Thus, the corresponding slow angle is $\tilde{\psi} \equiv j\psi - \omega_f t_k \simeq -\omega_f t_k$.

For the left wing of the peak of $\Delta E^{(-)}(\omega_f)$ (including also the maximum of the peak), the boundary of the chaotic layer of the separatrix map is formed by the lower part of the NR separatrix. The minimum energy along this separatrix occurs at $\tilde{\psi} = \pi$. Taking this into account, and also noting that $\tilde{\psi} \simeq -\omega_f t_k$, we conclude that $\cos(\omega_f t_k) \simeq -1$. So, $\Delta E \leq 0$, i.e. it does lower the minimum energy of the layer of the Hamiltonian system. The maximum reduction occurs at the right turning point q_{rp} :

$$\max(|\Delta E|) \simeq h(q_{rp} - q_{lp}) = \sqrt{2}h. \quad (57)$$

We conclude that the left wing of the j -th peak is described as follows:

$$\Delta E_l^{(j)}(\omega_f) \simeq \Delta E_{l, NR}^{(j)}(\omega_f) + \sqrt{2}h, \quad \omega_f \leq \omega_{\max}^{(j)}, \quad (58)$$

where $\Delta E_{l, NR}^{(j)}(\omega_f)$ is given by Eqs. (51)-(52). In particular, the maximum of the peak is:

$$\Delta E_{\max}^{(j)} \simeq (2\pi e + 1)\sqrt{2}h \approx 25.6h. \quad (59)$$

For the right wing of the peak, the minimum energy of the layer of the separatrix map occurs when $\tilde{\psi}$ coincides with $\tilde{\psi}_{saddle}$ (Fig. 1(c)) i.e. is equal to 0. As a result, $\cos(\omega_f t_k) \simeq 1$ and, hence, $\Delta E \geq 0$. So, this variation cannot lower the minimum energy of the layer for the main part of the wing, i.e. for $\omega_f \leq \omega_{bend}^{(j)}$ where $\omega_{bend}^{(j)}$ is defined by the condition $\Delta E_{r, NR}^{(j)} = \max(|\Delta E|) \equiv \sqrt{2}h$. For $\omega_f > \omega_{bend}^{(j)}$, the minimal energy in the layer occurs at $\tilde{\psi} = \pi$, and it is determined exclusively by the variation of energy during the velocity pulse (the NR contribution is close to zero at such $\tilde{\psi}$). Thus, we conclude that there is a bending of the wing at $\omega_f = \omega_{bend}^{(j)}$:

$$\begin{aligned} \Delta E_r^{(j)}(\omega_f) &= \Delta E_{r, NR}^{(j)}(\omega_f), & \omega_{\max}^{(j)} < \omega_f \leq \omega_{bend}^{(j)}, \\ \Delta E_r^{(j)}(\omega_f) &= \sqrt{2}h, & \omega_f \geq \omega_{bend}^{(j)}, \\ \omega_{bend}^{(j)} &= \frac{2\pi j}{\ln(8\sqrt{2}/h) + 1 - 2\pi}, \end{aligned} \quad (60)$$

where $\Delta E_{r, NR}^{(j)}(\omega_f)$ is given by Eqs. (54) and (55).

Analogously to the previous case, $\Delta E^{(-)}(\omega_f)$ may be approximated over the whole frequency range by Eq. (41) with $\Delta E_l^{(j)}$ and $\Delta E_r^{(j)}$ given by Eqs. (58) and (60) respectively. Moreover, unlike the previous case, the theory also describes accurately the range far beyond the peaks: $\Delta E^{(-)}$ is dominated in this range by the velocity pulse contribution ΔE , which is accurately taken into account both by Eqs. (58) and (60).

Fig. 5 shows very reasonable agreement between the theory and simulations, especially for the 1st peak⁷.

⁷ The disagreement between theory and simulations for the magnitude of the 2nd peak is about three times larger than that for the 1st peak, so that the height of the 2nd peak is about 30% smaller than that calculated from the asymptotic theory. This occurs because, for the energies relevant to the 2nd peak, the deviation from the separatrix is much higher than that for the 1st peak. Due to the latter, the Fourier coefficient $q_2(E)$ for the relevant E is significantly smaller than that obtained from the asymptotic formula (42). In addition, the velocity pulse contribution ΔE also significantly decreases while the separatrix split increases as ω_f becomes ~ 1 .

3.3.2 Pendulum with an oscillating suspension point

Consider the archetypal Hamiltonian [1, 18, 29, 34, 35]

$$H = H_0 + hV,$$

$$H_0 = \frac{p^2}{2} + \cos(q), \quad V = -\cos(q) \cos(\omega_f t), \quad h \ll 1. \quad (61)$$

Though the treatment is similar to that used in the previous case, there are also characteristic differences. One of them is the following: although the resonance Hamiltonian is similar to the Hamiltonian (16), instead of the Fourier component of the coordinate, q_n , there should be the Fourier component of $\cos(q)$, V_n , which can be shown to be:

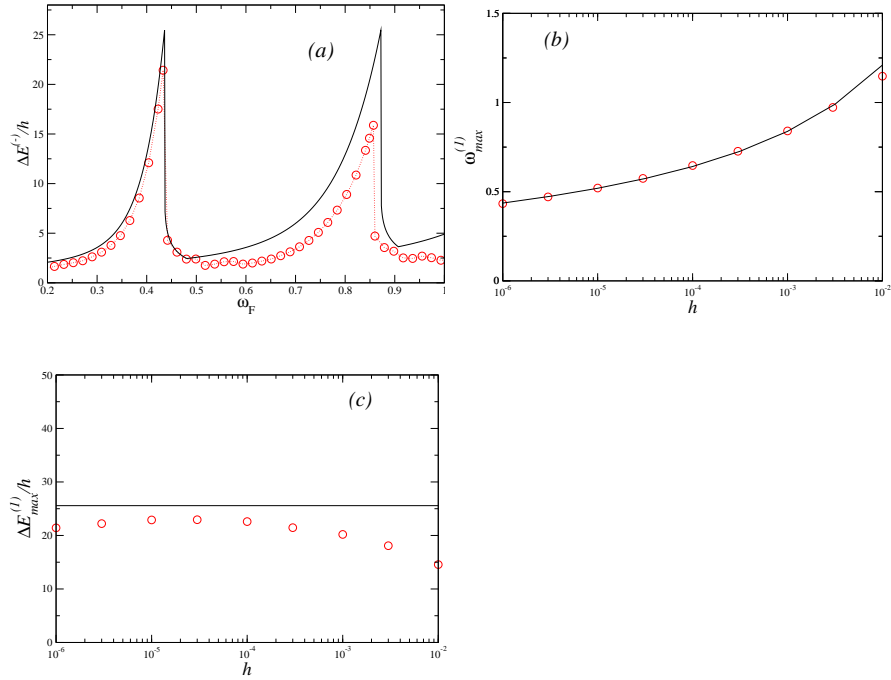


Fig. 5 An archetypal example of a type II system: the ac driven Duffing oscillator (42). Comparison of theory (solid lines) and simulations (circles): (a) the deviation $\Delta E^{(-)}(\omega_f)$ of the lower boundary of the chaotic layer from the separatrix, normalized by the perturbation amplitude h , as a function of the perturbation frequency ω_f , for $h = 10^{-6}$; the theory is from Eqs. (41), (50), (51), (52), (54), (55), (58) and (60) (note the discontinuous drop from the maximum to the right wing); (b) the frequency of the 1st maximum in $\Delta E^{(-)}(\omega_f)$ as a function of h ; the theory is from Eq. (50); (c) the 1st maximum in $\Delta E^{(-)}(\omega_f)/h$ as a function of h ; the theory is from Eq. (59).

$$\begin{aligned}
V_{2j} &\simeq (-1)^{j+1} \frac{4}{\pi} \omega(E), & E_s - E \ll 1, \\
V_{2j-1} &= 0, \\
j = 1, 2, \dots &\ll \frac{2\pi}{\omega(E)}, & V_n \equiv \frac{1}{2\pi} \int_0^{2\pi} d\psi \cos(q) \cos(n\psi).
\end{aligned} \tag{62}$$

The description of the chaotic layer of the separatrix map at the lowest order, i.e. within the NR approximation, is similar to that for the ac-driven Duffing oscillator. So we present only the results, marking them with the subscript “NR”.

The frequency of the maximum of a given j -th peak is:

$$\omega_{\max}^{(j)} \simeq \frac{2\pi j}{\ln(4/h)}, \quad j = 1, 2, \dots \ll \ln(4/h). \tag{63}$$

This expression agrees well with simulations for the Hamiltonian system (Fig. 6(b)). To logarithmic accuracy, Eq. (63) coincides with the formula following from Eq. (8) of [34] (reproduced in [35] as Eq. (21)) taken in the asymptotic limit $h \rightarrow 0$ (or, equivalently, $\omega_{\max}^{(j)} \rightarrow 0$). However, the numerical factor in the argument of the logarithm in the asymptotic formula following from the result of [34, 35] is half our value: this is because the nonlinear resonance is approximated in [34, 35] by the conventional pendulum model which is not valid near the separatrix (cf. our Sec. 3.1 above).

The left wing of the j th peak of $\Delta E_{NR}^{(-)}(\omega_f)$ is described by the function

$$\begin{aligned}
\Delta E_{l,NR}^{(j)}(\omega_f) &= 32(1+y) \exp\left(-\frac{2\pi j}{\omega_f}\right) \equiv \frac{8h}{\ln(1+y) - y/(1+y)}, \\
\omega_f &\leq \omega_{\max}^{(j)},
\end{aligned} \tag{64}$$

where y is the positive solution of the transcendental equation

$$(1+y) \ln(1+y) - y = \frac{h}{4} \exp\left(\frac{2\pi j}{\omega_f}\right), \quad y > 0. \tag{65}$$

Similarly to the previous cases, $1 + y(\omega_{\max}^{(j)}) = e$. Hence,

$$\Delta E_{\max,NR}^{(j)} = e(E_s - E_r^{(j)}(\omega_{\max}^{(j)})) = 8eh. \tag{66}$$

Eq. (66) confirms the rough estimate (13). The right wing of the peak is described by the function

$$\begin{aligned}
\Delta E_{r,NR}^{(j)}(\omega_f) &= 32z \exp\left(-\frac{2\pi j}{\omega_f}\right) \equiv \frac{8h}{1 + \ln(1/z)}, \\
\omega_f &> \omega_{\max}^{(j)},
\end{aligned} \tag{67}$$

where $z < 1$ is the solution of the transcendental equation

$$z(1 + \ln(1/z)) = \frac{h}{4} \exp\left(\frac{2\pi j}{\omega_f}\right), \quad 0 < z < 1. \quad (68)$$

Similarly to the previous cases, $z(\omega_f \rightarrow \omega_{\max}^{(j)}) \rightarrow 1$.

Now consider the variation of energy during a velocity pulse. Though the final result looks quite similar to the case with a single saddle, its derivation has some characteristic differences, and we present it in detail. Unlike the case with a single saddle, the pulse may start close to either the left or the right turning point, and the sign of the velocity in such pulses is opposite [55, 43]. The angle ψ in the pulse is close to $-\pi/2$ or $\pi/2$ respectively. So, let us calculate the change of energy from the beginning of the pulse, t_k , until a given instant t within the pulse:

$$\begin{aligned} \Delta E &= - \int_{t_k}^t d\tau \dot{q} h \partial V / \partial q = h \int_{t_k}^t d\tau \dot{q} (-\sin(q) \cos(\omega_f \tau)) \\ &\simeq h \cos(\omega_f t_k) \int_{t_k}^t d\tau \dot{q} (-\sin(q)) \simeq h \cos(\omega_f t_k) (\cos(q(t)) - 1). \end{aligned} \quad (69)$$

Here, the third equality assumes adiabaticity while the last equality takes into account that the turning points are close to the maxima of the potential i.e. close to a multiple of 2π (where the cosine is equal to 1).

The quantity ΔE (69) takes its maximal absolute value at $q = \pi$. So, we shall further consider

$$\Delta E_{\max} = -2h \cos(\omega_f t_k) \equiv -2h \cos(2j\psi_k - \tilde{\psi}_k) = (-1)^{j+1} 2h \cos(\tilde{\psi}_k). \quad (70)$$

The last equality takes into account that, as mentioned above, the relevant ψ_k is either $-\pi/2$ or $\pi/2$. For the left wing, the value of $\tilde{\psi}$ at which the chaotic layer of the separatrix map possesses a minimal energy corresponds to the minimum of the resonance separatrix. It is equal to π or 0 if the Fourier coefficient V_{2j} is positive or negative, i.e. for odd or even j , respectively: see Eq. (63). Thus $\Delta E_{\max} = -2h$ for any j and, therefore, it does lower the minimal energy of the boundary. We conclude that

$$\Delta E_l^{(j)}(\omega_f) \simeq \Delta E_{l, NR}^{(j)}(\omega_f) + 2h, \quad \omega_f \leq \omega_{\max}^{(j)}, \quad (71)$$

where $\Delta E_{l, NR}^{(j)}(\omega_f)$ is given by Eqs. (64)-(65). In particular, the maximum of the peak is:

$$\Delta E_{\max}^{(j)} \simeq (4e + 1)2h \approx 23.7h. \quad (72)$$

The expression (72) confirms the rough estimate (13) and agrees well with simulations (Fig. 6(c)). At the same time, it differs from the formula which can be obtained from Eq. (10) of [34] (using also Eqs. (1), (3), (8), (9) of [34]) in the asymptotic limit $h \rightarrow 0$: the latter gives for $\Delta E_{\max}^{(j)}$ the asymptotic value $32h$. Though this

result [34] (referred to also in [35]) provides for the correct functional dependence on h , it is quantitatively incorrect because (i) it is based on the pendulum approximation of the nonlinear resonance while this approximation is invalid in the vicinity of the separatrix (see the discussion of this issue in Sec. 3.1 above), and (ii) it does not take into account the variation of energy during the velocity pulse.

The right wing, by analogy to the case of the Duffing oscillator, possesses a bend at $\omega_f = \omega_{bend}^{(j)}$ where $\Delta E_{r, NR}^{(j)} = |\Delta E_{\max}| \equiv 2h$, corresponding to the shift of the relevant $\tilde{\psi}$ for π . We conclude that:

$$\begin{aligned} \Delta E_r^{(j)}(\omega_f) &= \Delta E_{r, NR}^{(j)}(\omega_f), & \omega_{\max}^{(j)} < \omega_f \leq \omega_{bend}^{(j)}, \\ \Delta E_r^{(j)}(\omega_f) &= 2h, & \omega_f \geq \omega_{bend}^{(j)}, \end{aligned}$$

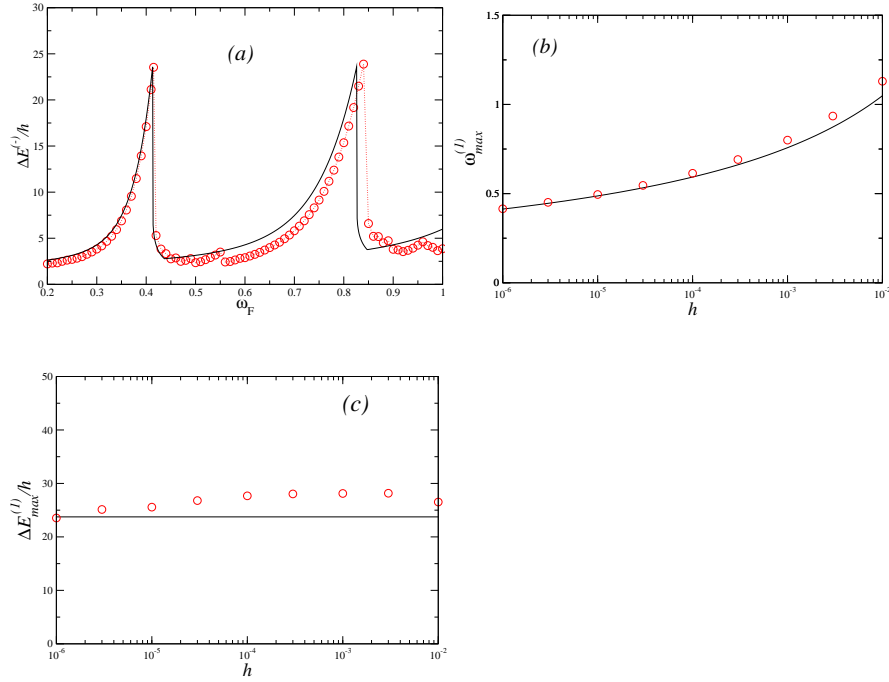


Fig. 6 An archetypal example of a type II system: the pendulum with an oscillating suspension point (61). Comparison of theory (solid lines) and simulations (circles): (a) The deviation $\Delta E^{(-)}(\omega_f)$ of the lower boundary of the chaotic layer from the separatrix, normalized by the perturbation amplitude h , as a function of the perturbation frequency ω_f , for $h = 10^{-6}$; the theory is by Eqs. (41), (63), (64), (65), (67), (68), (71) and (73) (note the discontinuous drop from the maximum to the right wing). (b) The frequency of the 1st maximum in $\Delta E^{(-)}(\omega_f)$ as a function of h ; the theory is from Eq. (63). (c) The 1st maximum in $\Delta E^{(-)}(\omega_f)/h$ as a function of h ; the theory is from Eq. (72).

$$\omega_{bend}^{(j)} = \frac{2\pi j}{\ln(16/h) - 3}, \quad (73)$$

where $\Delta E_{r, NR}^{(j)}(\omega_f)$ is given by Eqs. (66) and (67).

Similarly to the previous case, both the peaks and the frequency ranges far beyond the peaks are well approximated by Eq. (41), with $\Delta E_t^{(j)}$ and $\Delta E_r^{(j)}$ given by Eqs. (71) and (73) respectively (Fig. 6(a)).

3.4 Estimate of the next-order corrections

We have calculated explicitly only the leading term ΔE in the asymptotic expansion of the chaotic layer width. Explicit calculation of the next-order term $\Delta E^{(next)}$ is possible, but it is rather complicated and cumbersome: cf. the closely related case with two separatrices [43] (see also Sec. 4 below). In the present section, where the perturbation amplitude h in the numerical examples is 4 orders of magnitude smaller than that in [43], there is no particular need to calculate the next-order correction quantitatively. Let us estimate it, however, in order to demonstrate that its ratio to the leading term does vanish in the asymptotic limit $h \rightarrow 0$.

We shall consider separately the contribution $\Delta E_w^{(next)}$ stemming from the various corrections *within* the resonance approximation (16) and the contribution $\Delta E_t^{(next)}$ stemming from the corrections *to* the resonance approximation.

The former contribution may be estimated in a similar way to the case considered in [43]: it stems, in particular, from the deviation of the GSS curve from the separatrix (this deviation reaches δ at certain angles: see Eq. (7)) and from the difference between the exact resonance condition (20) and the approximate one (21). It can be shown that the absolute value of the ratio between $\Delta E_w^{(next)}$ and the leading term is logarithmically small (cf. [43]):

$$\frac{|\Delta E_w^{(next)}|}{\Delta E} \sim \frac{1}{\ln(1/h)}. \quad (74)$$

Let us turn to the analysis of the contribution $\Delta E_t^{(next)}$, i.e. the contribution stemming from the corrections to the resonance Hamiltonian (16). It is convenient to consider separately the cases of the left and right wings of the peak.

As described in Secs. 3.2 and 3.3 above, the left wing corresponds in the leading-order approximation to formation of the boundary of the layer by the *separatrix* of the resonance Hamiltonian (16). The resonance approximation (16) neglects time-periodic terms while the frequencies of oscillation of these terms greatly exceed the frequency of eigenoscillation of the resonance Hamiltonian (16) around its relevant elliptic point i.e. the elliptic point inside the area limited by the resonance separatrix. As is well known [18, 23, 29, 51, 52, 55], fast-oscillating terms acting on a system with a separatrix give rise to the onset of an *exponentially narrow* chaotic layer in place of the separatrix. In the present context, this means that the correction

to the maximal action \tilde{I} stemming from fast-oscillating corrections to the resonance Hamiltonian, i.e. $\Delta E_t^{(next)}$, is *exponentially small*, thus being negligible in comparison with the correction $\Delta E_w^{(next)}$ (see (74)).

The right wing, described in Secs. 3.2 and 3.3 above, corresponds in leading-order approximation to the formation of the boundary of the layer by the resonance trajectory *tangent* to the GSS curve. For the part of the right wing exponentially close in frequency to the frequency of the maximum, the tangent trajectory is close to the resonance separatrix, so that the correction stemming from fast-oscillating terms is exponentially small, similarly to the case of the left wing. As the frequency further deviates from the frequency of the maximum, the tangent trajectory further deviates from the resonance separatrix and the correction $\Delta E_t^{(next)}$ differs from the exponentially small correction estimated above. It may be estimated in the following way.

It follows from the second-order approximation of the averaging method [5] that the fast-oscillating terms lead, in the second-order approximation, to the onset of additional terms $h^2 T_{\tilde{I}}(\tilde{I}, \tilde{\psi})$ and $h^2 T_{\tilde{\psi}}(\tilde{I}, \tilde{\psi})$ in the dynamic equations for slow variables \tilde{I} and $\tilde{\psi}$ respectively, where $T_{\tilde{I}}(\tilde{I}, \tilde{\psi})$ and $T_{\tilde{\psi}}(\tilde{I}, \tilde{\psi})$ are of the order of the power-law-like function of $1/\ln(1/h)$ in the relevant range of \tilde{I} . The corresponding correction to the width of the chaotic layer in energy may be expressed as

$$\Delta E_t^{(next)} = \int_{t_{\min}}^{t_{\max}} dt h^2 T_{\tilde{I}} \omega(\tilde{I}), \quad (75)$$

where t_{\min} and t_{\max} are instants corresponding to the minimum and maximum deviation of the tangent trajectory from the separatrix of the unperturbed system (cf. Figs. 1(c) and 4(c)). The interval $t_{\max} - t_{\min}$ may be estimated as follows:

$$t_{\max} - t_{\min} \sim \frac{\pi}{|\langle \dot{\tilde{\psi}} \rangle|}, \quad (76)$$

where $\langle \dot{\tilde{\psi}} \rangle$ is the value of $\dot{\tilde{\psi}}$ averaged over the tangent trajectory. It follows from (16) that

$$|\langle \dot{\tilde{\psi}} \rangle| \sim \omega_f - \omega(E_s - \delta) \sim \frac{\omega(E_s - \delta)}{\ln(1/h)} \sim \frac{\omega_0}{\ln^2(1/h)}. \quad (77)$$

Taking together Eqs. (75)-(77) and allowing for the fact that $T_{\tilde{I}}$ is of the order of a power-law-like function of $1/\ln(1/h)$, we conclude that

$$\Delta E_t^{(next)} \sim h^2 P(\ln(1/h)), \quad (78)$$

where $P(x)$ is some power-law-like function.

The value $\Delta E_t^{(next)}$ is still asymptotically smaller than the absolute value of the correction within the resonance approximation, $|\Delta E_w^{(next)}|$, which is of the order of h or $h/\ln(1/h)$ for systems of type I or type II respectively.

Thus, we conclude that, both for the left and right wings of the peak, (i) the correction $\Delta E_t^{(next)}$ is determined by the correction within the resonance approximation

$\Delta E_w^{(next)}$, and (ii) in the asymptotic limit $h \rightarrow 0$, the overall next-order correction is negligible in comparison with the leading term:

$$\frac{|\Delta E^{(next)}|}{\Delta E} \equiv \frac{|\Delta E_w^{(next)} + \Delta E_t^{(next)}|}{\Delta E} \approx \frac{|\Delta E_w^{(next)}|}{\Delta E} \sim \frac{1}{\ln(1/h)} \xrightarrow{h \rightarrow 0} 0. \quad (79)$$

This estimate well agrees with results in Figs. 3-6.

3.5 Discussion

In this section, we briefly discuss the following issues: (i) the *scaled* asymptotic shape of the peaks; (ii) peaks in the range of *moderate* frequencies; (iii) *jumps* in the amplitude dependence of the layer width; and (iv) chaotic *transport*; (v) smaller peaks at *rational* frequencies; (vi) other separatrix maps; (vii) an application to the onset of *global chaos*.

1. Let us analyse the scaled asymptotic shape of the peaks. We consider first systems of type I. The peaks are then described in the leading-order approximation exclusively within separatrix map dynamics (approximated, in turn, by the NR dynamics). It follows from Eqs. (32), (34), (36), (39) and (40) that most of the peak for given j can be written in the universal scaled form:

$$\Delta E^{(j)}(\omega_f) = \Delta E_{\max}^{(j)} S \left(\frac{\pi(2j-1)}{(\omega_{\max}^{(j)})^2} (\omega_f - \omega_{\max}^{(j)}) \right), \quad (80)$$

where the universal function $S(\alpha)$ is strongly asymmetric:

$$S(\alpha) = \begin{cases} S_l(\alpha) & \text{for } \alpha \leq 0, \\ S_r(\alpha) & \text{for } \alpha > 0, \end{cases} \quad (81)$$

$$S_l(\alpha) = \frac{1}{e(\ln(1+y) - y/(1+y))}, \quad (1+y)\ln(1+y) - y = \exp(-\alpha),$$

$$S_r(\alpha) = \frac{1}{e(1 + \ln(1/z))}, \quad z(1 + \ln(1/z)) = \exp(-\alpha).$$

It is not difficult to show that

$$S_l(\alpha = 0) = 1, \quad S_r(\alpha \rightarrow +0) = e^{-1}, \quad (82)$$

$$\frac{dS_l(\alpha = 0)}{d\alpha} = 1 - e^{-1}, \quad \frac{dS_r(\alpha \rightarrow +0)}{d\alpha} \rightarrow -\infty,$$

$$S(\alpha \rightarrow \pm\infty) \propto \frac{1}{|\alpha|}.$$

Thus, the function $S(\alpha)$ is discontinuous at the maximum. To the left of the maximum, it approaches the far part of the wing (which decreases in a power-law-like way) relatively *slowly* while, to the right of the maximum, the function first drops *jump-wise* by a factor e and then *sharply* approaches the far part of the wing (which again decreases in a power-law-like way).

It follows from Eqs. (80), (81), (82) and (27) that the peaks are logarithmically narrow, i.e. the ratio of the half-width of the peak, $\Delta \omega^{(j)}$, to $\omega_{\max}^{(j)}$ is logarithmically small:

$$\frac{\Delta \omega^{(j)}}{\omega_{\max}^{(j)}} \sim \frac{1}{\ln(8(2j-1)/h)}. \quad (83)$$

We emphasize that the shape (81) is not restricted to the example (14): it is valid for any system of type I.

For systems of type II, contributions from the NR and from the variation of energy during the pulse of velocity, in relation to their h dependence, are formally of the same order but, numerically, the latter contribution is usually much smaller than the former. Thus, typically, the function (81) approximates well the properly scaled shape of the major part of the peak for systems of type II too.

2. The quantitative theory presented in the paper relates only to the peaks of *small* order n i.e. in the range of logarithmically small frequencies. At the same time, the magnitude of the peaks is still significant up to frequencies of order of one. This occurs because, for motion close to the separatrix, the order of magnitude of the Fourier coefficients remains the same up to logarithmically large numbers n . The shape of the peaks remains the same but their magnitude typically decreases (though in some cases, e.g. in case of the wave-like perturbation [23, 51, 52, 55] it may even increase in some range of frequencies). The quantitative description of this decrease, together with analyses of more sophisticated cases, requires a generalization of our theory.
3. Apart from the frequency dependence of the layer width, our theory is also relevant to amplitude dependence: it describes the jumps [40] in the dependence of the width on h and the transition between the jumps and the linear dependence. The values of h at which the jumps occur, $h_{\text{jump}}^{(j)}$, are determined by the same condition that determines $\omega_{\max}^{(j)}$ in the frequency dependence of the width. The formulæ relevant to the left wings of the peaks in the frequency dependence describe the ranges $h > h_{\text{jump}}^{(j)}$ while the formulæ relevant to the right wings describe the ranges $h < h_{\text{jump}}^{(j)}$.
4. Apart from the description of the boundaries, the approach allows us to describe *chaotic transport* within the layer. In particular, it allows us to describe quantitatively the effect of the stickiness of the chaotic trajectory to boundaries between the chaotic and regular areas of the phase space [51, 52]. Moreover, the presence of additional (resonance) saddles should give rise to an additional slowing down of the transport, despite a widening of the area of the phase space involved in the chaotic transport.

5. Our approach can be generalized in order to describe smaller peaks at non-integer rational frequencies i.e. $\omega_f \approx n/m\omega_r^{(\pm)}$ where n and m are integer numbers.
6. Apart from Hamiltonian systems of the one and a half degrees of freedom and corresponding Zaslavsky separatrix maps, our approach may be useful in the treatment of other chaotic systems and separatrix maps (see [29] for the most recent major review on various types of separatrix maps and related continuous chaotic systems).
7. Finally we note that, apart from systems with a separatrix, our work may be relevant to *nonlinear resonances* in any system. If the system is perturbed by a weak time-periodic perturbation, then nonlinear resonances arise and their dynamics is described by the model of the auxiliary time-periodically perturbed pendulum [10, 23, 55, 51, 52, 1, 18]. If the original perturbation has a single harmonic, then the effective perturbation of the auxiliary pendulum is necessarily a high-frequency one, and chaotic layers associated with the resonances are exponentially narrow [10, 23, 55, 51, 52, 1, 18] while our results are irrelevant. But, if either the amplitude or the angle of the original perturbation is slowly modulated, or if there is an additional harmonic of a slightly shifted frequency, then the effective perturbation of the auxiliary pendulum is a low-frequency one [43] and the layers become much wider⁸ while our theoretical approach becomes relevant. It may allow to find optimal parameters of the perturbation for the facilitation of the onset of global chaos associated with the overlap in energy between different-order nonlinear resonances [10]: the overlap may be expected to occur at a much smaller amplitude of perturbation in comparison with that one required for the overlap in case of a single-harmonic perturbation.

4 Double-separatrix chaos

There are many problems in physics where an unperturbed Hamiltonian model possesses two or more separatrices. A weak perturbation of the system typically destroys the separatrices, replacing them by thin chaotic layers. As the magnitude of the perturbation grows, the layers become wider and, at some critical value, they merge with each other: this may be described as the onset of *global chaos* between the separatrices. Such a connection of regions of different separatrices is important for transport in the system.

In the present section, following the paper [43], we consider the characteristic problem of the onset of global chaos between two close separatrices of a 1D Hamiltonian system perturbed by a time-periodic perturbation. As a characteristic example of a Hamiltonian system with two or more separatrices, we use a spatially periodic potential system with two different-height barriers per period (Fig. 7(a)):

⁸ This should not be confused with the widening occurring with the separatrix chaotic layer in the *original* pendulum if an originally single-harmonic perturbation of a high frequency is completed by one more harmonic of a slightly shifted frequency: see [47] and references therein.

$$H_0(p, q) = \frac{p^2}{2} + U(q), \quad U(q) = \frac{(\Phi - \sin(q))^2}{2}, \quad \Phi = \text{const} < 1. \quad (84)$$

This model may relate e.g. to a pendulum spinning about its vertical axis [3] or to a classical 2D electron gas in a magnetic field spatially periodic in one of the in-plane dimensions [49, 50]. Interest in the latter system arose in the 1990s due to technological advances allowing to manufacture magnetic superlattices of high-quality [6, 48], and thus leading to a variety of interesting behaviours of the charge carriers in semiconductors [49, 50, 6, 48, 36, 33].

Figs. 7(b) and 7(c) show respectively the separatrices of the Hamiltonian system (1) in the $p-q$ plane and the dependence of the frequency ω of its oscillation, often called its *eigenfrequency*, on its energy $E \equiv H_0(p, q)$. The separatrices correspond to energies equal to the value of the potential barrier tops $E_b^{(1)} \equiv (1 - \Phi)^2/2$ and $E_b^{(2)} \equiv (1 + \Phi)^2/2$ (Fig. 7(a)). The function $\omega(E)$ possesses a local maximum $\omega_m \equiv \omega(E_m)$. Moreover, $\omega(E)$ is close to ω_m for most of the range $[E_b^{(1)}, E_b^{(2)}]$ while sharply decreasing to zero as E approaches either $E_b^{(1)}$ or $E_b^{(2)}$.

We now consider the addition of a time-periodic perturbation: as an example, we use an AC drive, which corresponds to a dipole [55, 21] perturbation of the Hamiltonian:

$$\begin{aligned} \dot{q} &= \partial H / \partial p, & \dot{p} &= -\partial H / \partial q, \\ H(p, q) &= H_0(p, q) - hq \cos(\omega_f t). \end{aligned} \quad (85)$$

The *conventional* scenario for the onset of global chaos between the separatrices of the system (84)-(85) is illustrated by Fig. 8. The figure presents the evolution of

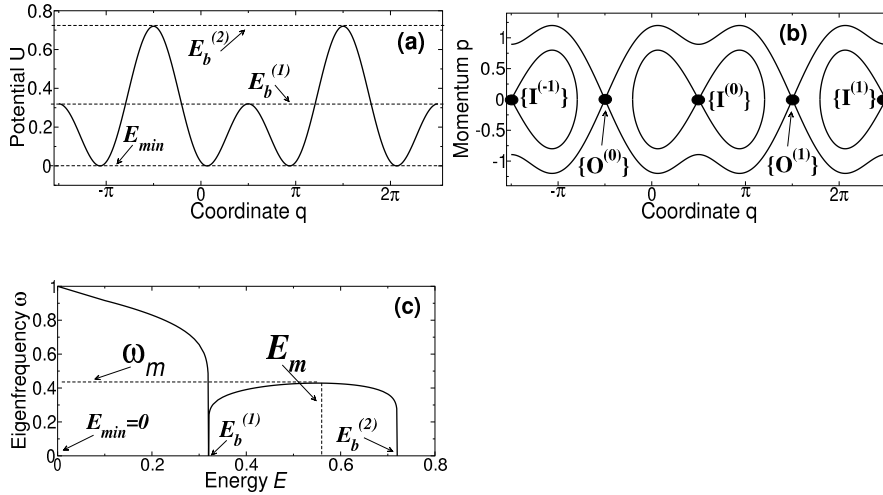
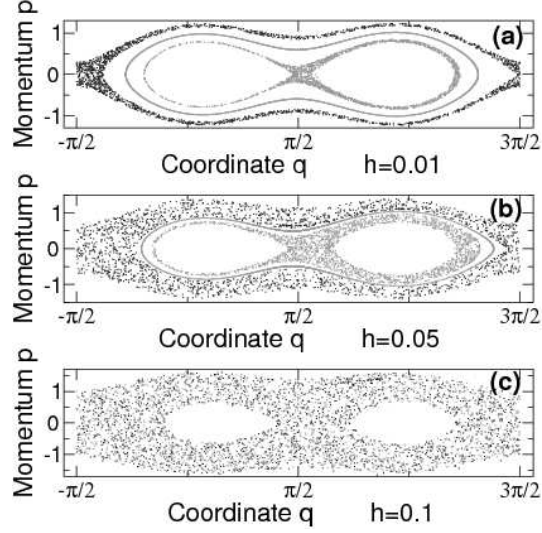


Fig. 7 The potential $U(q)$, the separatrices in the phase space, and the eigenfrequency $\omega(E)$ for the unperturbed system (84) with $\Phi = 0.2$, in (a), (b) and (c) respectively.

Fig. 8 The evolution of the stroboscopic (at $t = n2\pi/\omega_f$ with $n = 0, 1, 2, \dots$) Poincaré section of the system (84)-(85) with $\Phi = 0.2$ as h grows while $\omega_f = 0.3$. The number of points in each trajectory is 2000. In (a) and (b), three characteristic trajectories are shown: the inner trajectory starts from the state $\{I^{(0)}\} \equiv \{p = 0, q = \pi/2\}$ and is chaotic but bounded in space; the outer trajectory starts from $\{O^{(0)}\} \equiv \{p = 0, q = -\pi/2\}$ and is chaotic and unbounded in coordinate; the third trajectory is an example of a regular trajectory separating the two chaotic ones. In (c), the chaotic trajectories mix.



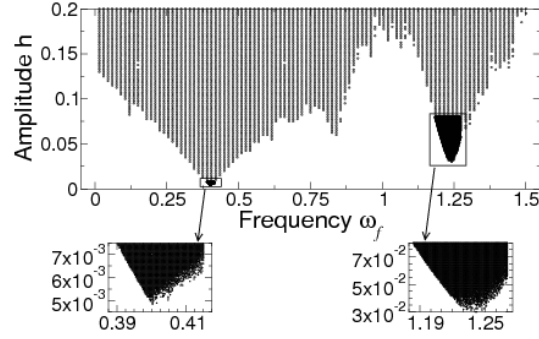
the stroboscopic Poincaré section as h grows while ω_f is fixed at an arbitrarily chosen value *away* from ω_m and its harmonics. At small h , there are two thin chaotic layers around the inner and outer separatrices of the unperturbed system. Unbounded chaotic transport takes place only in the outer chaotic layer i.e. in a *narrow* energy range. As h grows, so also do the layers. At some critical value $h_{gc} \equiv h_{gc}(\omega_f)$, the layers merge. This may be considered as the onset of global chaos: the whole range of energies between the barrier levels is involved, with unbounded chaotic transport. The states $\{I^{(l)}\} \equiv \{p = 0, q = \pi/2 + 2\pi l\}$ and $\{O^{(l)}\} \equiv \{p = 0, q = -\pi/2 + 2\pi l\}$ (where l is any integer) in the Poincaré section are associated respectively with the inner and outer saddles of the unperturbed system, and necessarily belong to the inner and outer chaotic layers, respectively. Thus, the necessary and sufficient condition for global chaos onset may be formulated as the possibility for the system placed initially in the state $\{I^{(0)}\}$ to pass beyond the neighbourhood of the “outer” states, $\{O^{(0)}\}$ or $\{O^{(1)}\}$, i.e. for the coordinate q to become $< -\pi/2$ or $> 3\pi/2$ at sufficiently large times $t \gg 2\pi/\omega_f$.

A diagram in the $h - \omega_f$ plane, based on the above criterion, is shown in Fig. 9. The lower boundary of the shaded area represents the function $h_{gc}(\omega_f)$. It has deep *spikes* i.e. cusp-like local minima. The most pronounced spikes are situated at frequencies $\omega_f = \omega_s^{(j)}$ that are slightly less than the odd multiples of ω_m ,

$$\omega_s^{(j)} \approx \omega_m(2j - 1), \quad j = 1, 2, \dots \quad (86)$$

The deepest minimum occurs at $\omega_s^{(1)} \approx \omega_m$: the value of h_{gc} at the minimum, $h_s^{(1)} \equiv h_{gc}(\omega_s^{(1)})$, is approximately 40 times smaller than the value in the neighbouring pronounced local maximum of $h_{gc}(\omega_f)$ at $\omega_f \approx 1$. As n increases, the n th minimum becomes shallower. The function $h_{gc}(\omega_f)$ is very sensitive to ω_f in the vicinity of

Fig. 9 Diagram indicating the range of perturbation parameters (shaded) for which global chaos exists. The integration time for each point of the grid is 12000π .



the minima: for example, a reduction of ω_f from $\omega_s^{(1)} \approx 0.4$ of only 1% causes an increase in h_{gc} of $\approx 30\%$.

The origin of the spikes is related to the involvement of the resonance dynamics in separatrix chaos, similar to that considered in Sec. 3. In particular, the minima of the spikes correspond to the situation when the resonances almost touch, or slightly overlap with, the separatrices of the unperturbed system while overlapping each other. This is illustrated by the evolution of the Poincaré section as h grows while $\omega_f \approx \omega_s^{(1)}$ (Fig. 10) and by its comparison with the corresponding evolution of resonance separatrices calculated in the resonance approximation (Fig. 11).

Sec. 4.1 below presents the self-consistent asymptotic theory of the minima of the spikes, based on an accurate analysis of the overlap of resonances with each other and on the matching between the separatrix map and the resonance Hamiltonian (details of the matching are developed in Appendix). Sec. 4.2 presents the theory of the wings of the spikes. Generalizations and applications are discussed in Sec. 4.3.

4.1 Asymptotic Theory For The Minima Of The Spikes

The eigenfrequency $\omega(E)$ stays close to its local maximum ω_m for most of the relevant range $[E_b^{(1)}, E_b^{(2)}]$ (Fig. 7(c)). As shown below, $\omega(E)$ approaches a *rectangular* form in the asymptotic limit $\Phi \rightarrow 0$. Hence, if the perturbation frequency ω_f is close to ω_m or its odd multiples, $|\omega_f - (2j-1)\omega_m| \ll \omega_m$, then the energy widths of nonlinear resonances become comparable to the width of the whole range between the barriers (i.e. $E_b^{(2)} - E_b^{(1)} \approx 2\Phi$) at a rather small perturbation magnitude $h \ll \Phi$. Note that Φ determines the characteristic magnitude of the perturbation required for the conventional overlap of the separatrix chaotic layers, when ω_f is not close to any odd multiple of ω_m (Fig. 8 (c)). Thus, if $\omega_f \approx \omega_s^{(j)}$, the nonlinear resonances should play a crucial role in the onset of global chaos (cf. Fig. 10).

We note that it is not entirely obvious *a priori* whether it is indeed possible to calculate $h_s^{(j)} \equiv h_{gc}(\omega_s^{(j)})$ within the resonance approximation: in fact, it is essential for the separatrices of the nonlinear resonances to nearly touch the barrier levels, but the

Fig. 10 (Color version may be found in the online version of [43] as Fig. 5). The evolution of the stroboscopic Poincaré section of the system (84)-(85) with $\Phi = 0.2$, as the amplitude h of the perturbation grows, while the frequency remains fixed at $\omega_f = 0.401$. The number of points in each trajectory is 2000. The chaotic trajectories starting from the states $\{I^{(0)}\}$ and $\{O^{(0)}\}$ are drawn in green and blue respectively. The stable stationary points of Eq. (98) for $n = 1$ (i.e. for the 1st-order nonlinear resonances) are indicated by the red and cyan crosses. The chaotic layers associated with the resonances are indicated in red and cyan respectively, unless they merge with those associated with the green/blue chaotic trajectories. Examples of regular trajectories embracing the state $\{I^{(0)}\}$ while separating various chaotic trajectories are shown in brown.

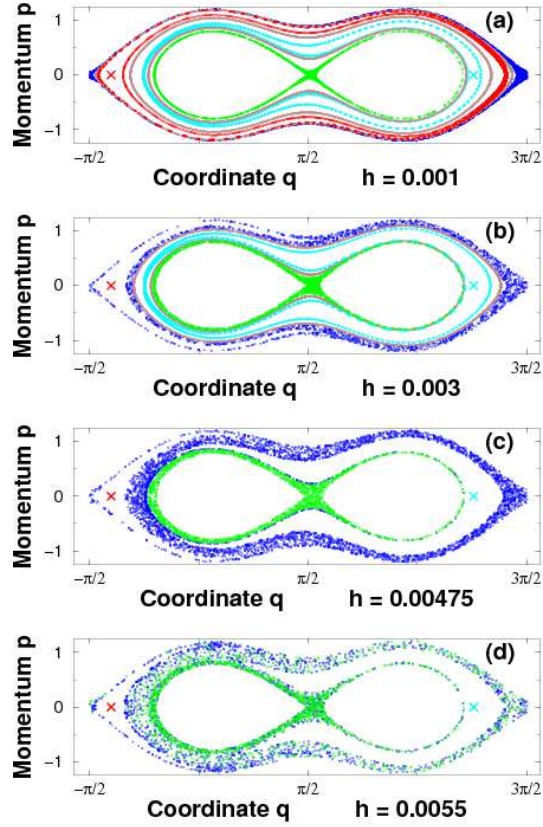
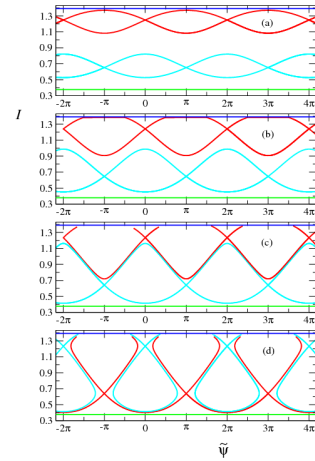


Fig. 11 (Color version may be found in the online version of [43] as Fig. 6). The evolution of the separatrices of the 1st-order resonances within the resonance approximation (described by (16) with $n = 1$) in the plane of action I and slow angle $\tilde{\psi}$, for the same parameters as in Fig. 10 (boxes (a), (b), (c), (d) correspond to those in Fig. 10). Horizontal levels mark the values of I corresponding to the barriers.



resonance approximation is invalid in the close vicinity of the barriers; furthermore, numerical calculations of resonances show that, if $\omega_f \approx \omega_s^{(j)}$, the perturbation amplitude h at which the resonance separatrix touches a given energy level in the close vicinity of the barriers is very sensitive to ω_f , apparently making the calculation of $h_s^{(j)}$ within the resonance approximation even more difficult.

Nevertheless, we show below in a self-consistent manner that, in the asymptotic limit $\Phi \rightarrow 0$, the relevant boundaries of the chaotic layers lie in the range of energies E where $\omega(E) \approx \omega_m$. Therefore, the resonant approximation is valid and it allows us to obtain *explicit* asymptotic expressions both for $\omega_s^{(j)}$ and $h_s^{(j)}$, and for the wings of the spikes in the vicinities of $\omega_s^{(j)}$.

The *asymptotic* limit $\Phi \rightarrow 0$ is the most interesting one from a theoretical point of view because it leads to the strongest facilitation of the onset of global chaos, and it is most accurately described by the self-contained theory. Most of the theory presented below assumes this limit and concentrates therefore on the results to the *lowest* (i.e. leading) order in the small parameter.

On the applications side, the range of *moderately small* Φ is more interesting, since the chaos facilitation is still pronounced (and still described by the asymptotic theory) while the area of chaos between the separatrices is not too small (comparable with the area inside the inner separatrix): cf. Figs. 7, 8 and 10. To increase the accuracy of the theoretical description in this range, we estimate the next-order corrections and develop an efficient numerical procedure allowing for further corrections.

4.1.1 Resonant Hamiltonian and related quantities

Let ω_f be close to the n th odd⁹ harmonic of ω_m , $n \equiv (2j - 1)$. Over most of the range $[E_b^{(1)}, E_b^{(2)}]$, except in the close vicinities of $E_b^{(1)}$ and $E_b^{(2)}$, the n th harmonic of the eigenoscillation is nearly resonant with the perturbation. Due to this, the (slow) dynamics of the action $I \equiv I(E) = (2\pi)^{-1} \oint dq p$ and the angle ψ [10, 23, 55, 51, 52, 41, 21] can be described by means of a resonance Hamiltonian similar in form to (16). The lower integration limit in the expression for \tilde{H} may be chosen arbitrarily, and it will be convenient for us to use presently $I(E_m)$ (instead of $I(E_s)$ in (16)) where E_m is the energy of the local maximum of $\omega(E)$ (Fig. 7(c)). To avoid confusion, we write the resonance Hamiltonian explicitly below after making this change:

$$\begin{aligned} \tilde{H}(I, \tilde{\psi}) &= \int_{I(E_m)}^I d\tilde{I} (n\omega - \omega_f) - nhq_n \cos(\tilde{\psi}) \\ &\equiv n(E - E_m) - \omega_f(I - I(E_m)) - nhq_n \cos(\tilde{\psi}), \end{aligned} \quad (87)$$

⁹ Even harmonics are absent in the eigenoscillation due to the symmetry of the potential.

$$\begin{aligned}
I \equiv I(E) &= \int_{E_{\min}}^E \frac{d\tilde{E}}{\omega(\tilde{E})}, & E &\equiv H_0(p, q), \\
\tilde{\psi} &= n\psi - \omega_f t, \\
\psi &= \pi + \text{sign}(p)\omega(E) \int_{q_{\min}(E)}^q \frac{d\tilde{q}}{\sqrt{2(E-U(\tilde{q}))}} + 2\pi l, \\
q_n \equiv q_n(E) &= \frac{2}{\pi} \int_0^{\pi/2} d\psi q(E, \psi) \cos(n\psi), \\
|n\omega - \omega_f| &\ll \omega, & n &\equiv 2j - 1, & j &= 1, 2, 3, \dots
\end{aligned}$$

Let us derive explicit expressions for various quantities in (87). In the unperturbed case ($h = 0$), the equations of motion (85) with H_0 (84) can be integrated [50] (see also Eq. (144) below), so that we can find $\omega(E)$:

$$\omega(E) = \frac{\pi(2E)^{1/4}}{2K[k]}, \quad k = \frac{1}{2} \sqrt{\frac{(\sqrt{2E} + 1)^2 - \Phi^2}{\sqrt{2E}}}, \quad (88)$$

where

$$K[k] = \int_0^{\frac{\pi}{2}} \frac{d\phi}{\sqrt{1 - k^2 \sin^2(\phi)}},$$

is the complete elliptic integral of first order [2]. Using its asymptotic expression,

$$K[k \rightarrow 1] \simeq \frac{1}{2} \ln \left(\frac{16}{1 - k^2} \right),$$

we derive $\omega(E)$ in the asymptotic limit $\Phi \rightarrow 0$:

$$\begin{aligned}
\omega(E) &\simeq \frac{\pi}{\ln \left(\frac{64}{(\Phi - \Delta E)(\Phi + \Delta E)} \right)}, & (89) \\
\Delta E &\equiv E - \frac{1}{2}, & |\Delta E| < \Phi, & \Phi \rightarrow 0.
\end{aligned}$$

As mentioned above, the function $\omega(E)$ (89) remains close to its maximum

$$\omega_m \equiv \max_{[E_b^{(1)}, E_b^{(2)}]} \{\omega(E)\} \simeq \frac{\pi}{2 \ln(8/\Phi)} \quad (90)$$

for most of the interbarrier range of energies $[1/2 - \Phi, 1/2 + \Phi]$ (note that $E_b^{(1,2)} \approx 1/2 \mp \Phi$ to first order in Φ); on the other hand, in the close vicinity of the barriers, where either $|\ln(1/(1 - \Delta E/\Phi))|$ or $|\ln(1/(1 + \Delta E/\Phi))|$ become comparable with, or larger than, $\ln(8/\Phi)$, $\omega(E)$ decreases rapidly to zero as $|\Delta E| \rightarrow \Phi$. The range where this takes place is $\sim \Phi^2$, and its ratio to the whole interbarrier range, 2Φ , is $\sim \Phi$ i.e. it goes to zero in the asymptotic limit $\Phi \rightarrow 0$: in other words, $\omega(E)$

approaches a *rectangular* form. As it will be clear from the following, *it is this almost rectangular form of $\omega(E)$ which determines many of the characteristic features of the global chaos onset in systems with two or more separatrices.*

One more quantity which strongly affects (ω_s, h_s) is the Fourier harmonic $q_n \equiv q_n(E)$. The system stays most of the time very close to one of the barriers. Consider the motion within one of the periods of the potential $U(q)$, between neighboring upper barriers $[q_{ub}^{(1)}, q_{ub}^{(2)}]$ where $q_{ub}^{(2)} \equiv q_{ub}^{(1)} + 2\pi$. If the energy $E \equiv 1/2 + \Delta E$ lies in the relevant range $[E_b^{(1)}, E_b^{(2)}]$, then the system will stay close to the lower barrier $q_{lb} \equiv q_{ub}^{(1)} + \pi$ for a time¹⁰

$$T_l \approx 2 \ln \left(\frac{1}{\Phi + \Delta E} \right) \quad (91)$$

during each period of eigenoscillation, while it will stay close to one of the upper barriers $q_{ub}^{(1,2)} \equiv q_{lb} \pm \pi$ for most of the remainder of the eigenoscillation,

$$T_u \approx 2 \ln \left(\frac{1}{\Phi - \Delta E} \right) \quad . \quad (92)$$

Hence, the function $q(E, \psi) - q_{lb}$ may be approximated by the following piecewise even periodic function:

$$q(E, \psi) - q_{lb} = \begin{cases} \pi & \text{at } \psi \in [0, \frac{\pi}{2} \frac{T_u}{T_l + T_u}] \cup [\pi - \frac{\pi}{2} \frac{T_u}{T_l + T_u}, \pi], \\ 0 & \text{at } \psi \in]\frac{\pi}{2} \frac{T_u}{T_l + T_u}, \pi - \frac{\pi}{2} \frac{T_u}{T_l + T_u}[, \end{cases} \quad (93)$$

$$q(E, -\psi) - q_{lb} = q(E, \psi) - q_{lb}, \quad q(E, \psi \pm 2\pi i) = q(E, \psi), \quad i = 1, 2, 3, \dots$$

Substituting the above approximation for $q(E, \psi)$ into the definition of q_n (87), one can obtain:

$$q_{2j-1} \equiv q_{2j-1}(E) = \frac{2}{2j-1} \sin \left(\frac{(2j-1)\pi/2}{1 + \frac{\ln(\frac{1}{\Phi + \Delta E})}{\ln(\frac{1}{\Phi - \Delta E})}} \right), \quad (94)$$

$$\Phi \rightarrow 0, \quad q_{2j} = 0, \quad j = 1, 2, 3, \dots$$

At barrier energies, q_{2j-1} takes the values

$$q_{2j-1}(E_b^{(1)}) = 0, \quad q_{2j-1}(E_b^{(2)}) = -(-1)^j \frac{2}{(2j-1)}. \quad (95)$$

As E varies in between its values at the barriers, q_{2j-1} varies monotonically if $j = 1$ and non-monotonically otherwise (cf. Fig. 16). But in any case, the significant

¹⁰ We omit corrections $\sim (\ln(1/\Phi))^{-1}$ here and in Eq. (92) since they vanish in the asymptotic limit $\Phi \rightarrow 0$.

variations occur mostly in the close vicinity of the barrier energies $E_b^{(1)}$ and $E_b^{(2)}$ while, for most of the range $[E_b^{(1)}, E_b^{(2)}]$, the argument of the sine in Eq. (94) is close to $\pi/4$ and q_{2j-1} is then almost constant:

$$q_{2j-1} \approx (-1)^{\lfloor \frac{2j-1}{4} \rfloor} \frac{\sqrt{2}}{2j-1}, \quad j = 1, 2, 3, \dots, \quad (96)$$

$$\left| \ln \left(\frac{1 + \Delta E / \Phi}{1 - \Delta E / \Phi} \right) \right| \ll 2 \ln \left(\frac{1}{\Phi} \right),$$

where $\lfloor \dots \rfloor$ means the integer part.

In the asymptotic limit $\Phi \rightarrow 0$, the range of ΔE for which the approximate equality (96) for q_{2j-1} is valid approaches the whole range $]-\Phi, \Phi[$.

We emphasize that $|q_n|$ determines the “strength” of the nonlinear resonances: therefore, apart from the nearly rectangular form of $\omega(E)$, the non-smallness of $|q_n|$ is an important additional factor strongly facilitating the onset of global chaos.

We shall need also an asymptotic expression for the action I . Substituting $\omega(E)$ (89) into the definition of $I(E)$ (87) and carrying out the integration, we obtain

$$I(E) = I(1/2) + \frac{\Delta E \ln \left(\frac{64e^2}{\Phi^2 - (\Delta E)^2} \right) + \Phi \ln \left(\frac{\Phi - \Delta E}{\Phi + \Delta E} \right)}{\pi}, \quad \Phi \rightarrow 0. \quad (97)$$

4.1.2 Reconnection of resonance separatrices

We now turn to analysis of the *phase space* of the resonance Hamiltonian (87). The evolution of the Poincaré section (Fig. 10) suggests that we need to find a *separatrix* of (87) that undergoes the following evolution as h grows: for sufficiently small h , the separatrix does not overlap chaotic layers associated with the barriers while, for $h > h_{gc}(\omega_f)$, it does overlap them. The relevance of such a condition will be further justified.

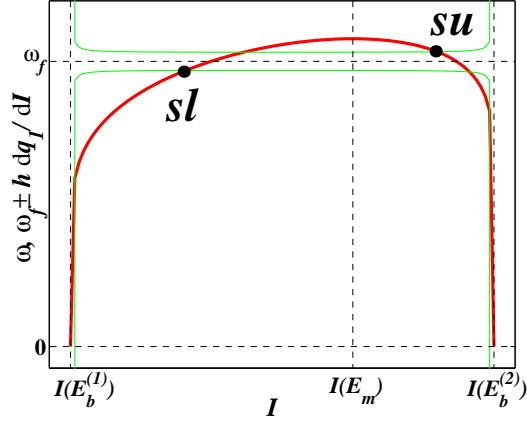
Consider $\omega_f \approx n\omega_m$ with a given odd n . For the sake of convenience, let us write down the equations of motion (87) explicitly:

$$\dot{I} = -\frac{\partial \tilde{H}}{\partial \tilde{\psi}} \equiv -nhq_n \sin(\tilde{\psi}), \quad \dot{\tilde{\psi}} = \frac{\partial \tilde{H}}{\partial I} \equiv n\omega - \omega_f - nh \frac{dq_n}{dI} \cos(\tilde{\psi}). \quad (98)$$

Any separatrix necessarily includes one or more unstable stationary points. The system of dynamic equations (98) may have several stationary points per 2π interval of $\tilde{\psi}$. Let us first exclude those points which are irrelevant to a separatrix undergoing the evolution described above.

Given that $q_n(E_b^{(1)}) = 0$, there are two unstable stationary points with I corresponding to $E = E_b^{(1)}$ and $\tilde{\psi} = \pm\pi/2$. They are irrelevant because, even for an

Fig. 12 (Color version may be found in the online version of [43] as Fig. 7). A schematic example illustrating the graphical solutions of Eqs. (99) for $n = 1$, as intersections of the curve $\omega(I)$ (thick solid red line) with the curves $\omega_f \pm h dq_n(I)/dI$ (thin solid green lines). The solutions corresponding to the lower and upper relevant saddles (defined by Eq. (100)) are marked by dots and by the labels sl and su respectively (we do not mark other solutions because they are irrelevant).



infinitely small h , each of them necessarily lies inside the corresponding barrier chaotic layer.

If $E \neq E_b^{(1)}$, then $q_n \neq 0$, so $\dot{I} = 0$ only if $\tilde{\psi}$ is equal either to 0 or to π . Substituting these values into the second equation of (98) and putting $\tilde{\psi} = 0$, we obtain the equations for the corresponding actions:

$$X_{\mp}(I) \equiv n\omega - \omega_f \mp nhdq_n/dI = 0, \quad (99)$$

where the signs “-” and “+” correspond to $\tilde{\psi} = 0$ and $\tilde{\psi} = \pi$ respectively. A typical example of the graphical solution of equations (99) for $n = 1$ is shown in Fig. 12. Two of the roots corresponding to $\tilde{\psi} = \pi$ are very close to the barrier values of I (recall that the relevant values of h are small). These roots arise due to the divergence of dq/dI as I approaches any of the barrier values. The lower/upper root corresponds to a stable/unstable point, respectively. However, for any n , both these points and the separatrix generated by the unstable point necessarily lie in the ranges covered by the barrier chaotic layers. Therefore, they are also irrelevant¹¹. For $n > 1$, the number of roots of (99) in the vicinity of the barriers may be larger (due to oscillations of the modulus and sign of dq_n/dI in the vicinity of the barriers) but they all are irrelevant for the same reason, at least to leading-order terms in the expressions for the spikes’ minima.

Consider the stationary points corresponding to the remaining four roots of equations (99). Just these points are conventionally associated with *nonlinear resonances* [10, 23, 55, 51, 52, 41]. It follows from the analysis of equations (98) linearized near the stationary points (cf. [10, 23, 55, 51, 52, 41]), two of them are stable (elliptic)

¹¹ For sufficiently small Φ and h , the separatrix generated by the unstable point forms the boundary of the upper chaotic layer, but this affects only the higher-order terms in the expressions for the spikes minima (see below).

points¹², while two others are unstable (hyperbolic) points, often called *saddles*. These saddles are of central interest in the context of our work. They belong to the *separatrices* dividing the $I - \tilde{\psi}$ plane for regions with topologically different trajectories.

We shall identify the relevant saddles as those with the *lower* action/energy (using the subscript “*sl*”) and *upper* action/energy (using the subscript “*su*”). The positions of the saddles in the $I - \tilde{\psi}$ plane are defined by the following equations (cf. Figs. 11 and 12):

$$\begin{aligned} g &\equiv \text{sgn}(q_n(I_{su,sl})) = \text{sgn}\left((-1)^{\lfloor \frac{n}{4} \rfloor}\right), \\ \tilde{\psi}_{sl} &= \pi(1+g)/2, \quad \tilde{\psi}_{su} = \pi(1-g)/2, \\ X_g(I_{sl}) &= X_{-g}(I_{su}) = 0, \quad \frac{dX_g(I_{sl})}{dI_{sl}} > 0, \quad \frac{dX_{-g}(I_{su})}{dI_{su}} < 0, \end{aligned} \quad (100)$$

where [...] means an integer part, $X_{\pm}(I)$ are defined in Eq. (99) while I_{sl} and I_{su} are closer to $I(E_m)$ than any other solution of (100) (if any) from below and from above, respectively.

Given that the values of h relevant to the minima of the spikes asymptotically approach 0 in the asymptotic limit $\Phi \rightarrow 0$, one may neglect the last term in the definition of X_{\mp} in Eq. (99) in the lowest-order approximation¹³, so that the equations $X_{\mp} = 0$ reduce to the simplified resonance condition

$$n\omega(I_{su,sl}) = \omega_f. \quad (101)$$

Substituting here Eq. (89) for ω , we obtain explicit expressions for the energies in the saddles:

$$\begin{aligned} E_{su,sl} &\approx \frac{1}{2} \pm \Delta E^{(1)}, \\ \Delta E^{(1)} &\equiv \sqrt{\Phi^2 - 64 \exp\left(-\frac{n\pi}{\omega_f}\right)}, \quad \omega_f \leq n\omega_m. \end{aligned} \quad (102)$$

The corresponding actions $I_{su,sl}$ are expressed via $E_{su,sl}$ by means of Eq. (97).

For $\omega_f \approx n\omega_m$, the values of $E_{su,sl}$ (102) lie in the range where the expression (96) for q_n holds true. This will be confirmed by the results of calculations based on this assumption.

Using (100) for the angles and (102) for the energies, and the asymptotic expressions (89), (96) and (97) for $\omega(E)$, $q_n(E)$ and $I(E)$ respectively, and allowing for

¹² In the Poincaré sections shown in Fig. 10, the points which correspond to such stable points of equations (98) are indicated by the crosses.

¹³ As will become clear in what follows, the remaining terms are much larger in the asymptotic limit than the neglected term: cf. the standard theory of the nonlinear resonance [10, 23, 51, 52, 55].

the resonance condition (101), we obtain explicit expressions for the values of the Hamiltonian (87) at the saddles:

$$\tilde{H}_{sl} = -\tilde{H}_{su} = \frac{\omega_f}{\pi} \left[2\Delta E^{(1)} - \Phi \ln \left(\frac{\Phi + \Delta E^{(1)}}{\Phi - \Delta E^{(1)}} \right) \right] + h\sqrt{2}. \quad (103)$$

As the analysis of simulations suggests and as it is self-consistently shown further, one of the main conditions which should be satisfied in the spikes is the overlap in phase space between the separatrices of the nonlinear resonances, which is known as *separatrix reconnection* [41, 19, 20, 11, 12, 26]. Given that the Hamiltonian \tilde{H} is constant along any trajectory of the system (87), the values of \tilde{H} in the lower and upper saddles of the *reconnected* separatrices are equal to each other:

$$\tilde{H}_{sl} = \tilde{H}_{su}. \quad (104)$$

This may be considered as the necessary and sufficient¹⁴ condition for the reconnection. Taking into account that $\tilde{H}_{sl} = -\tilde{H}_{su}$ (see (103)), it follows from (104) that

$$\tilde{H}_{sl} = \tilde{H}_{su} = 0. \quad (105)$$

Explicitly, the relations in (105) reduce to

$$h \equiv h(\omega_f) = \frac{\omega_f}{\sqrt{2}\pi} \left[\Phi \ln \left(\frac{\Phi + \Delta E^{(1)}}{\Phi - \Delta E^{(1)}} \right) - 2\Delta E^{(1)} \right], \quad (106)$$

$$\Delta E^{(1)} \equiv \sqrt{\Phi^2 - 64 \exp\left(-\frac{n\pi}{\omega_f}\right)}, \quad 0 < \omega_m - \omega_f/n \ll \omega_m \equiv \frac{\pi}{2 \ln(8/\Phi)},$$

$$n = 1, 3, 5, \dots$$

The function $h(\omega_f)$ (106) decreases monotonically to zero as ω_f grows from 0 to $n\omega_m$, where the line abruptly stops. Fig. 15 shows the portions of the lines (106) relevant to the left wings of the 1st and 2nd spikes (for $\Phi = 0.2$).

4.1.3 Barrier chaotic layers

The next step is to find the minimum value of h for which the resonance separatrix overlaps the chaotic layer related to a potential barrier. With this aim, we study how the relevant outer boundary of the chaotic layer behaves as h and ω_f vary. Assume that the relevant ω_f is close to $n\omega_m$ while the relevant h is sufficiently large for $\omega(E)$ to be close to ω_m at all points of the outer boundary of the layer (the results will confirm these assumptions). Then the motion along the regular trajectory

¹⁴ Eq. (104) is the *sufficient* (rather than just necessary) condition for separatrix reconnection since there is no any other separatrix which would lie in between the separatrices generated by the saddles “sl” and “su”.

infinitesimally close to the layer boundary may be described within the resonance approximation (87). Hence the boundary may also be described as a trajectory of the resonant Hamiltonian (87). This is explicitly proved in the Appendix, using a separatrix map analysis allowing for the validity of the relation $\omega(E) \approx \omega_m$ for all E relevant to the boundary of the chaotic layer. The main results are presented below. For the sake of clarity, we present them for each layer separately, although they are similar in practice.

4.1.3.1 Lower Layer

Let ω_f be close to any of the spikes' minima.

One of the key roles in the formation of the upper boundary of the layer is played by the angle-dependent quantity $\delta_l |\sin(\tilde{\psi})|$ which we call the *generalized separatrix split* (GSS) for the lower layer, alluding to the conventional *separatrix split* [51] for the lower layer $\delta_l \equiv |\varepsilon^{(low)}(\omega_f)|h$ with $\varepsilon^{(low)}$ given by Eq. (172)¹⁵ (cf. also (4)). Accordingly, we use the term ‘‘lower GSS curve’’ for the following curve in the $I - \tilde{\psi}$ plane:

$$I = I_{\text{GSS}}^{(l)}(\tilde{\psi}) \equiv I(E_b^{(1)} + \delta_l |\sin(\tilde{\psi})|). \quad (107)$$

4.1.3.1.1 Relatively Small Values Of h

If $h < h_{cr}^{(l)}(\omega_f)$, where the critical value $h_{cr}^{(l)}(\omega_f)$ is determined by Eq. (125) (its origin will be explained further), then there are differences in the boundary formation for the frequency ranges of *odd* and *even* spikes. We describe these ranges separately.

1. Odd spikes

In this case, the boundary is formed by the trajectory of the Hamiltonian (87) *tangent* to the GSS curve (see Fig. 22(a); cf. also Figs. 1(c), 13(a), 14(b), 14(c)). There are two tangencies in the angular range $]-\pi, \pi[$: they occur at the angles $\pm \tilde{\psi}_t^{(l)}$ where $\tilde{\psi}_t^{(l)}$ is determined by Eq. (182).

In the ranges of h and ω_f relevant to the spike minimum, the asymptotic expressions for δ_l and $\tilde{\psi}_t^{(l)}$ are:

$$\delta_l = \sqrt{2}\pi h, \quad (108)$$

$$\tilde{\psi}_t^{(l)} = (-1)^{\lfloor \frac{n}{4} \rfloor} \sqrt{\frac{n\pi}{8 \ln(1/\Phi)}} + \pi \frac{1 - (-1)^{\lfloor \frac{n}{4} \rfloor}}{2}. \quad (109)$$

¹⁵ The quantity δ_l may also be interpreted as the magnitude of the corresponding Melnikov integral [10, 23, 55, 51, 52], sometimes called as the Poincaré-Melnikov integral [29].

Hence, the asymptotic value for the deviation of the tangency energy $E_t^{(l)}$ from the lower barrier reduces to:

$$E_t^{(l)} - E_b^{(1)} \equiv \delta_l \sin(\tilde{\psi}_t^{(l)}) = \frac{\pi^{3/2}}{2} \frac{h}{\sqrt{\ln(1/\Phi)/n}}. \quad (110)$$

The minimum energy on the boundary, $E_{\min}^{(l)}$, corresponds to $\tilde{\psi} = 0$ or π for even or odd values of $[n/4]$ respectively. Thus, it can be found from the equality

$$\tilde{H} \left(I(E_{\min}^{(l)}), \tilde{\psi} = \pi(1 - (-1)^{[n/4]})/2 \right) = \tilde{H} \left(I_t^{(l)} \equiv I(E_t^{(l)}), \tilde{\psi}_t^{(l)} \right). \quad (111)$$

At $\Phi \rightarrow 0$, Eq. (111) yields the following expression for the minimal deviation of energy on the boundary from the barrier:

$$\delta_{\min}^{(l)} \equiv E_{\min}^{(l)} - E_b^{(1)} = (E_t^{(l)} - E_b^{(1)})/\sqrt{e} = \frac{\pi^{3/2}}{2\sqrt{e}} \frac{h}{\sqrt{\ln(1/\Phi)/n}}. \quad (112)$$

In the context of the onset of global chaos, the most important property of the boundary is that the *maximum* deviation of its energy from the barrier, $\delta_{\max}^{(l)}$, should greatly exceed both $\delta_{\min}^{(l)}$ and δ_l . As $h \rightarrow h_{cr}^{(l)}$, the maximum of the boundary approaches the saddle “ sl ”.

2. Even spikes

In this case, the Hamiltonian (87) possesses saddles “ s ” in the close vicinity to the lower barrier (see Fig. 22(b)). Their angles differ by π from those of “ sl ”:

$$\tilde{\psi}_s = \pi \frac{1 - (-1)^{[n/4]}}{2} + 2\pi m, \quad m = 0, \pm 1, \pm 2, \dots, \quad (113)$$

while the deviation of their energies from the barrier still lies in the relevant (resonant) range and reads, in the lowest-order approximation,

$$\delta_s = \frac{\pi}{2\sqrt{2}} \frac{h}{\ln(\ln(1/\Phi))}. \quad (114)$$

The lower whiskers of the separatrix generated by these saddles intersect the GSS curve while the upper whiskers in the asymptotic limit do not intersect it (Fig. 22(b)). Thus, it is the upper whiskers of the separatrix which form the boundary of the chaotic layer in the asymptotic limit. The energy on the boundary takes the minimal value right on the saddle “ s ”, so that

$$\delta_{\min}^{(l)} = \delta_s = \frac{\pi}{2\sqrt{2}} \frac{h}{\ln(\ln(1/\Phi))}. \quad (115)$$

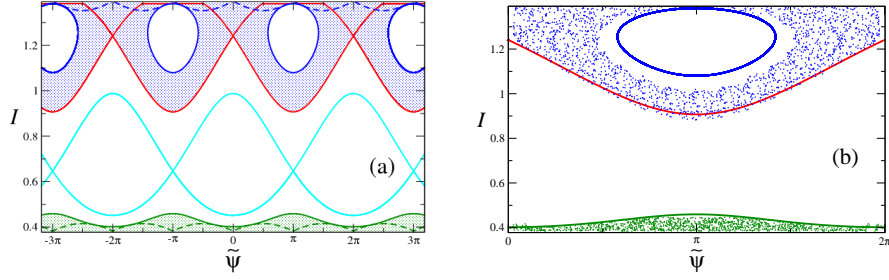


Fig. 13 (Color version may be found in the online version of [43] as Fig. 8). (a) Chaotic layers (shaded in green and blue, for the upper and lower layers respectively) in the plane of action I and slow angle $\tilde{\psi}$, as described by our theory. Parameters are the same as in Figs. 10(b) and 11(b). The lower and upper boundaries of the figure box coincide with $I(E_b^{(1)})$ and $I(E_b^{(2)})$ respectively. The resonance separatrices are drawn by the cyan and red solid lines (for the lower and upper resonances respectively). Dashed green and blue lines mark the curves $I = I_{\text{GSS}}^{(l)}(\tilde{\psi}) \equiv I(E = E_b^{(1)} + \delta_l |\sin(\tilde{\psi})|)$ and $I = I_{\text{GSS}}^{(u)}(\tilde{\psi}) \equiv I(E = E_b^{(2)} - \delta_u |\sin(\tilde{\psi})|)$ respectively, where δ_l and δ_u are the values of the separatrix split related to the lower and upper barrier respectively. The upper boundary of the lower layer is formed by the trajectory of the resonant Hamiltonian system (87) tangent to the curve $I = I_{\text{GSS}}^{(l)}(\tilde{\psi})$. The lower boundary of the upper layer is formed by the lower part of the upper (red) resonance separatrix. The periodic closed loops (solid blue lines) are the trajectories of the system (87) tangent to the curve $I_{\text{GSS}}^{(u)}(\tilde{\psi})$: they form the boundaries of the major stability islands inside the upper chaotic layer. (b) Comparison of the chaotic layers obtained from computer simulations (dots) with the theoretically calculated boundaries (solid lines) shown in the box (a).

Similar to the case of the odd spikes, the *maximal* deviation of the energy from the barrier (measured along the boundary) greatly exceeds both $\delta_{\min}^{(l)}$ and δ_l . As $h \rightarrow h_{cr}^{(l)}$, the maximum of the boundary approaches the saddle “ sl ”.

4.1.3.1.2 Relatively Large Values Of h

If $h > h_{cr}^{(l)}(\omega_f)$, the previously described trajectory (either the tangent one or the separatrix, for the odd or even spike ranges respectively) is encompassed by the separatrix of the lower nonlinear resonance and typically forms the boundary of a major stability island inside the lower layer (reproduced periodically in $\tilde{\psi}$ with the period 2π). The upper *outer* boundary of the layer is formed by the upper part of the *resonance separatrix*. This may be interpreted as the absorption of the lower resonance by the lower chaotic layer.

4.1.3.2 Upper Layer

Let ω_f be close to any of the spikes’ minima.

One of the key roles in the formation of the lower boundary of the layer is played by the angle-dependent quantity $\delta_u |\sin(\tilde{\psi})|$ which we call the *generalized separatrix split* (GSS) for the upper layer; δ_u is the separatrix split for the upper layer:

$\delta_u = |\varepsilon^{(up)}(\omega_f)|h$ with $\varepsilon^{(up)}$ given by Eq. (204). Accordingly, we use the term ‘‘upper GSS curve’’ for the following curve in the $I - \tilde{\psi}$ plane:

$$I = I_{\text{GSS}}^{(u)}(\tilde{\psi}) \equiv I(E_b^{(2)} - \delta_u |\sin(\tilde{\psi})|). \quad (116)$$

4.1.3.2.1 Relatively Small Values Of h

If $h < h_{cr}^{(u)}(\omega_f)$, where the critical value $h_{cr}^{(u)}(\omega_f)$ is determined by Eq. (126) (its origin will be explained further), then there are some differences in the boundary formation in the frequency ranges of *odd* and *even* spikes: for odd spikes, the formation is similar to the one for even spikes in the lower-layer case and vice versa.

1. Odd spikes

In the case of odd spikes, the Hamiltonian (87) possesses saddles ‘‘ \tilde{s} ’’ in the close vicinity of the upper barrier, analogous to the saddles ‘‘ s ’’ near the lower barrier in the case of even spikes. Their angles are shifted by π from those of ‘‘ s ’’:

$$\tilde{\psi}_{\tilde{s}} = \tilde{\psi}_s + \pi = \pi \frac{1 + (-1)^{\lfloor \frac{q}{4} \rfloor}}{2} + 2\pi m, \quad m = 0, \pm 1, \pm 2, \dots \quad (117)$$

The deviation of their energies from the upper barrier coincides, in the lowest-order approximation, with $\delta_{\tilde{s}}$:

$$\delta_{\tilde{s}} = \delta_s = \frac{\pi}{2\sqrt{2}} \frac{h}{\ln(\ln(1/\Phi))}. \quad (118)$$

The upper whiskers of the separatrix generated by these saddles intersect the upper GSS curve while the lower whiskers in the asymptotic limit do not intersect it. Thus, it is the lower whiskers of the separatrix which form the boundary of the chaotic layer in the asymptotic limit. The deviation of the energy from the upper barrier takes its minimal value (measured along the boundary) right on the saddle ‘‘ \tilde{s} ’’,

$$\delta_{\min}^{(u)} = \delta_{\tilde{s}} = \frac{\pi}{2\sqrt{2}} \frac{h}{\ln(\ln(1/\Phi))}. \quad (119)$$

The *maximal* deviation of the energy from the barrier (along the boundary) greatly exceeds both $\delta_{\min}^{(u)}$ and δ_u . As $h \rightarrow h_{cr}^{(u)}$, the maximum of the boundary approaches the saddle ‘‘ su ’’.

2. Even spikes

The boundary is formed by the trajectory of the Hamiltonian (87) *tangent* to the GSS curve. There are two tangencies in the angle range $]-\pi, \pi[$: they occur at the angles $\pm \tilde{\psi}_t^{(u)}$ where $\tilde{\psi}_t^{(u)}$ is determined by Eq. (202).

In the ranges of h and ω_f relevant to the spike minimum, the expressions for δ_u and $\tilde{\psi}_t^{(u)}$ in the asymptotic limit $\Phi \rightarrow 0$ are similar to the analogous quantities in the

lower-layer case:

$$\delta_u = \sqrt{2}\pi h, \quad (120)$$

$$\tilde{\psi}_t^{(u)} = -(-1)^{\lfloor \frac{n}{4} \rfloor} \sqrt{\frac{n\pi}{8 \ln(\frac{1}{\Phi})}} + \pi \frac{1 + (-1)^{\lfloor \frac{n}{4} \rfloor}}{2}. \quad (121)$$

Hence, the asymptotic value for the deviation of the tangency energy $E_t^{(u)}$ from the upper barrier reduces to:

$$E_b^{(2)} - E_t^{(u)} \delta_u \left| \pi \frac{1 + (-1)^{\lfloor \frac{n}{4} \rfloor}}{2} - \tilde{\psi}_t^{(u)} \right| = \frac{\pi^{3/2}}{2} \frac{h}{\sqrt{\ln(1/\Phi)/n}}. \quad (122)$$

The maximal energy on the boundary, $E_{\max}^{(u)}$, corresponds to $\tilde{\psi} = \pi(1 + (-1)^{\lfloor n/4 \rfloor})/2$. Thus, it can be found from the equality

$$\tilde{H}(I = I(E_{\max}^{(u)}), \tilde{\psi} = \pi(1 + (-1)^{\lfloor n/4 \rfloor})/2) = \tilde{H}(I_t^{(u)} \equiv I(E_t^{(u)}), \tilde{\psi}_t^{(u)}). \quad (123)$$

At $\Phi \rightarrow 0$, Eq. (123) yields the following expression for the minimal deviation of energy from the barrier (measured along the boundary):

$$\delta_{\min}^{(u)} \equiv E_b^{(2)} - E_{\max}^{(u)} = (E_b^{(2)} - E_t^{(u)})/\sqrt{e} = \frac{\pi^{3/2}}{2e^{1/2}} \frac{h}{\sqrt{\ln(1/\Phi)/n}}. \quad (124)$$

4.1.3.2.2 Relatively Large Values Of h

If $h > h_{cr}^{(u)}(\omega_f)$ (cf. Fig. 13(a)), the previously described trajectory (either the tangent one or the separatrix, for the even and odd spikes ranges respectively) is encompassed by the separatrix of the upper nonlinear resonance and typically forms the boundary of a major stability island inside the upper layer (reproduced periodically in $\tilde{\psi}$ with the period 2π). The lower *outer* boundary of the layer is formed in this case by the lower part of the *resonance separatrix*. This may be interpreted as the absorption of the upper resonance by the upper chaotic layer.

The self-consistent description of chaotic layers given above, and in more detail in the Appendix, is the first main result of this section. It provides a *rigorous basis* for our intuitive assumption that the minimal value of h at which the layers overlap corresponds to the reconnection of the nonlinear resonances with each other while the reconnected resonances touch one of the layers and also touch/overlap another layer. It is gratifying that we have obtained a *quantitative* theoretical description of the chaotic layer boundaries in the *phase space*, including even the major stability islands, that agrees well with the results of simulations (see Fig. 13(b)). To the best of our knowledge it was the first ever [43] quantitative description of the layer boundaries in the phase space.

4.1.4 Onset of global chaos: the spikes' minima

The condition for the merger of the lower resonance and the lower chaotic layer may be written as

$$\tilde{H}(I = I(E = E_b^{(1)} + \delta_{\min}^{(l)}), \tilde{\psi} = \pi(1 - (-1)^{\lfloor n/4 \rfloor})/2) = \tilde{H}_{sl}. \quad (125)$$

The condition for the merger of the upper resonance and the upper chaotic layer may be written as

$$\tilde{H}(I = I(E = E_b^{(2)} - \delta_{\min}^{(u)}), \tilde{\psi} = \pi(1 + (-1)^{\lfloor n/4 \rfloor})/2) = \tilde{H}_{su}. \quad (126)$$

For the onset of global chaos related to the spike minimum, either of Eqs. (125) and (126) should be combined with the condition of the separatrix reconnection (104). Let us seek first only the leading terms of $h_s \equiv h_s(\Phi)$ and $\omega_s \equiv \omega_s(\Phi)$. Then (104) may be replaced by its lowest-order approximation (105) or, equivalently, (106). Using also the lowest-order approximation for the barriers ($E_b^{(1,2)} \approx 1/2 \mp \Phi$), we reduce Eqs. (125), (126) respectively to

$$\tilde{H}(I = I(E = 1/2 - \Phi + \delta_{\min}^{(l)}), \tilde{\psi} = \pi(1 - (-1)^{\lfloor n/4 \rfloor})/2) = 0, \quad (127)$$

$$\tilde{H}(I = I(E = 1/2 + \Phi - \delta_{\min}^{(u)}), \tilde{\psi} = \pi(1 + (-1)^{\lfloor n/4 \rfloor})/2) = 0, \quad (128)$$

where $\delta_{\min}^{(l)}$ is given by (112) or (115) for the odd or even spikes respectively, while $\delta_{\min}^{(u)}$ is given by (119) or (124) for the odd or even spikes respectively.

To the *leading* order, the solution $(h_s^{(l)}, \omega_s^{(l)})$ of the system of equations (106),(127) and the solution $(h_s^{(u)}, \omega_s^{(u)})$ of the system of equations (106),(128) turn out *identical*. For the sake of brevity, we derive below just $(h_s^{(l)}, \omega_s^{(l)})$, denoting the latter, in short, as (h_s, ω_s) ¹⁶.

The system of algebraic equations (106) and (127) is still too complicated for us to find its exact solution. However, we need only the *lowest-order* solution – and this simplifies the problem. Still, even this simplified problem is not trivial, both because the function $h_s(\Phi)$ turns out to be non-analytic and because $\Delta E^{(1)}$ in (106) is very sensitive to ω_f in the relevant range. Despite these difficulties, we have found the solution in a *self-consistent* way, as briefly described below.

Assume that the asymptotic dependence $h_s(\Phi)$ is:

¹⁶ With account taken of the next-order corrections, the spike minimum (h_s, ω_s) coincides with $(h_s^{(l)}, \omega_s^{(l)})$ in case of an odd spike, or with $(h_s^{(u)}, \omega_s^{(u)})$ in case of an even spike. This occurs because, in case of odd spikes, $|q_n(E)|$ increases/decreases as E approaches the relevant vicinity of the upper/lower barrier, while it is *vice versa* in the case of even spikes. And the larger $|q_n|$ the further the resonance separatrix extends: in other words, the reconnection of the barrier chaotic layer with the resonance separatrix requires a smaller value of h at the barrier where $|q_n|$, in the relevant vicinity of the barrier, is larger.

$$h_s = a \frac{\Phi}{\ln(4e/\Phi)}, \quad (129)$$

where the constant a may be found from the asymptotic solution of (106), (127), (129).

Substituting the energies $E = 1/2 - \Phi + \delta_{\min}^{(l)}$ and $E = 1/2 + \Phi - \delta_{\max}^{(u)}$ in (89) and taking account of (112), (115), (119), (124) and (129), we find that, both for the odd and even spikes, the inequality

$$\omega_m - \omega(E) \ll \omega_m \quad (130)$$

holds over the whole relevant range of energies, i.e. for

$$\Delta E \in [-\Phi + \delta_{\min}^{(l)}, \Phi - \delta_{\min}^{(u)}]. \quad (131)$$

Thus, the resonant approximation is valid over the whole range (131). Eq. (96) for $q_n(E)$ is valid over the whole relevant range of energies too.

Consider Eq. (127) in an explicit form. Namely, we express ω_f from (127), using Eqs. (87), (96), and (97), using also (112) or (115) for odd or even spikes and (129):

$$\omega_f = \frac{n\pi}{2\ln\left(\frac{4e}{\Phi}\right)} \left\{ 1 + \frac{h\sqrt{2}}{n\Phi} + O\left(\frac{1}{\ln^2(4e/\Phi)}\right) \right\}. \quad (132)$$

We emphasize that the value of $\delta_{\min}^{(l)}$ enters explicitly only the term $O(\dots)$ while, as is clear from the consideration below, this term does not affect the leading terms in (h_s, ω_s) . Thus, $\delta_{\min}^{(l)}$ does not affect the leading term of ω_s at all, while it affects the leading term of h_s only *implicitly*: $\delta_{\min}^{(l)}$ lies in the range of energies where $nq_n(E) \approx \sqrt{2}$. This latter quantity is present in the second term in the curly brackets in (132) and, as becomes clear from further consideration, h_s is proportional to it.

Substituting (132) into the expression for $\Delta E^{(1)}$ in (106), using (129) and keeping only the leading terms, we obtain

$$\Delta E^{(1)} = \Phi \sqrt{1 - 4e^{c-2}}, \quad c \equiv \frac{2\sqrt{2}}{n}a. \quad (133)$$

Substituting $\Delta E^{(1)}$ from (133) into Eq. (106) for $h(\omega_f)$ and allowing for (129) once again, we arrive at a transcendental equation for c :

$$\ln\left(\frac{1 + \chi(c)}{1 - \chi(c)}\right) - 2\chi(c) = c, \quad \chi(c) \equiv \sqrt{1 - 4e^{c-2}}. \quad (134)$$

An approximate numerical solution of Eq. (134) is:

$$c \simeq 0.179. \quad (135)$$

Thus, the final leading-order asymptotic formulæ for ω_f and h in the minima of the spikes are the following:

$$\omega_{s0} \equiv \omega_{s0}^{(n+1)} = n \frac{\pi}{2 \ln\left(\frac{4e}{\Phi}\right)}, \quad h_{s0} \equiv h_{s0}^{(n+1)} = n \frac{c}{2\sqrt{2}} \frac{\Phi}{\ln\left(\frac{4e}{\Phi}\right)}, \quad (136)$$

$$n = 1, 3, 5, \dots, \quad \Phi \rightarrow 0,$$

where the constant $c \simeq 0.179$ is the solution of Eq. (134).

The self-consistent derivation of the explicit asymptotic formulæ for the minima of $h_{gc}(\omega_f)$ constitutes the second main result of this section. These formulæ allow one to predict immediately the parameters for the weakest perturbation that may lead to global chaos.

4.1.5 Numerical example and next-order corrections

For $\Phi = 0.2$, the numerical simulations give the following values for the frequencies at the minima of the first two spikes (see Fig. 9):

$$\omega_s^{(1)} \approx 0.4005 \pm 0.0005, \quad \omega_s^{(2)} \approx 1.24 \pm 0.005. \quad (137)$$

By the lowest-order formula (136), the values are:

$$\omega_{s0}^{(1)} \approx 0.393, \quad \omega_{s0}^{(2)} \approx 1.18, \quad (138)$$

in rather good agreement with the simulations.

The next-order correction for ω_s can immediately be found from Eq. (132) for ω_f and from Eq. (136) for h_{s0} , so that

$$\omega_{s1} \simeq \omega_{s0} \left(1 + \frac{c}{2 \ln\left(\frac{4e}{\Phi}\right)}\right) \approx \frac{n\pi \left(1 + \frac{0.09}{\ln\left(\frac{4e}{\Phi}\right)}\right)}{2 \ln\left(\frac{4e}{\Phi}\right)}, \quad n = 1, 3, 5, \dots \quad (139)$$

The formula (139) agrees with the simulations even better than the lowest-order approximation:

$$\omega_{s1}^{(1)} \approx 0.402, \quad \omega_{s1}^{(2)} \approx 1.21. \quad (140)$$

For h in the spikes minima, the simulations give the following values (see Fig. 9):

$$h_s^{(1)} \approx 0.0049, \quad h_s^{(2)} \approx 0.03. \quad (141)$$

The values according to the lowest-order formula (52) are:

$$h_{s0}^{(1)} \approx 0.0032, \quad h_{s0}^{(2)} \approx 0.01. \quad (142)$$

The theoretical value $h_{s0}^{(1)}$ gives reasonable agreement with the simulation value $h_s^{(1)}$. The theoretical value $h_{s0}^{(2)}$ gives the correct order of magnitude for the simulation

value $h_s^{(2)}$. Thus, the accuracy of the lowest-order formula (136) for h_s is much lower than that for ω_s : this is due to the steepness of $h_{gc}(\omega_f)$ in the ranges of the spikes (the steepness, in turn, is due to the flatness of the function $\omega(E)$ near its maximum). Moreover, as the number of the spike j increases, the accuracy of the lowest-order value $h_{s0}^{(j)}$ significantly decreases. The latter can be explained as follows. For the next-order correction to $h_{s0}^{(j)}$, the dependence on Φ reads as:

$$\frac{h_{s1}^{(j)} - h_{s0}^{(j)}}{h_{s0}^{(j)}} \propto \frac{1}{\ln(4e/\Phi)}. \quad (143)$$

At least some of the terms in this correction are positive and proportional to $h_{s0}^{(j)}$ (e.g. due to the difference between the exact equation (99) and its approximate version (101)), while $h_{s0}^{(j)}$ is proportional to $n \equiv 2j - 1$. Thus, for $\Phi = 0.2$, the relative correction for the 1st spike is ~ 0.25 while the correction for the 2nd spike is a few times larger i.e. ~ 1 . But the latter means that, for $\Phi = 0.2$, the asymptotic theory for the 2nd spike cannot pretend to be a quantitative description of $h_s^{(2)}$, but only provides the correct order of magnitude. Besides, if $n > 1$ while Φ exceeds some critical value, then the search of the minimum involves Eq. (150) rather than Eq. (104), as explained below in Sec. 4.2 (cf. Figs. 15(b) and 16). Altogether, this explains why $h_s^{(1)}$ is larger than $h_{s0}^{(1)}$ only by 50% while $h_s^{(2)}$ is larger than $h_{s0}^{(2)}$ by 200%.

To provide a consistent explicit derivation of the correction to $h_{s0}^{(j)}$ is complicated. A reasonable alternative may be a proper *numerical* solution of the algebraic system of Eqs. (104)¹⁷ and (125) for the odd spikes, or (126) for the even spikes¹⁶. To this end, in Eqs. (104)¹⁷ and (125) or (126) we use: (i) the exact values of the saddle energies obtained from the exact relations (100) instead of the approximate relations (101); (ii) the exact formula (88) for $\omega(E)$ instead of the asymptotic expression (89); (iii) the exact functions $q_n(E)$ instead of the asymptotic formula (86); (iv) the relation (111) and the calculation of the ‘‘tangent’’ state $(\tilde{\psi}_t^{(l)}, I_t^{(l)})$ by Eqs. (172), (183) for the odd spikes, or relation (123) and the calculation of the ‘‘tangent’’ state $(\tilde{\psi}_t^{(u)}, I_t^{(u)})$ by Eqs. (202)-(204) for the even spikes. Note that, to find the exact function $q_n(E)$, we substitute into the definition of $q_n(E)$ in (87) the explicit¹⁸ solution for $q(E, \psi)$:

$$q(E, \psi) = \arcsin\left(\frac{\eta - \sqrt{2E} + \Phi}{1 - \eta}\right) \quad \text{for } \psi \in \left[0, \frac{\pi}{2}\right],$$

$$q(E, \psi) = \pi - q(E, \pi - \psi) \quad \text{for } \psi \in \left[\frac{\pi}{2}, \pi\right],$$

¹⁷ For $n > 1$, it is also necessary to check if the solution lies above the line (150). If it does not, then (104) should be replaced here by (150).

¹⁸ In the general case of an arbitrary potential $U(q)$, when the explicit expression for $q(E, \psi)$ and $\omega(E)$ cannot be obtained, these functions can be calculated numerically.

$$\begin{aligned}
q(E, \psi) &= q(E, 2\pi - \psi) && \text{for } \psi \in [\pi, 2\pi], \\
\eta &\equiv \frac{1}{2}(\sqrt{2E} - \Phi + 1)\text{sn}^2\left(\frac{2K}{\pi}\psi\right), && (144)
\end{aligned}$$

where $\text{sn}(x)$ is the elliptic sine [2] with the same modulus k as the full elliptic integral K defined in (88). The numerical solution described above gives:

$$\begin{aligned}
\left(\omega_s^{(1)}\right)_{num} &\approx 0.401, && \left(h_s^{(1)}\right)_{num} \approx 0.005, \\
\left(\omega_s^{(2)}\right)_{num} &\approx 1.24, && \left(h_s^{(2)}\right)_{num} \approx 0.052.
\end{aligned} \tag{145}$$

The agreement with the simulation results is: (i) excellent for ω_s for the both spikes and for h_s for the 1st spike, (ii) reasonable for h_s for the 2nd spike. Thus, if Φ is *moderately* small, a much more accurate prediction for h_s than that by the lowest-order formula is provided by the numerical procedure described above.

4.2 Theory of the Spikes' Wings

The goal of this section is to find the mechanisms responsible for the formation of the spikes' wings (i.e. the function $h_{gc}(\omega_f)$ in the ranges of ω_f slightly deviating from $\omega_s^{(j)}$), and to provide for their theoretical description.

Before developing the theory, we briefly analyze the simulation data (Fig. 9), concentrating on the 1st spike. The left wing of the spike is smooth and nearly straight. The initial part of the right wing is also nearly straight¹⁹, though less steep. But at some small distance from $\omega_s^{(1)}$ its slope changes jump-wise by a few times: compare the derivative $dh_{gc}/d\omega_f \approx 0.1$ at $\omega_f = 0.4 \div 0.41$ (see the left inset in Fig. 9) and $dh_{gc}/d\omega_f \approx 0.4$ at $\omega_f = 0.45 \div 0.55$ (see the main part of Fig. 9). Thus, even prior to the theoretical analysis, one may assume that there are a number of different mechanisms responsible for formation of the wings.

Consider the arbitrary j th spike. We have shown in the previous section that, in the asymptotic limit $\Phi \rightarrow 0$, the minimum of the spike corresponds to the intersection between the line (104) with (125) or (126) for odd or even spikes respectively. We recall that: (i) Eq. (104) corresponds to the overlap in phase space between non-linear resonances of the same order $n \equiv 2j - 1$; (ii) Eq. (125) or (126) corresponds to the onset of the overlap between the resonance separatrix associated respectively with the lower or upper saddle and the chaotic layer associated with the lower or upper potential barrier; (iii) for $\omega_f = \omega_s^{(j)}$, the condition (125) or (126) also guarantees the overlap between the upper or lower resonance separatrix, respectively, and the chaotic layer associated with the upper or lower barrier¹⁶.

¹⁹ Provided $h_{gc}(\omega_f)$ is smoothed over small fluctuations.

If ω_f becomes slightly smaller than $\omega_s^{(j)}$, the resonances shift closer to the barriers while moving apart from each other. Hence, as h increases, the overlap of the resonances with the chaotic layers associated with the barriers occurs earlier than with each other. Therefore, at $0 < \omega_s^{(j)} - \omega_f \ll \omega_m$, the function $h_{gc}(\omega_f)$ should correspond approximately to the reconnection of resonances of the order $n \equiv 2j - 1$ (Fig. 14(a)). Fig. 15(a) demonstrates that even the asymptotic formula (106) for the separatrix reconnection line fits the left wing of the 1st spike quite well, and that the numerically calculated line (104) agrees with the simulations perfectly.

If ω_f becomes slightly larger than $\omega_s^{(j)}$ then, on the contrary, the resonances shift closer to each other and further from the barriers. Therefore, the mutual overlap of the resonances occurs at smaller h than the overlap between any of them and the chaotic layer associated with the lower/upper barrier (cf. Figs. 10(c) and 10(d) as well as 11(c) and 11(d)). Hence, it is the latter overlap which determines the function $h_{gc}(\omega_f)$ in the relevant range of ω_f (Fig. 14(b)). Fig. 15 shows that $h_{gc}(\omega_f)$ is indeed well-approximated in the close vicinity to the right from $\omega_s^{(j)}$ by the numerical solution of Eq. (125) or (126), for an odd or even spike respectively and, for the 1st spike and the given Φ , even by its asymptotic form,

$$h \equiv h(\omega_f) = n \frac{-\Phi + \frac{\omega_f}{n\pi} \left[\Phi \left\{ 2 \ln \left(\frac{4e}{\Phi} \right) + \ln \left(\frac{\Phi + \Delta E^{(1)}}{\Phi - \Delta E^{(1)}} \right) \right\} - 2\Delta E^{(1)} \right]}{2\sqrt{2}},$$

$$\Delta E^{(1)} \equiv \sqrt{\Phi^2 - 64 \exp\left(-\frac{n\pi}{\omega_f}\right)}, n \equiv 2j - 1, \quad |\omega_f - \omega_s^{(j)}| \ll \omega_m. \quad (146)$$

The mechanism described above determines $h_{gc}(\omega_f)$ only in the close vicinity of $\omega_s^{(j)}$. If ω_f/n becomes too close to ω_m or exceeds it, then the resonances are not of immediate relevance: they may even disappear or, if they still exist, their closed loops shrink, so that they can no longer provide for connection of the chaotic layers in the relevant range of h . At the same time, the closeness of the frequency

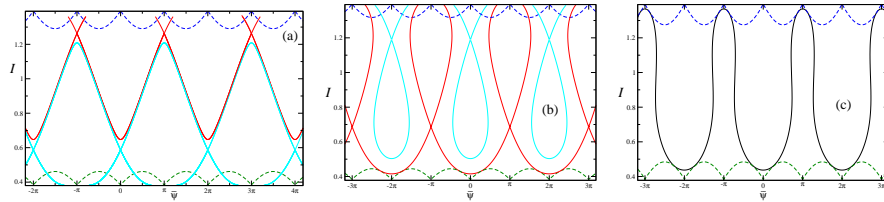


Fig. 14 (Color version may be found in the online version of [43] as Fig. 9). Illustrations of the mechanisms of the formation of the 1st spike wings and of the corresponding theoretical lines in Fig. 15(a). Boxes (a), (b) and (c) illustrate the lines of Eqs. (104), (125) and (148) respectively: the corresponding perturbation parameters are $(\omega_f = 0.39, h = 0.0077)$, $(\omega_f = 0.41, h = 0.00598)$ and $(\omega_f = 0.43, h = 0.01009)$ respectively. Resonance separatrices are drawn in red and cyan. The dashed lines show the functions $I_{GSS}^{(l)}(\tilde{\psi})$ and $I_{GSS}^{(u)}(\tilde{\psi})$. The black line in (c) is the trajectory of the resonant Hamiltonian system (87) which is tangent to both dashed lines.

to ω_m may still give rise to a large variation of action along the trajectory of the Hamiltonian system (87). For the odd/even spikes, the boundaries of the chaotic layers in the asymptotic limit $\Phi \rightarrow 0$ are formed in this case by the trajectory of (87) which is tangent to the lower/upper GSS curves (for the lower/upper layer) or by the lower/upper part of the separatrix of (87) generated by the saddle “ \tilde{s} ”/“ s ” (for the upper/lower layer). The overlap of the layers occurs when these trajectories coincide with each other, which may be formulated as the equality of \tilde{H} in the corresponding tangency and saddle:

$$\begin{aligned} \tilde{H}(I_t^{(l)}, \tilde{\psi}_t^{(l)}) &= \tilde{H}(I_{\tilde{s}}, \tilde{\psi}_{\tilde{s}}) \quad \text{for } j = 1, 3, 5, \dots, \\ \tilde{H}(I_s, \tilde{\psi}_s) &= \tilde{H}(I_t^{(u)}, \tilde{\psi}_t^{(u)}) \quad \text{for } j = 2, 4, 6, \dots, \\ I_{\tilde{s}} &\equiv I(E_b^{(2)} - \delta_{\tilde{s}}), \quad I_s \equiv I(E_b^{(1)} + \delta_s). \end{aligned} \quad (147)$$

Note however that, for *moderately* small Φ , the tangencies may be relevant both to the lower layer and to the upper one (see the Appendix). Indeed, such a case occurs for our example with $\Phi = 0.2$: see Fig. 14(c). Therefore, the overlap of the layers corresponds to the equality of \tilde{H} in the tangencies:

$$\tilde{H}(I_t^{(l)}, \tilde{\psi}_t^{(l)}) = \tilde{H}(I_t^{(u)}, \tilde{\psi}_t^{(u)}). \quad (148)$$

To the lowest order, Eq. (147) and Eq. (148) read as:

$$h \equiv h(\omega_f) = \frac{\sqrt{2}\Phi \ln\left(\frac{4\epsilon}{\Phi}\right)}{\pi} \left(\omega_f - \frac{n\pi}{2 \ln\left(\frac{4\epsilon}{\Phi}\right)} \right). \quad (149)$$

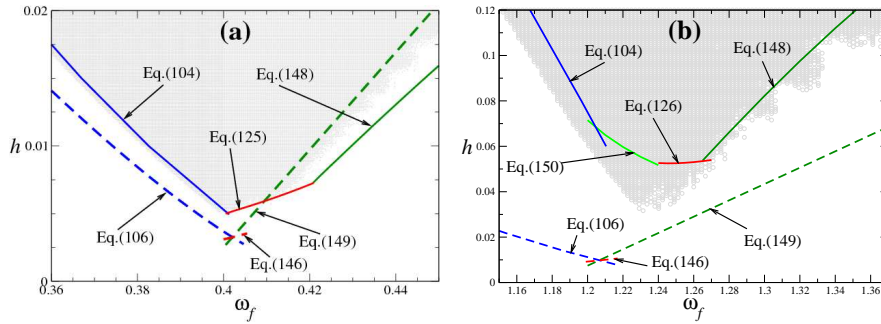


Fig. 15 (Color version may be found in the online version of [43] as Fig. 10). The 1st (a) and 2nd (b) spike in $h_{gc}(\omega_f)$: comparison between the results of the numerical simulations (the lower boundary of the shaded area) and the theoretical estimates. The estimates are indicated by the corresponding equation numbers and are drawn by different types of lines, in particular the dashed lines represent the explicit asymptote for the solid line of the same color.

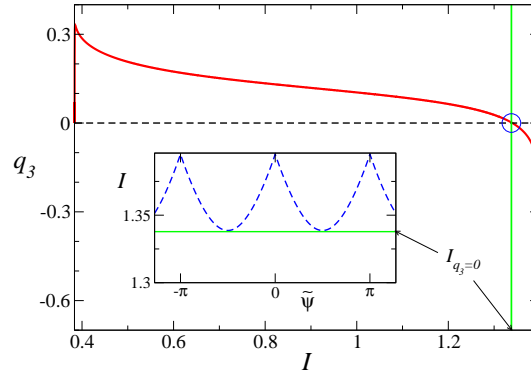
Both the line (148) and the asymptotic line (149) well agree with the part of the right wing of the 1st spike situated to the right from the fold at $\omega_f \approx 0.42$ (Fig. 15(a)). The fold corresponds to the change of the mechanisms of the chaotic layers overlap.

If Φ is moderately small while $n > 1$, the description of the far wings by the numerical lines (104) and (148) may be still quite good but the asymptotic lines (106) and (149) cannot pretend to describe the wings quantitatively any more (Fig. 15(b)). As for the minimum of the spike and the wings in its close vicinity, one more mechanism may become relevant for their formation (Figs. 15(b) and 16). It may be explained as follows. If $n > 1$, then $q_n(E)$ becomes zero in the close vicinity ($\sim \Phi^2$) of the relevant barrier (the upper or lower barrier, in the case of even or odd spikes respectively: cf. Fig. 16). It follows from the equations of motion (98) that no trajectory can cross the line $I = I_{q_n=0}$. In the asymptotic limit $\Phi \rightarrow 0$, provided h is from the range relevant for the spike minimum, almost the whole GSS curve is further from the barrier than the line $I = I_{q_n=0}$, and the latter becomes irrelevant. But, for a moderately small Φ , the line may separate the whole GSS curve from the rest of the phase space. Then the resonance separatrix cannot connect to the GSS curve even if there is a state on the latter curve with the same value of \tilde{H} as on the resonance separatrix. For a given ω_f , the connection then requires a higher value of h : for such a value, the GSS curve itself crosses the line $I = I_{q_n=0}$. In the relevant range of h , the resonance separatrix passes very close to this line, so that the connection is well approximated by the condition that the GSS curve *touches* this line (see the inset in Fig. 16):

$$\begin{aligned} \delta_u &= E_b^{(2)} - E_{q_{2j-1}=0} & \text{for } j = 2, 4, 6, \dots, \\ \delta_l &= E_{q_{2j-1}=0} - E_b^{(1)} & \text{for } j = 3, 5, 7, \dots \end{aligned} \quad (150)$$

This mechanism is relevant to the formation of the minimum of the 2nd spike at $\Phi = 0.2$, and in the close vicinity of the spike on the left (Fig. 15(b)).

Fig. 16 (Color version may be found in the online version of [43] as Fig. 11). Amplitude of the 3rd Fourier harmonic as a function of action (solid red line). The dashed black line shows the zero level. Its intersection with the solid red line is marked by the circle. The green line indicates the value of action where $q_3 = 0$. The inset illustrates the line (150) in Fig. 15(b): the GSS curve touches the horizontal line $I = I_{q_3=0}$.



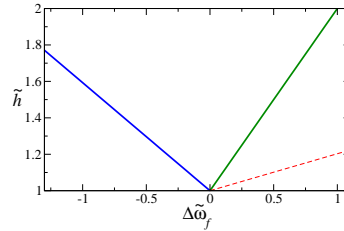
Finally, let us find explicitly the *universal asymptotic shape* of the spike in the vicinity of its minimum. First, we note that the lowest-order expression (146) for the spike between the minimum and the fold can be written as the *half-sum* of the expressions (106) and (149) (which represent the lowest-order approximations for the spike to the left of the minimum, and to the right of the fold respectively). Thus, all three lines (106), (146) and (149) intersect at a single point. This means that, in the asymptotic limit $\Phi \rightarrow 0$, the fold merges with the minimum: ω_f and h in the fold asymptotically approach ω_s and h_s respectively. Thus, though the fold is a generic feature of the spikes, it is not of major significance: the spike is formed basically from two straight lines. The ratio between their slopes is universal. So, introducing a proper scaling, we reduce the spike shape to the universal function (Fig. 17):

$$\begin{aligned}\tilde{h}(\Delta\tilde{\omega}_f) &= \tilde{h}^{(lw)}(\Delta\tilde{\omega}_f) \equiv 1 - \sqrt{1 - 4e^{c-2}}\Delta\tilde{\omega}_f \approx \\ &\approx 1 - 0.593\Delta\tilde{\omega}_f \quad \text{for } \Delta\tilde{\omega}_f < 0, \\ \tilde{h}(\Delta\tilde{\omega}_f) &= \tilde{h}^{(rw)}(\Delta\tilde{\omega}_f) \equiv 1 + \Delta\tilde{\omega}_f \quad \text{for } \Delta\tilde{\omega}_f > 0, \\ \tilde{h}^{(fold)}(\Delta\tilde{\omega}_f) &= \frac{\tilde{h}^{(lw)}(\Delta\tilde{\omega}_f) + \tilde{h}^{(rw)}(\Delta\tilde{\omega}_f)}{2} \equiv \\ &\equiv 1 + \frac{1 - \sqrt{1 - 4e^{c-2}}}{2}\Delta\tilde{\omega}_f \approx 1 + 0.203\Delta\tilde{\omega}_f, \\ \tilde{h} &\equiv \frac{h}{h_{s0}}, \quad \Delta\tilde{\omega}_f \equiv \frac{\omega_f - \omega_{s1}}{\omega_{s1} - \omega_{s0}}, \quad \Phi \rightarrow 0,\end{aligned}\tag{151}$$

where ω_{s0} and h_{s0} are the lowest-order expressions (136) respectively for the frequency and amplitude in the spike minimum, ω_{s1} is the expression (139) for the frequency in the spike minimum, including the first-order correction, and c is a constant (135).

In addition to the left and right wings of the universal shape (the solid lines in Fig. 17), we include in (151) the function $\tilde{h}^{(fold)}(\Delta\tilde{\omega}_f)$ (the dashed line in Fig. 17): its purpose is to show, on one hand, that the fold merges asymptotically with the minimum but, on the other hand, that the fold is generic and the slope of the spike

Fig. 17 (Color version may be found in the online version of [43] as Fig. 12). The universal shape of the spike minimum (151) (solid lines). The dashed line indicates the universal slope of the spike in between the minimum and the fold, which have merged in the universal (asymptotic) function (151).



between the minimum and the fold has a universal ratio to any of the slopes of the major wings.

Even for a moderately small Φ , as in our example, the ratios between the three slopes related to the 1st spike in the simulations are reasonably well reproduced by those in Eq. (151): cf. Figs. 15(a) and 17. It follows from (151) that the asymptotic scaled shape is universal i.e. independent of Φ (but still assuming the asymptotic limit $\Phi \rightarrow 0$), n or any other parameter.

The description of the wings of the spikes near their minima, in particular the derivation of the spike universal shape, constitutes the third main result of this section.

4.3 Generalizations and Applications

The *facilitation of the onset of global chaos* between adjacent separatrices has a number of possible generalizations and applications. We discuss an application in Sec. 5, but first list some of generalizations below.

1. The spikes in $h_{gc}(\omega_f)$ may occur for an *arbitrary Hamiltonian* system with two or more separatrices. The asymptotic theory can be generalized accordingly.
2. The absence of pronounced spikes at *even* harmonics $2j\omega_m$ is explained by the symmetry of the potential (84): the even Fourier harmonics of the coordinate, q_{2j} , are equal to zero. For time-periodic perturbation of the dipole type, as in Eq. (85), there are no resonances of even order on account of this symmetry [10, 23, 55, 51, 52, 41]. If either the potential is *non-symmetric*, or the additive perturbation of the Hamiltonian is not an *odd* function of the coordinate, then even-order resonances do exist, resulting in the presence of the spikes in $h_{gc}(\omega_f)$ at $\omega_f \approx 2j\omega_m$.
3. There may also be an additional facilitation of the onset of global chaos that could reasonably be described as a “secondary” facilitation. Let the frequency ω_f be close to the frequency ω_s of the spike minimum, while the amplitude h be $\sim h_s$ but still lower than $h_{gc}(\omega_f)$. Then there are two resonance separatrices in the $I - \tilde{\psi}$ plane that are not connected by chaotic transport (cf. Fig. 11(b)). This system possesses the zero-dispersion property. The trajectories of the resonant Hamiltonian (87) which start in between the separatrices oscillate in I (as well as in $d\tilde{\psi}/dt$). The frequency $\tilde{\omega}$ of such oscillations along a given trajectory depends on the corresponding value of \tilde{H} analogously to the way in which ω depends on E for the original Hamiltonian H_0 : $\tilde{\omega}(\tilde{H})$ is equal to zero for the values of \tilde{H} corresponding to the separatrices (being equal in turn to \tilde{H}_{sl} and \tilde{H}_{su} : see Eq. (103)) while possessing a nearly rectangular shape in between, provided the quantity $|\tilde{H}_{sl} - \tilde{H}_{su}|$ is much smaller than the variation of \tilde{H} within each of the resonances,

$$|\tilde{H}_{sl} - \tilde{H}_{su}| \ll \tilde{H}_{var} \sim |\tilde{H}_{sl} - \tilde{H}_{et}| \sim |\tilde{H}_{su} - \tilde{H}_{eu}|, \quad (152)$$

where \tilde{H}_{el} and \tilde{H}_{eu} are the values of \tilde{H} at the elliptic point of the lower and upper resonance respectively. The maximum of $\tilde{\omega}(\tilde{H})$ in between \tilde{H}_{sl} and \tilde{H}_{su} is described by the asymptotic formula:

$$\tilde{\omega}_m \approx \frac{\pi}{\ln(\tilde{H}_{var}/|\tilde{H}_{sl} - \tilde{H}_{su}|)}. \quad (153)$$

If we additionally perturb the system in such a way that an additional time-periodic term of frequency $\tilde{\omega}_f \approx \tilde{\omega}_m$ arises in the resonance Hamiltonian, then the chaotic layers associated with the resonance separatrices may be connected by chaotic transport even for a rather small amplitude of the additional perturbation, due to a scenario similar to the one described in this paper.

There may be various types of such additional perturbation [37]. For example, one may *add* to H (85) one more dipole time-periodic perturbation of *mixed* frequency (i.e. $\approx \omega_m + \tilde{\omega}_m$). Alternatively, one may directly perturb the *angle* of the original perturbation by a *low-frequency* perturbation, i.e. the time-periodic term in H (85) is replaced by the term

$$-hq \cos(\omega_f t + A \cos(\tilde{\omega}_f t)), \quad \omega_f \approx \omega_m, \quad \tilde{\omega}_f \approx \tilde{\omega}_m. \quad (154)$$

Recently discussed physical problems where a similar situation is relevant are: chaotic mixing and transport in a meandering jet flow [30] and reflection of light rays in a corrugated waveguide [22].

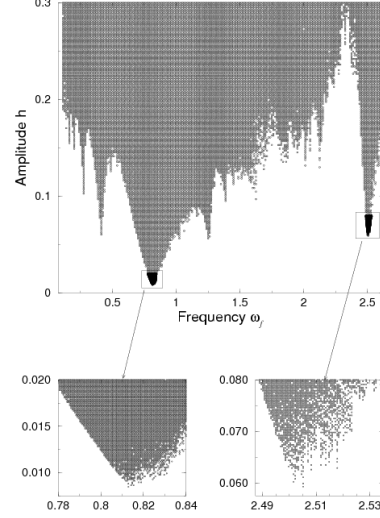
4. If the time-periodic perturbation is *multiplicative* rather than additive, the resonances become *parametric* (cf. [21]). Parametric resonance is more complicated and much less studied than nonlinear resonance. Nevertheless, the main mechanism for the onset of global chaos remains the same, namely the combination of the reconnection between resonances of the same order and of their overlap in energy with the chaotic layers associated with the barriers. At the same time, the frequencies of the main spikes in $h_{gc}(\omega_f)$ may change (though still being related to ω_m). We consider below an example when the periodically driven parameter is²⁰ Φ in (84). The Hamiltonian is

$$\begin{aligned} H &= p^2/2 + (\Phi - \sin(q))^2/2, \\ \Phi &= \Phi_0 + h \cos(\omega_f t), \quad \Phi_0 = \text{const} < 1. \end{aligned} \quad (155)$$

The term $(\Phi - \sin(q))^2/2$ in H (155) may be rewritten as $(\Phi_0 - \sin(q))^2/2 + (\Phi_0 - \sin(q))h \cos(\omega_f t) + h^2 \cos^2(\omega_f t)/2$. The last term in the latter expression does not affect the equations of motion. Thus, we end up with an additive perturbation $(\Phi_0 - \sin(q))h \cos(\omega_f t)$. In the asymptotic limit $\Phi_0 \rightarrow 0$, the n th-order Fourier component of the function $(\Phi_0 - \sin(q))$ can be shown to differ from zero only for the orders $n = 2, 6, 10, \dots$. Therefore one may expect the main spikes in

²⁰ In the case of a 2D electron gas in a magnetic superlattice, this may correspond e.g. to the time-periodic electric force applied perpendicular to the direction of the periodic magnetic field [49, 50].

Fig. 18 Diagram analogous to that in Fig. 9, but for the system (155) (with $\Phi_0 = 0.2$).



$h_{gc}(\omega_f)$ to be at frequencies twice larger than those for the dipole perturbation (85):

$$\omega_{sp}^{(j)} \approx 2\omega_s^{(j)} \approx 2(2j-1)\omega_m, \quad j = 1, 2, 3, \dots \quad (156)$$

This agrees well with the results of simulations (Fig. 18).

Moreover, the asymptotic theory for the dipole perturbation may immediately be generalized to the present case: it is necessary only to replace the Fourier component of the coordinate q by the Fourier component of the function $(\Phi_0 - \sin(q))$:

$$(\Phi_0 - \sin(q))_n = \begin{cases} \frac{4}{\pi n} & \text{at } n=2(2j-1), \\ 0 & \text{at } n \neq 2(2j-1), \end{cases} \quad j = 1, 2, 3, \dots, \quad \Phi_0 \rightarrow 0 \quad (157)$$

(cf. Eq. (96) for q_n). We obtain:

$$\omega_{sp0} \equiv \omega_{sp0}^{(\frac{n+2}{4})} = n \frac{\pi}{2 \ln\left(\frac{4e}{\Phi_0}\right)}, \quad h_{sp0} \equiv h_{sp0}^{(\frac{n+2}{4})} = n \frac{c\pi}{8} \frac{\Phi_0}{\ln\left(\frac{4e}{\Phi_0}\right)}, \quad (158)$$

$$n = 2, 6, 10, \dots, \quad \Phi_0 \rightarrow 0,$$

where c is given in Eqs. (134) and (135).

For $\Phi_0 = 0.2$, Eq. (158) gives, for the 1st spike, values differing from the simulation data by about 3% in frequency and by about 10% in amplitude. Thus, the lowest-order formulæ accurately describe the 1st spike even for a moderately small Φ .

5. One more generalization relates to *multi-dimensional* Hamiltonian systems with two or more saddles with different energies: the perturbation may not necessarily be time-periodic, in this case. The detailed analysis has not yet been done.

The paper [43] presents a rather detailed discussion of possible applications to the electron gas in a magnetic superlattice, a spinning pendulum, cold atoms in an optical lattice as well as to problems of noise-induced escape and the stochastic web formation. We review briefly in the next section the further development of the latter application.

5 Enlargement of a low-dimensional stochastic web

The stochastic web concept dates back to the 1960s when Arnold showed [4] that, in non-degenerate Hamiltonian systems of dimension exceeding 2, resonance lines necessarily intersect, forming an infinite-sized web in the Poincaré section. It provides in turn for a slow chaotic (sometimes called “stochastic”) diffusion for infinite distances in relevant dynamical variables.

It was discovered towards the end of 1980s [54, 7, 8, 9] that, in degenerate or nearly-degenerate systems, a stochastic web may arise even if the dimension is $3/2$. One of the archetypal examples of such a low-dimensional stochastic web arises in the 1D harmonic oscillator perturbed by a weak traveling wave the frequency of which coincides with a multiple of the natural frequency of the oscillator [51, 8, 55]. Perturbation plays a dual role: on the one hand, it gives rise to a slow dynamics characterized by an auxiliary Hamiltonian that possesses an infinite web-like separatrix; on the other hand, the perturbation destroys this self-generated separatrix, replacing it by a thin chaotic layer. Such a low-dimensional stochastic web may be relevant to a variety of physical systems and plays an important role in corresponding transport phenomena: see [51, 8, 55] for reviews on relevant classical systems. In addition, there are quantum systems in which the dynamics of transport reduces to that in the classical model described above. The latter concerns e.g. nanometre-scale semiconductor superlattices with an applied voltage and magnetic field [15, 16].

One might assume that, like the Arnold web, the low-dimensional stochastic web described above should be infinite, so that it can provide for transport between the centre of the web and states situated arbitrarily far away in coordinate and momentum. However the numerical integration of the equations of motion shows that this is not so: even for a rather non-weak perturbation, the real web is limited to the region within *a few* inner loops of the infinite web-like resonant separatrix (Fig. 19(a)) while chaotic layers associated with outer loops are distinctly separated from each other and from the web-like chaotic layer formed by the few inner loops. The reason is apparently as follows. The single infinite web-like separatrix is possessed by the resonant Hamiltonian only in the first-order approximation of the averaging method [5] whereas, with the account taken of the next-order approximations, the separatrix apparently splits into many separate complex loops successively embedded into each other. Non-resonant terms of the perturbation dress the separatrices by expo-

nentially narrow chaotic layers. If the perturbation is not small, the chaotic layers manage to connect neighbouring separatrix loops situated close to the centre. However, the width of the chaotic layer decreases exponentially sharply as the distance from the centre grows [51, 8, 55]. As a result, the merger between chaotic layers associated with neighbouring loops takes place only within the few loops closest to the centre, provided that the perturbation is not exponentially strong.

If the resonance between the perturbation and the oscillator is inexact, or if the oscillator is nonlinear, the splitting between the neighbouring loops is typically much larger: it appears even in the first-order approximation of the averaging method [51, 9, 55]. So the number of loops connected to the centre by chaotic transport is even smaller [51, 9, 55] than in the case of the exact resonance.

A natural question arises: how can the perturbation be modified in order for the transport to be unlimited or, at least, significantly extended? One of the answers was obtained in the very beginning of studies of the low-dimensional webs [54, 7]: if the perturbation consists of repeated in time short kicks that are also periodic space, and if the frequency of the kicks is equal to a multiple of the natural frequency, then a so-called uniform web covering the whole of phase space is formed. However such a perturbation is absent in many cases and, even where present, the chaotic transport is still exponentially slow if the perturbation is weak [51, 55].

It is reasonable then to pose the following question: is it possible to obtain a web of form similar to the original one [8] but substantially extended in phase space? A positive answer was suggested in [43] and explicitly realized recently [46] using the following simple idea. The chaotic layer in the webs is *exponentially* narrow since the frequency of the non-resonant perturbation of the resonant Hamiltonian is necessarily much higher than the frequency of small eigenoscillation in the cell of the web-like separatrix [51, 54, 7, 8, 9, 55]. So we need to modify the perturbation in such a way that the resonant Hamiltonian does not change while its perturbation contains, in addition to the conventional terms, a low-frequency one. One may do this modulating the wave angle with a low frequency or adding one more wave with the frequency slightly shifted from the original one. The latter option, together with a generalization for the uniform web leading to a huge enhancement of the chaotic transport through it, have not yet been considered in detail while the work [46] and the present section concentrate on the former option since it may have immediate applications to nanometre-scale semiconductor superlattices in electric and magnetic fields [15, 16].

5.1 *Slow modulation of the wave angle*

Fig. 19 demonstrates the validity of our idea. We integrate the equation

$$\ddot{q} + q = 0.1 \sin[15q - 4t - h \sin(0.02t)], \quad (159)$$

first for $h = 0$ (i.e. for the conventional case with parameters as in [51, 8, 55]), and secondly for $h = 0.1$. Although the modulation in the latter case is weak (its amplitude is about 63 times smaller than the 2π period of the wave angle which is a characteristic scale in this problem), the resultant increase in the size of the web in coordinate and momentum is large: by a factor of ~ 6 .

An analytic theory can be developed to account for these results. It can be generalized for the off-resonant case [51, 9, 55] too, using the general method developed in [43, 44, 38, 39] and described above in the previous sections.

It is anticipated that the method can also be generalized for uniform webs [51, 54, 55] too, leading to an exponentially strong enhancement of chaotic transport through them.

5.2 Application to semiconductor superlattices

The works [15, 16] consider quantum electron transport in 1D semiconductor superlattices (SLs) on the nanometre scale, subject to a constant electric field along the SL axis and to a constant magnetic field. The spatial periodicity with a period of the nanometre scale gives rise to the onset of minibands for electrons. In the tight-binding approximation, the electron motion in the lowest mini-band is described by the following dispersion relation for the electron energy E versus momentum \mathbf{p} :

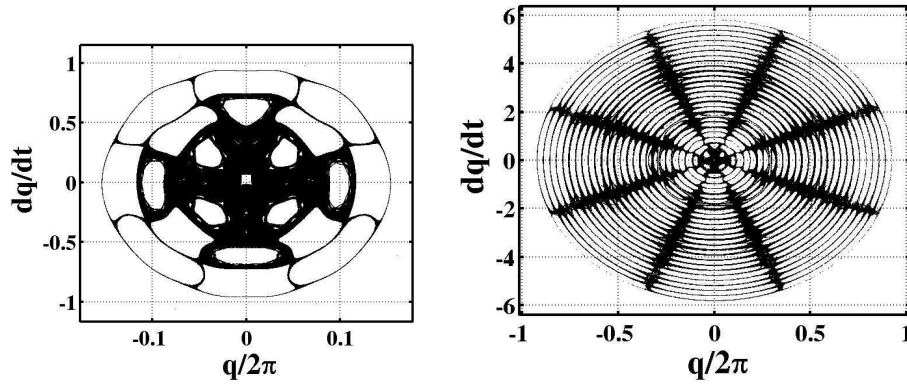


Fig. 19 The Poincaré section for a trajectory of the system (159) with initial state $q = 0.1$, $\dot{q} = 0$ (at instants $t_n = nT$ where $T \equiv 2\pi/0.02$ is the period of the modulation and $n = 1, 2, 3, \dots, 600000$) for $h = 0$ (left panel) and $h = 0.1$ (right panel). A symplectic integration scheme of the fourth order is used, with an integration step $t_{int} = \frac{2\pi}{40000} \approx 1.57 \times 10^{-4}$, so that the inaccuracy at each step is of the order of $t_{int}^5 \approx \times 10^{-19}$. The left panel corresponds to the example of the conventional case considered in [51, 8, 55]. The right panel demonstrates that the modulation, although weak, greatly enlarges the web sizes.

$$E(\mathbf{p}) = \frac{\Delta[1 - \cos(p_x d/\hbar)]}{2} + \frac{p_y^2 + p_z^2}{2m^*}, \quad (160)$$

where x is the direction along the SL axis, Δ is the miniband width, d is the SL period, m^* is the electron effective mass for the motion in the transverse (i.e. $y-z$) direction.

Thus, the quasi-classical motion of electron in an electric field \mathbf{F} and a magnetic field \mathbf{B} is described by the following equation:

$$\frac{d\mathbf{p}}{dt} = -e\{\mathbf{F} + [\nabla_{\mathbf{p}}E(\mathbf{p}) \times \mathbf{B}]\}. \quad (161)$$

where e is the electron charge

It was shown in [15] that, with a constant electric field along the SL axis $\mathbf{F} = (-F_0, 0, 0)$ and a constant magnetic field with a given angle θ to the axis $\mathbf{B} = (B \cos(\theta), 0, B \sin(\theta))$, the dynamics of the z -component of momentum p_z reduces to the equation of motion of an auxiliary harmonic oscillator in a plane wave. At certain values of the parameters, the ratio of the wave and oscillator frequencies takes integer values (like in Eq. (159) with $h = 0$) which gives rise to the onset of the stochastic web, leading in turn to a delocalization of the electron in the x -direction and, as a result, to an increase of the dc-conductivity along the SL axis. The experiment [16] appears to provide evidence in favor of this exciting hypothesis.

At the same time, the finite size of the web and, yet more so, the exponentially fast decrease in the transport rate as the distance from the centre of the web increases, seems to put strong limitations on the use of the effect. We suggest a simple and efficient way to overcome these limitations. Indeed, one can show that, if we add to the original (constant) electric field F_0 a small time-periodic (ac) component $F_{ac} \sin(\Omega_{ac}t)$, then the wave angle in the equation of motion of p_z is modulated by the term (cf. Eq. (159)):

$$h \sin(\Omega t) \equiv \frac{F_{ac}}{F_0} \frac{\Omega_0}{\Omega_{ac}} \sin\left(\frac{\Omega_{ac}}{\Omega_0} t\right), \quad \Omega_0 \equiv \frac{eF_0 d}{\hbar}. \quad (162)$$

This allows us to increase drastically the size of the web and the rate of chaotic transport through it. For example, for the case shown in Fig. 19, where we have an increase of the web size by a factor of $6\times$, it is sufficient to add an ac component of the electric field with the frequency $0.02 \cdot \Omega_0$ and an amplitude $F_{ac} = 0.1 \cdot 0.02 \cdot F_0$ i.e. an amplitude smaller than that of the original constant field F_0 by a factor of $500\times$.

5.3 Discussion

We have presented above just initial results on the subject [46]. There are still many unsolved interesting problems –

1. It can be shown that, in the off-resonance case, there may be a facilitation of the onset of global chaos similar to that described in Sec. 4 above, i.e. the critical value of the modulation amplitude h required for the onset of global chaos between neighbouring separatrix loops possesses deep spikes (minima) as a function of the modulation frequency Ω_{ac} . The detailed theory of this facilitation has yet to be developed.
2. Our conjecture that, in the resonant case, taking account of the next-order approximations of the averaging method could explain the split between different separatrix loops, should be proved rigorously. If the corresponding theory is developed, it will provide the possibility of calculating both the optimal modulation frequency, i.e. that at which the web sizes are maximal, for a given amplitude of modulation, and the maximum sizes themselves.
3. It would be interesting to study the case with an additive perturbation (rather than an angular modulation) in detail, both numerically and theoretically.

6 Conclusions

We have reviewed the recently developed method for the theoretical treatment of separatrix chaos in regimes when it involves resonance dynamics. It has been applied both to single-separatrix chaotic layers and to the onset of global chaos between two close separatrices. The method is based on a matching between the discrete chaotic dynamics of the separatrix map and the continuous regular dynamics of the resonance Hamiltonian. For single-separatrix chaos, the method has allowed:

1. Development of the first asymptotic (i.e. for $h \rightarrow 0$) description of the high peaks in the width of the separatrix chaotic layer as a function of the perturbation frequency, thus describing its dominant feature and, in particular, its maxima.
2. Classification of all systems into two types, based on the asymptotic dependence of the maximum width on the perturbation amplitude h : the maximum width is proportional to $h \ln(1/h)$ or h for systems of type I or type II respectively.

For systems with two or more separatrices, the method has allowed us to develop an accurate asymptotic theory of the facilitation of the onset of global chaos between neighbouring separatrices which occurs at frequencies close to multiples of a local maximum in the eigenoscillation frequency as a function of the energy: the local maximum necessarily exists in the range between the separatrices.

Finally, for an oscillator perturbed by a plane wave of frequency equal to or close to the frequency of a small eigenoscillation, the method has allowed us to suggest how to enlarge substantially the size of the stochastic web using a rather weak perturbation, and it promises to provide an accurate theoretical description of the enlargement.

Acknowledgements We are very much indebted to George Zaslavsky: numerous discussions with him, and his friendly attitude and interest in our research, have greatly stimulated the work. We

also acknowledge financial support from the grant within the Convention between the Institute of Semiconductor Physics and University of Pisa for 2008-2009, from a Royal Society International Joint Project grant 2007/R2-IJP, and from the German Physical Society grant SFB-TR12. Finally, S.M.S. acknowledges the hospitality of Pisa and Lancaster Universities during his visits to both places and, in turn, R.M. and P.V.E.McC. acknowledge the hospitality of the Institute of Semiconductor Physics during their visits there.

7 Appendix

This appendix follows the appendix of the paper [43]. The chaotic layers of the system (85) associated with the separatrices of the unperturbed system (84) are described here by means of the separatrix map. To derive the map, we follow the method described in [55], but the analysis of the map significantly differs from formerly existing ones [23, 55, 51, 52, 29] (cf. also the recently published paper [35] where the analysis of the map has some similarity to ours but still differs significantly). Using our approach, we are able to calculate the chaotic layer boundaries in the *phase space* (rather than only in energy), throughout the resonance frequency ranges, and we can quantitatively describe the *transport* within the layer in a manner different from existing ones (cf. [29, 32] and references therein).

7.1 Lower chaotic layer

We now present a detailed consideration of the lower chaotic layer. The upper layer may be considered in a very similar way.

7.1.1 Separatrix map

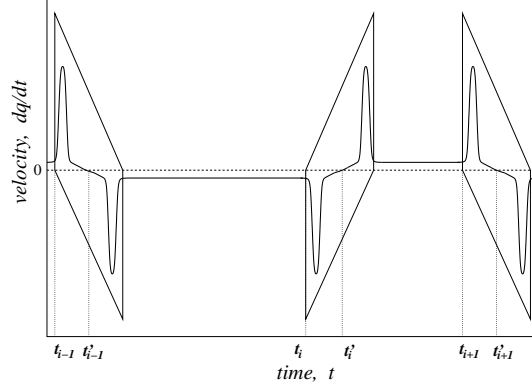
A typical form of trajectory $\dot{q}(t)$ close to the inner separatrix (that corresponding to the lower potential barrier) is shown in Fig. 20. One can resolve pulses in $\dot{q}(t)$. Each of them consists of two approximately antisymmetric spikes²¹. The pulses are separated by intervals during which $|\dot{q}|$ is relatively small. In general, successive intervals differ between each other. Let us introduce the pair of variables E and φ :

$$E \equiv H_0, \quad \varphi \equiv \omega_f t + \varphi_a, \quad (163)$$

where the constant φ_a may be chosen arbitrarily.

²¹ Spikes correspond to motion over any of the minima of the potential, first in one and then (after the reflection from one of the upper barriers) in the opposite direction. If Φ is small, then the spikes within the pulse are separated by long intervals since the reflection point is situated close to the top of the upper barrier, where the motion is slow.

Fig. 20 Schematic example of the time dependence of the velocity of the perturbed system (thick solid line) in the case when the energy of motion varies in the close vicinity of the top of the lower potential barrier. The dashed line marks the zero level of the velocity. Pulses of the velocity are schematically singled out by the parallelograms (drawn by a thin solid line). The two sequences of time instants $(\dots, t_{i-1}, t_i, t_{i+1}, \dots)$ and $(\dots, t'_{i-1}, t'_i, t'_{i+1}, \dots)$ correspond to beginnings and centers of the pulses, respectively.



The energy E changes only during the pulses of $\dot{q}(t)$ and remains nearly unchanged during the intervals between the pulses, when $|\dot{q}(t)|$ is small [55]. We assign numbers i to the pulses and introduce the sequences of (E_i, φ_i) corresponding to the initial instants t_i of the pulses. In such a way, we obtain the following map (cf. [55]):

$$E_{i+1} = E_i + \Delta E_i, \quad \varphi_{i+1} = \varphi_i + \frac{\omega_f \pi (3 - \text{sign}(E_{i+1} - E_b^{(1)}))}{2\omega(E_{i+1})},$$

$$\Delta E_i \equiv h \int_{i \text{ th pulse}} dt \dot{q}(t) \cos(\omega_f t), \quad (164)$$

where $\int_{i \text{ th pulse}}$ means integration over the i th pulse. Before deriving a more explicit expression for ΔE_i , we make two remarks.

1. Let us denote with t'_i the instant within the i th pulse when \dot{q} is equal to zero (Fig. 20). The function $\dot{q}(t - t'_i)$ is an odd function within the i th pulse and it is convenient to transform the cosine in the integrand in ΔE_i (164) as

$$\cos(\omega_f t) \equiv \cos(\omega_f(t - t'_i) + \omega_f t'_i) \equiv \cos(\omega_f(t - t'_i)) \cos(\omega_f t'_i) - \sin(\omega_f(t - t'_i)) \sin(\omega_f t'_i),$$

and to put $\varphi_a = \omega_f(t'_i - t_i)$, so that $\varphi_i \equiv \omega_f t'_i$.

2. Each pulse of \dot{q} contains one positive and one negative spike. The first spike can be either positive or negative. If E changes during the given n th pulse so that its value at the end of the pulse is *smaller* than $E_b^{(1)}$, then the first spikes of the i th and $(i + 1)$ st pulses have the *same* signs. On the contrary, if E at the end of the i th pulse is *larger* than $E_b^{(1)}$, then the first spikes of the i th and $(i + 1)$ st pulses

have *opposite* signs. Note that Fig. 20 corresponds to the case when the energy remains above $E_b^{(1)}$ during the whole interval shown in the figure. This obviously affects the sign of ΔE_i , and it may be explicitly accounted for in the map if we introduce a new discrete variable $\sigma_i = \pm 1$ which characterizes the sign of \dot{q} at the beginning of a given i th pulse,

$$\sigma_i \equiv \text{sign}(\dot{q}(t_i)) , \quad (165)$$

and changes from pulse to pulse as

$$\sigma_{i+1} = \sigma_i \text{sign}(E_b^{(1)} - E_{i+1}) . \quad (166)$$

With account taken of the above remarks, we can rewrite the map (164) as follows:

$$\begin{aligned} E_{i+1} &= E_i + \sigma_i h \varepsilon^{(low)} \sin(\varphi_i), & (167) \\ \varphi_{i+1} &= \varphi_i + \frac{\omega_f \pi (3 - \text{sign}(E_{i+1} - E_b^{(1)}))}{2\omega(E_{i+1})}, \\ \sigma_{i+1} &= \sigma_i \text{sign}(E_b^{(1)} - E_{i+1}), \\ \varepsilon^{(low)} &\equiv \varepsilon^{(low)}(\omega_f) = -\sigma_i \int_{\text{ith pulse}} dt \dot{q}(t - t'_i) \sin(\omega_f(t - t'_i)) \\ &\approx -2\sigma_i \int_{t'_i}^{t_{i+1}} dt \dot{q}(t - t'_i) \sin(\omega_f(t - t'_i)). \end{aligned}$$

A map similar to (167) was introduced in [53], and it is often called the Zaslavsky separatrix map. It was re-derived mathematically rigorously in [31]; see also the recent mathematical review [29]. The latter review also describes generalizations of the Zaslavsky map as well as other types of separatrix map. The analysis presented below relates immediately to the Zaslavsky map but it is hoped that it will prove possible to generalize it for other types of separatrix maps too.

The variable $\varepsilon^{(low)}$ introduced in (167) will be convenient for the further calculations since it does not depend on i in the lowest-order approximation. A quantity like $\delta_i \equiv h|\varepsilon^{(low)}|$ is sometimes called the *separatrix split* [51] since it is conventionally assumed that the maximal deviation of energy on the chaotic trajectory from the separatrix energy is of the order of δ_i [23, 55, 51, 52]. As in the main text, we shall use this term, but we emphasize that the maximal deviation may be much larger.

In the adiabatic limit $\omega_f \rightarrow 0$, the excess of the upper boundary $E_{cl}^{(1)}$ of the lower layer over the lower barrier $E_b^{(1)}$ does not depend on angle and is equal to $2\pi h$ (cf. [14]). But ω_f relevant for the spike of $h_{gc}(\omega_f)$ cannot be considered as an adiabatic frequency, despite its smallness, because it is close to ω_m or to its multiple while all energies at the boundary lie in the range where the eigenfrequency is also close to ω_m :

$$\omega_f \approx (2j - 1)\omega_m \approx (2j - 1)\omega(E_{cl}^{(1)}), \quad j = 1, 2, 3, \dots \quad (168)$$

The validity of (168) (confirmed by the results) is *crucial* for the description of the layer boundary in the relevant case.

7.1.2 Separatrix split

Let us evaluate $\varepsilon^{(low)}$ explicitly. Given that the energy is close to $E_b^{(1)}$, the velocity $\dot{q}(t - t'_i)$ in $\varepsilon^{(low)}$ (167) may be replaced by the corresponding velocity along the separatrix associated with the lower barrier, $\dot{q}_s^{(low)}(t - t'_i)$, while the upper limit of the integral may be replaced by infinity. In the asymptotic limit $\Phi \rightarrow 0$, the interval between spikes within the pulse becomes infinitely long²³ so that only the short ($\sim \omega_0^{-1}$) intervals corresponding to the spikes contribute to the integral in $\varepsilon^{(low)}$ (167). In the scale ω_f^{-1} , they may be considered just as the two instants:

$$t_{sp}^{(1,2)} - t'_i \approx \pm \frac{\pi}{4\omega_m}, \quad \Phi \rightarrow 0. \quad (169)$$

In the definition of $\varepsilon^{(low)}$ (167), we substitute the argument of the sine by the corresponding constants for the positive and negative spikes respectively:

$$\varepsilon^{(low)} \approx 2 \sin\left(\frac{\pi\omega_f}{4\omega_m}\right) \int_{\text{positive spike}} dt \dot{q}_s^{(low)}(t - t'_i) \approx 2\pi \sin\left(\frac{\pi\omega_f}{4\omega_m}\right), \quad (170)$$

$\Phi \rightarrow 0.$

In the derivation of the first equality in (170), we have also taken into account that the function $\dot{q}_s^{(low)}(x)$ is odd. In the derivation of the second equality in (170), we have taken into account that the right turning point of the relevant separatrix is the top of the lower barrier and the distance between this point and the left turning point of the separatrix approaches π in the limit $\Phi \rightarrow 0$.

For the frequencies relevant to the minima of the spikes of $h_{gc}(\omega_f)$, i.e. for $\omega_f = \omega_s^{(j)} \approx (2j - 1)\omega_m$, we obtain:

$$\varepsilon^{(low)}(\omega_s^{(j)}) \approx 2\pi \sin\left((2j - 1)\frac{\pi}{4}\right) = \sqrt{2}\pi(-1)^{\lfloor \frac{2j-1}{4} \rfloor},$$

$j = 1, 2, 3, \dots, \quad \Phi \rightarrow 0. \quad (171)$

For moderately small Φ , it is better to use the more accurate formula:

$$\varepsilon^{(low)}(\omega_f) = 2 \int_0^\infty dt \dot{q}_s^{(low)}(t) \sin(\omega_f t), \quad (172)$$

where the instant $t = 0$ corresponds to the turning point of the separatrix to the left of the lower barrier, i.e. $\dot{q}_s^{(low)}(t = 0) = 0$ while $\dot{q}_s^{(low)}(t) > 0$ for all $t > 0$. The dependence

$|\varepsilon^{(low)}(\omega_f)|$ by Eq. (172) is shown for $\Phi = 0.2$ in Fig. 21(a). For small frequencies, the asymptotic formula (170) fits well the formula (172).

7.1.3 Dynamics of the map

Consider the *dynamics* of the map (167) when ω_f is close to the spikes' minima: $\omega_f \approx n\omega_m$ where $n \equiv 2j - 1$ while $j = 1, 2, 3, \dots$. Let the energy at the step $i = -1$ be equal to $E_b^{(1)}$. The trajectory passing through the state with this energy is chaotic since $(\omega(E))^{-1}$ diverges as $E \rightarrow E_b^{(1)}$ and, therefore, the angle φ_{-1} is not correlated with the angle on the previous step φ_{-2} . The quantity σ_{-1} is not correlated with σ_{-2} either. Thus, $\sin(\varphi_{-1})$ may take any value in the range $[-1, 1]$ and σ_{-1} may equally take the values 1 or -1. Therefore, the energy may change on the next step by an arbitrary value in the interval $[-h|\varepsilon^{(low)}|, h|\varepsilon^{(low)}|]$. Thus, $E_0 - E_b^{(1)}$ may have a positive value²² $\sim h|\varepsilon^{(low)}|$. Then, the approximate equality $n\omega(E_0) \approx \omega_m$ holds, provided that the value of h is from the relevant range. Allowing for this and recalling that we are interested only in those realizations of the map such that $E_0 > E_b^{(1)}$, the relevant realization of the map $i = -1 \rightarrow i = 0$ may be written as:

$$\begin{aligned} E_0 &= E_b^{(1)} + \sigma_{-1}h\varepsilon^{(low)} \sin(\varphi_{-1}) = E_b^{(1)} + h|\varepsilon^{(low)} \sin(\varphi_{-1})|, \\ \varphi_0 &\approx \varphi_{-1} + n\pi, \\ \sigma_0 &= -\sigma_{-1}. \end{aligned} \quad (173)$$

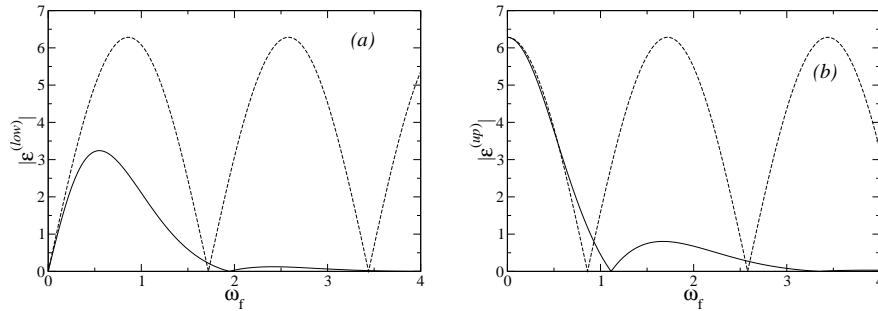


Fig. 21 Theoretical estimates for the normalized separatrix split (for $\Phi = 0.2$) as a function of the perturbation frequency, for the lower and upper layers in (a) and (b) respectively. The solid lines are calculated from Eqs. (172) and (204) for (a) and (b) respectively, while the dashed lines represent the asymptotic expressions (170) and (205) respectively.

²² The latter is valid for any φ_{-1} except in the close vicinity of multiples of π while the state E_0, φ_0 (167) in the latter range of φ_{-1} turns out irrelevant to the boundary, as shown further down.

One may expect that further evolution of the map will, for some time, approximately follow the trajectory of the system (87) with the initial energy E_0 (173) and an arbitrary φ_{-1} and initial slow angle $\tilde{\psi}$ somehow related to $\varphi_0 \approx \varphi_{-1} + n\pi$. Let us prove this explicitly.

Consider two subsequent iterations of the map (167): $2i \rightarrow 2i+1$ and $2i+1 \rightarrow 2i+2$ with an arbitrary $i \geq 0$. While doing this, we shall assume the validity of (168) (it will be clarified below when this is true) from which it follows that: (i) $\omega(E_{k+1}) \approx \omega(E_k)$, (ii) $\varphi_{k+1} - \varphi_k \approx n\pi \equiv (2j-1)\pi$. It will follow from the results that the neglected corrections are small in comparison with the characteristic scales of the variation of E and φ (cf. the conventional treatment of the nonlinear resonance dynamics [10, 23, 55, 51, 52, 41]). Furthermore it follows from (167) that, while the energy remains above the barrier energy, σ_k oscillates, so that $\sigma_{2i} = \sigma_0$ and $\sigma_{2i+1} = -\sigma_0$. Then,

$$\begin{aligned} E_{2i+1} &= E_{2i} + \sigma_0 h \varepsilon^{(low)} \sin(\varphi_{2i}), \\ \varphi_{2i+1} &= \varphi_{2i} + \frac{\omega_f}{\omega(E_{2i+1})} \pi \approx \varphi_{2i} + n\pi + \pi \frac{\omega_f - n\omega(E_{2i})}{\omega(E_{2i})}, \end{aligned} \quad (174)$$

$$\begin{aligned} E_{2i+2} &= E_{2i+1} - \sigma_0 h \varepsilon^{(low)} \sin(\varphi_{2i+1}) = \\ &= E_{2i+1} + \sigma_0 h \varepsilon^{(low)} \sin(\varphi_{2i+1} - n\pi) \approx E_{2i} + \sigma_0 2h \varepsilon^{(low)} \sin(\varphi_{2i}), \\ \varphi_{2i+2} &= \varphi_{2i+1} + \frac{\omega_f}{\omega(E_{2i+2})} \pi \approx \varphi_{2i} + 2\pi n + 2\pi \frac{\omega_f - n\omega(E_{2i})}{\omega(E_{2i})} \end{aligned} \quad (175)$$

(the second equality in the map for E_{2i+2} takes into account that n is odd so that $\sin(\varphi - n\pi) = -\sin(\varphi)$.)

The quantity $\varphi_{2i+2} - \varphi_{2i} - 2\pi n$ is small, so the map $2i \rightarrow 2i+2$ (175) may be approximated by differential equations for E_{2i} and $\tilde{\varphi}_{2i} \equiv \varphi_{2i} - 2\pi ni$:

$$\begin{aligned} \frac{dE_{2i}}{d(2i)} &= \sigma_0 h \varepsilon^{(low)} \sin(\tilde{\varphi}_{2i}), & \frac{d\tilde{\varphi}_{2i}}{d(2i)} &= \frac{\pi}{\omega(E_{2i})} (\omega_f - n\omega(E_{2i})), \\ \tilde{\varphi}_{2i} &\equiv \varphi_{2i} - 2\pi ni. \end{aligned} \quad (176)$$

Let us (i) use for $\varepsilon^{(low)}$ the asymptotic formula (171), (ii) take into account that the increase of i by 1 corresponds to an increase of time by $\pi/\omega(E)$, and (iii) transform from the variables $(E, \tilde{\varphi})$ to the variables $(I, \tilde{\psi} \equiv n\pi(1 - \sigma_0)/2 - \tilde{\varphi})$. Equations (176) reduce then to:

$$\begin{aligned} \frac{dI}{dt} &= -h\sqrt{2}(-1)^{\lfloor \frac{n}{4} \rfloor} \sin(\tilde{\psi}), & \frac{d\tilde{\psi}}{dt} &= n\omega - \omega_f, \\ \tilde{\psi} &\equiv n\pi \frac{1 - \sigma_0}{2} - \tilde{\varphi}, & n &\equiv 2j - 1. \end{aligned} \quad (177)$$

Equations (177) are identical to the equations of motion of the system (87) in their lowest-order approximation, i.e. to equations (98) where q_n is replaced by its asymptotic value (96) and the last term in the right-hand part of the second equation is neglected, being of higher order in comparison with the term $n\omega - \omega_f$.

Apart from the formal identity of Eqs. (177) and (98), $\tilde{\psi}$ in (177) and $\tilde{\psi}$ in (98) are identical to. Necessarily t'_i corresponds to a turning point (see Fig. 20) while the corresponding ψ is equal to $2\pi i$ or $\pi + 2\pi i$ for the right and left turning points respectively (see (87)) i.e. $\psi = 2\pi i + \pi(1 - \sigma_i)/2$, so that $\tilde{\psi}_{(98)} \equiv n\psi - \omega_f t = n\pi(1 - \sigma)/2 - \tilde{\varphi} \equiv \tilde{\psi}_{(177)}$.

The relevant initial conditions for (177) follow from (173) and from the relationship between $\tilde{\psi}$ and φ :

$$I(0) = I(E = E_b^{(1)} + h\sqrt{2}\pi|\sin(\tilde{\psi}(0))|), \quad (178)$$

while $\tilde{\psi}(0) \equiv n\pi(1 - \sigma_0)/2 - \varphi_0$ may be an arbitrary angle from the ranges where

$$(-1)^{\lfloor n/4 \rfloor} \sin(\tilde{\psi}(0)) < 0. \quad (179)$$

For moderately small Φ , it is better to use the more accurate dynamic equations (98) instead of (177) and the more accurate initial value of action instead of (178):

$$I(0) = I(E = E_b^{(1)} + \delta_l |\sin(\tilde{\psi}(0))|), \quad \delta_l \equiv h|\varepsilon^{(low)}|, \quad (180)$$

with $\varepsilon^{(low)}$ calculated by (172).

We name the quantity $\delta_l |\sin(\tilde{\psi})|$ the *generalized separatrix split* (GSS) for the lower layer. Unlike the conventional separatrix split δ_l [51], it is *angle-dependent*. The curve $I(\tilde{\psi}) = I(E = E_b^{(1)} + \delta_l |\sin(\tilde{\psi})|)$ may be called then the GSS curve for the lower barrier and denoted as $I_{GSS}^{(l)}(\tilde{\psi})$.

Finally, let us investigate an important issue: whether the transformation from the discrete separatrix map (i.e. (174) and (A14)) to the differential equations (176) is valid for the very first step and, if it is so, for how long it is valid after that. The transformation is valid as long as $\omega(E_k) \approx n\omega_f$ i.e. as long as E_k is not too close to the barrier energy $E_b^{(1)}$. At the step $k = 0$, the system stays at the GSS curve, with a given (random) angle $\tilde{\psi}(0)$ from the range (179). Thus, at this stage, the relation (168) is certainly valid (for the relevant range of h and for any angle except for the close vicinity of the multiples of π). The change of energy at the next step is positive too:

$$\begin{aligned} E_1 - E_0 &\equiv \sigma_0 h \varepsilon^{(low)} \sin(\tilde{\varphi}_0) \approx -\sigma_{-1} h \varepsilon^{(low)} \sin(\tilde{\varphi}_{-1} - n\pi) = \\ &= \sigma_{-1} h \varepsilon^{(low)} \sin(\tilde{\varphi}_{-1}) \equiv E_0 - E_{-1} > 0. \end{aligned}$$

This may also be interpreted as a consequence of the first equation in (177) and of the inequality (179).

Hence, (168) is valid at the step $k = 1$ too. Similarly, one can show that $E_2 - E_1 > 0$, etc. Thus, the transformation (174,175)→(176) is valid at this initial stage indeed,

and the evolution of $(E, \tilde{\varphi})$ does reduce to the resonant trajectory (14) with an initial angle from the range (179) and the initial action (180). This lasts until the resonant trajectory meets the GSS curve in the adjacent π range of $\tilde{\psi}$ i.e. at t such that the state $(I(t), \tilde{\psi}(t))$ satisfies the conditions:

$$I(t) = I_{\text{GSS}}^{(l)}(\tilde{\psi}(t)), \quad [\tilde{\psi}(t)/\pi] - [\tilde{\psi}(0)/\pi] = 1. \quad (181)$$

At this instant, the absolute value of the change of energy E_k in the separatrix map (174) is equal to $E_k - E_b^{(1)}$ (just because the state belongs to the GSS curve) but the sign of this change is negative because the sign of $\sin(\varphi_k)$ is opposite to that of $\sin(\varphi_0)$. Therefore, at the step $k + 1$, the system gets to the separatrix itself, and the regular-like evolution stops: at the next step of the map, the system may either again get to the GSS curve but with a new (random) angle from the range (179), and start a new regular-like evolution as described above; or it may get to the similar GSS curve *below* the barrier and start an analogous regular-like evolution in the energy range below the barrier, until it stops in the same manner as described above, etc.

This approach makes it possible to describe all features of the transport within the chaotic layer. In the present context, it is most important to describe the *upper outer boundary* of the layer.

7.1.4 Boundary of the layer

We may now analyze the evolution of the boundary of the layer as h grows. Some of the stages of the evolution are illustrated by Figs. 13, 14 and 22.

It follows from the analysis carried out in the previous subsection that *any* state (in the $I - \tilde{\psi}$ plane) lying beyond the GSS curve but belonging to any trajectory following the equations (98) which possesses common points with the GSS curve belongs to the chaotic layer: the system starting from such a state will, sooner or later, reach the separatrix where the chaotization will necessarily occur. Therefore, the *upper boundary* of the chaotic layer coincides with the trajectory following equations (98) with the initial action (180) and an initial angle $\tilde{\psi}(0)$ from the range (179) such that the trajectory deviates from the barrier energy by more than does a trajectory (98)-(179)-(180) with any other initial angle. There may be only two topologically different options for such a trajectory: either it is *tangent* to the GSS curve, or it is the separatrix trajectory which *intersects* the GSS curve (some schematic examples are shown in Figs. 22(a) and 22(b) respectively; some real calculations are shown in Figs. 13 and 14).

1. Relatively small h

Consider first values of h which are large enough for the condition (168) to be satisfied (the explicit criterion will be given in (192)) but which are smaller than the value $h_{cr}^{(l)} \equiv h_{cr}^{(l)}(\omega_f)$ determined by Eq. (125) (its meaning is explained below). The

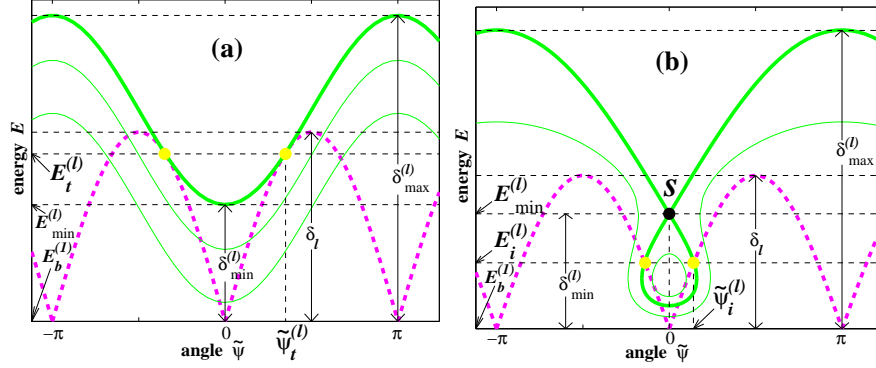


Fig. 22 (Color version may be found in the online version of [43] as Fig. 16). A schematic figure illustrating the formation of the boundary of the lower chaotic layer for $h < h_{cr}^{(l)}(\omega_f)$ in the ranges of ω_f relevant to (a) odd, and (b) even spikes. The dashed magenta line shows the GSS curve in the energy-angle plane: $E(\tilde{\psi}) = E_{\text{GSS}}^{(l)}(\tilde{\psi}) \equiv E_b^{(l)} + \delta_l |\sin(\tilde{\psi})|$. Green lines show examples of those trajectories (98) which have points in common with the GSS curve. One of them (shown by the *thick green line*) relates to the formation of the upper boundary of the lower chaotic layer: in (a), the boundary is the trajectory *tangent* to the GSS curve; in (b), the boundary is the upper part of the *separatrix* generated by the saddle “s”. Yellow dots indicate the relevant common points of the GSS curve and the thick green line. They have angles $\pm \tilde{\psi}_t^{(l)}$ and energy $E_t^{(l)}$ in the case (a), and angles $\pm \tilde{\psi}_i^{(l)}$ and energy $E_i^{(l)}$ in the case (b). The minimum and maximum deviation of energy on the boundary from the barrier energy are denoted as $\delta_{\min}^{(l)}$ and $\delta_{\max}^{(l)}$ respectively. The maximum deviation on the GSS curve is equal to δ_l .

further analysis within this range of h differs for the ranges of ω_f relevant to *odd* and *even* spikes, and so we consider them separately.

A. Odd spikes

The relevant frequencies are:

$$\omega_f \approx n\omega_m, \quad n \equiv 2j - 1, \quad j = 1, 3, 5, \dots \quad (182)$$

Let us seek the state $\{I_t^{(l)}, \tilde{\psi}_t^{(l)}\}$ (with $\tilde{\psi}_t^{(l)}$ within the range $]0, \pi[$) where the resonant trajectory is *tangent* to the GSS curve. With this aim, we equalise both the actions and the derivatives of both curves. The equality of actions immediately yields $I_t^{(l)}$ via $\tilde{\psi}_t^{(l)}$: $I_t^{(l)} \equiv I(E = E_t^{(l)}) = I_{\text{GSS}}^{(l)}(\tilde{\psi}_t^{(l)})$. The derivative along the GSS curve is obtained by differentiation of $I_{\text{GSS}}^{(l)}(\tilde{\psi})$. The derivative along a resonant trajectory can be found by dividing the first dynamic equation in (14) by the second one. Substituting the expression of $I_t^{(l)}$ via $\tilde{\psi}_t^{(l)}$ into the equality of the derivatives, we obtain a closed equation for $\tilde{\psi}_t^{(l)}$, and its solution immediately gives us the relevant $\tilde{\psi}(0)$:

$$\begin{aligned}
& \left[\varepsilon^{(low)} |\cos(\tilde{\psi}_t^{(l)}) \left(1 - \frac{\omega_f}{n\omega(E)} - h \frac{dq_n(E)}{dE} \cos(\tilde{\psi}_t^{(l)}) \right) + q_n(E) \sin(\tilde{\psi}_t^{(l)}) \right]_{E=E_t^{(l)}} \\
& = 0, \\
& E_t^{(l)} \equiv E_b^{(1)} + h |\varepsilon^{(low)}| \sin(\tilde{\psi}_t^{(l)}), \quad \tilde{\psi}_t^{(l)} \in [0, \pi], \\
& n \equiv 2j - 1, \quad j = 1, 3, 5, \dots, \quad \tilde{\psi}(0) = \tilde{\psi}_t^{(l)}. \tag{183}
\end{aligned}$$

A careful analysis of the phase space structure shows that, in the present case (i.e. when $h < h_{cr}^{(l)}(\omega_f)$ while j is odd), there is no separatrix of the resonant Hamiltonian (4) which would both intersect the GSS curve and possess points above the tangent trajectory²³. Thus, for this range of h , the outer boundary of the chaotic layer is formed by the trajectory following the dynamical equations (98) with the initial angle given by (183) and the initial action by (180) (Fig. 22(a)).

Lest us find the lowest-order solution of Eq. (183). We neglect the term $1 - \omega_f/(n\omega(E))$ (the result will justify this) and use the lowest-order expression for the relevant quantities: namely, Eqs. (171) and (96) for $\varepsilon^{(low)}$ and q_n respectively, and the lowest-order expression for dq_n/dE which can be derived from Eq. (95):

$$\begin{aligned}
\frac{dq_n(E)}{dE} &= (-1)^{\lfloor \frac{n}{4} \rfloor} \frac{\pi}{4\sqrt{2} (E - E_b^{(1)}) \ln(\Phi^{-1})}, \\
n &\equiv 2j - 1, \quad E - E_b^{(1)} \ll \Phi \rightarrow 0. \tag{184}
\end{aligned}$$

Then Eq. (183) reduces to the following equation

$$\tan^2(\tilde{\psi}_t^{(l)}) = \frac{n\pi}{8 \ln(\Phi^{-1})}. \tag{185}$$

The lowest-order solution of (185) in the range $]0, \pi[$ is

$$\tilde{\psi}_t^{(l)} = (-1)^{\lfloor \frac{n}{4} \rfloor} \sqrt{\frac{n\pi}{8 \ln(1/\Phi)}} + \pi \frac{1 - (-1)^{\lfloor \frac{n}{4} \rfloor}}{2}. \tag{186}$$

It follows from the definition $E_t^{(l)}$ (183) and from (186) that the lowest-order expression for $E_t^{(l)} - E_b^{(1)}$ is

$$E_t^{(l)} - E_b^{(1)} = \delta_l \sin(\tilde{\psi}_t^{(l)}) = \frac{\pi^{3/2}}{2} \frac{h}{\sqrt{\ln(1/\Phi)/n}}. \tag{187}$$

The next step is to find the *minimum* value of the energy on the boundary of the layer, $E_{\min}^{(l)}$. It follows from the analysis of the dynamical equations (98) that the corresponding angle $\tilde{\psi}_{\min}$ is equal to 0 if $\text{sign}(q_{2j-1}) > 0$ (i.e. $j = 1, 5, 9, \dots$) or to π if $\text{sign}(q_{2j-1}) < 0$ (i.e. $j = 3, 7, 11, \dots$): cf. Fig. 8(a). Given that the Hamiltonian

²³ For odd numbers $j \geq 3$, there are separatrices which lie in the range of E where $\omega(E) \ll \omega_n$ i.e. much closer to the barrier than the tangent trajectory: these separatrices are therefore irrelevant.

(87) is constant along any trajectory (98) while the boundary coincides with one such trajectory, the values of the Hamiltonian (87) in the states $\{I(E_{\min}^{(l)}), \tilde{\Psi} = \tilde{\Psi}_{\min}\}$ and $\{I_t^{(l)}, \tilde{\Psi}_t^{(l)}\}$ should be equal to each other. In explicit form, this equality may be written as

$$\int_{E_{\min}^{(l)}}^{E_t^{(l)}} dE \left(1 - \frac{\omega_f}{n\omega(E)} \right) - h \left(q_n(E_t^{(l)}) \cos(\tilde{\Psi}_t^{(l)}) - (-1)^{\lfloor \frac{n}{4} \rfloor} q_n(E_{\min}^{(l)}) \right) = 0. \quad (188)$$

Let us find the lowest-order solution of Eq. (188). Assume that $E_{\min}^{(l)}$ still belongs to the range of E where $\omega(E) \approx \omega_m$ (the result will confirm this assumption). Then the integrand in (188) goes to zero in the asymptotic limit $\Phi \rightarrow 0$. Hence the integral may be neglected (again, to be justified by the result). The remaining terms in Eq. (188) should be treated very carefully. In particular, it is insufficient to use the lowest-order value (96) for q_n since it is the difference between $q_n(E_t^{(l)})$ and $q_n(E_{\min}^{(l)})$ that matters. Moreover, the approximate equality $q_n(E_t^{(l)}) - q_n(E_{\min}^{(l)}) \approx dq_n(E_t^{(l)})/dE_t^{(l)}(E_t^{(l)} - E_{\min}^{(l)})$ does not apply here either since, as follows from Eq. (184), the derivative $dq_n(E)/dE$ may vary strongly in the range $[E_{\min}^{(l)}, E_t^{(l)}]$ if $(E_t^{(l)} - E_{\min}^{(l)})/(E_{\min}^{(l)} - E_b^{(1)}) \gtrsim 1$ (again, to be justified by the result). That is why it is necessary to use the more accurate expression (95) for q_n . Allowing for the asymptotic expression (186) of $\tilde{\Psi}_t^{(l)}$ and keeping only the lowest-order terms, one can finally reduce Eq. (188) to the relation

$$\ln \left(\frac{E_t^{(l)} - E_b^{(1)}}{E_{\min}^{(l)} - E_b^{(1)}} \right) = \frac{1}{2}. \quad (189)$$

Substituting here the asymptotic value of $E_t^{(l)}$ (187), we obtain the final lowest-order expression for the minimum deviation (along the boundary) of the energy from the barrier:

$$\delta_{\min}^{(l)} \equiv E_{\min}^{(l)} - E_b^{(1)} = (E_t^{(l)} - E_b^{(1)})/\sqrt{e} = \frac{\pi^{3/2}}{2e^{1/2}} \frac{h}{\sqrt{\ln(1/\Phi)/n}}. \quad (190)$$

It is necessary and sufficient that the condition $\omega(E) \approx \omega_m$ is satisfied at the *minimal* and *maximal* energies of the boundary to ensure that the second equality in (168) holds true, i.e. that $\omega(E)$ is close to ω_m for *all* points of the boundary.

At the *minimal* energy, this condition is

$$\omega_m - \omega(E_b^{(1)} + \delta_{\min}^{(l)}) \ll \omega_m. \quad (191)$$

Eq. (191) determines the lower limit of the relevant range of h . The asymptotic form of (191) is:

$$\frac{\ln\left(\frac{\Phi\sqrt{\ln(1/\Phi)}}{h}\right)}{\ln(1/\Phi)} \ll 1. \quad (192)$$

We emphasize that any h of the order of h_{s0} (136) satisfies this condition. In the asymptotic limit $\Phi \rightarrow 0$, the left-hand part of Eq. (192) goes to zero.

As for the *maximal* energy, it may take values up to the energy of the lower saddle “ sl ”, i.e. E_{sl} (102). Obviously, (168) is valid at this saddle, too.

B. Even spikes

The relevant frequencies are:

$$\omega_f \approx n\omega_m, \quad n \equiv 2j-1, \quad j = 2, 4, 6, \dots \quad (193)$$

In this case, $q_n(E)$ and $dq_n(E)/dE$ have different signs for all E within the relevant range (i.e. where $\omega(E) \approx \omega_m$, $q_n(E) \approx q_n(E_m)$): cf. (96) and (184). Then, in the asymptotic limit $\Phi \rightarrow 0$, Eq. (183) for the tangency does not have any solution for $\tilde{\psi}_t^{(l)}$ in the relevant range²⁴. There may only be solutions very close to some of π integers, and the corresponding energies $E_t^{(l)}$ are then very close to $E_b^{(1)}$ i.e. $\omega(E_t^{(l)}) \ll \omega_m$: therefore they are irrelevant.

At the same time, unlike for the odd spikes, there exists a saddle with an angle

$$\tilde{\psi}_s^{(l)} = \pi \frac{1 - (-1)^{\lfloor \frac{n}{2} \rfloor}}{2}, \quad (194)$$

while the energy (which may be found as the appropriate solution of Eq. (99)) lies in the relevant vicinity of the lower barrier (Fig. 22(b)). In the lowest-order approximation, this saddle energy is:

$$E_s^{(l)} \equiv E_b^{(1)} + \delta_s, \quad \delta_s = \frac{\pi}{2\sqrt{2}} \frac{h}{\ln(\ln(4e/\Phi))}. \quad (195)$$

This saddle (denoted in Fig. 22(b) as “ s ”) generates a separatrix. Its upper whiskers go to the similar adjacent saddles (shifted in $\tilde{\psi}$ by 2π). In the asymptotic limit $\Phi \rightarrow 0$, the upper whiskers are much steeper than the GSS curve and hence they do not intersect it²⁵. The lower whiskers do intersect the GSS curve and, moreover, two intersections lie in the relevant energy range (Fig. 22(b)). Let us show this explicitly. We write the expression for the Hamiltonian (87) in the relevant vicinity of the barrier energy (i.e. where $\omega_m - \omega(E) \ll \omega_m$), keeping in the expression both the lowest-order terms and the terms of next order (in particular, we use Eq. (95) for

²⁴ In case of a *moderately* small Φ , tangency may exist in the relevant range of energies. The boundary of the layer is then formed by the tangent trajectory.

²⁵ In case of a *moderately* small Φ , they may intersect the GSS curve. Then, the tangent trajectory lying above the separatrix necessarily exists, so the boundary of the layer is formed by this tangent trajectory.

$q_n(E)$ and take into account that $0 < \sqrt{2} - nq_n(E) \ll \sqrt{2}$ for the relevant range of E):

$$\begin{aligned} \tilde{H}(I = I(E = E_b^{(1)} + \delta), \tilde{\psi}) &= -\frac{n\delta \ln\left(\frac{2\Phi}{\delta}\right)}{2\ln\left(\frac{4e}{\Phi}\right)} + \left(\omega_f - \frac{n\pi}{2\ln\left(\frac{4e}{\Phi}\right)}\right) \frac{2\Phi}{\pi} \ln\left(\frac{4e}{\Phi}\right) - \\ &- (-1)^{\lfloor \frac{n}{4} \rfloor} h\sqrt{2} \left(1 + \frac{n\pi \ln\left(\frac{2\Phi}{\delta}\right)}{8\ln\left(\frac{4e}{\Phi}\right)}\right) \cos(\tilde{\psi}), \\ \omega_m - \omega(E + \delta) &\ll \omega_m. \end{aligned} \quad (196)$$

The Hamiltonian \tilde{H} should possess equal values at the saddle “s” and at the intersections of the separatrix and the GSS curve. Let us denote the angle of the intersection in the range $]0, \pi[$ as $\tilde{\psi}_i^{(l)}$, and let us denote the deviation of its energy $E_i^{(l)}$ from $E_b^{(1)}$ as $\delta_i^{(l)} \equiv \delta_l \sin(\tilde{\psi}_i^{(l)})$.

Assuming that $|\tilde{\psi}_i^{(l)} - \tilde{\psi}_s^{(l)}| \ll 1$ (the result will confirm this) so that

$$\begin{aligned} \cos(\tilde{\psi}_i^{(l)}) &\approx (-1)^{\lfloor n/4 \rfloor} (1 - (\tilde{\psi}_i^{(l)} - \tilde{\psi}_s^{(l)})^2/2) \approx \\ &\approx (-1)^{\lfloor n/4 \rfloor} (1 - (\delta_i^{(l)}/\delta_l)^2/2) \approx (-1)^{\lfloor n/4 \rfloor} (1 - (\delta_i^{(l)}/h)^2/4), \end{aligned}$$

the equality of the values of \tilde{H} is:

$$\frac{n}{2\ln\left(\frac{4e}{\Phi}\right)} \left(\delta_s \ln\left(\frac{2\Phi}{\delta_s}\right) - \delta_i^{(l)} \ln\left(\frac{2\Phi}{\delta_i^{(l)}}\right) \right) = h\sqrt{2} \frac{n\pi}{8} \frac{\ln\left(\frac{\delta_s}{\delta_i^{(l)}}\right)}{\ln\left(\frac{4e}{\Phi}\right)} - \frac{(\delta_i^{(l)})^2}{2\sqrt{2}h}. \quad (197)$$

Let us assume that, in the asymptotic limit $\Phi \rightarrow 0$, $\delta_i^{(l)} \ll \delta_s$ (the result will confirm this). Then the left-hand part is asymptotically smaller than the first term in the right-hand part. So, Eq. (197) implies, in the asymptotic limit, that the right-hand side equals zero. Expressing h via δ_s from Eq. (195), we finally obtain a closed transcendental equation for $\delta_s/\delta_i^{(l)}$:

$$\left(\frac{\delta_s}{\delta_i^{(l)}}\right)^2 \ln\left(\frac{\delta_s}{\delta_i^{(l)}}\right) = \frac{\pi \ln\left(\frac{4e}{\Phi}\right)}{n \left(\ln\left(\ln\left(\frac{4e}{\Phi}\right)\right)\right)^2} \equiv A. \quad (198)$$

In the asymptotic limit $\Phi \rightarrow 0$, the quantity A diverges and, hence, the lowest-order asymptotic solution of Eq. (198) reads as

$$\frac{\delta_s}{\delta_i^{(l)}} = \sqrt{\frac{2A}{\ln(A)}}. \quad (199)$$

Substituting here the expression (195) for δ_s and the expression (198) for A , we obtain:

$$\delta_i^{(l)} = h \frac{1}{4} \sqrt{\frac{n\pi \ln(\ln(\frac{4\epsilon}{\Phi}))}{\ln(\frac{4\epsilon}{\Phi})}}. \quad (200)$$

Thus, we have proved the following asymptotic properties of the separatrix generated by the saddle “ s ”: (i) the lower whiskers of the separatrix do intersect the GSS curve in the relevant range of E (i.e. where the resonant approximation is valid); and (ii) the upper whiskers of the separatrix do *not* intersect the GSS curve (there is no solution of Eq. (197) in the range $\delta_i^{(l)} > \delta_s$). The former property confirms the self-consistency of the asymptotic theory for even spikes; the latter property means that the *upper outer boundary* of the lower chaotic layer is formed by the *upper whiskers of the separatrix generated by the saddle “ s ”*.

Finally, we note explicitly that the minimal (along the boundary) deviation of energy from the barrier energy occurs exactly at the saddle “ s ”, i.e.

$$\delta_{\min}^{(l)} = \delta_s. \quad (201)$$

2. Relatively large h .

As h grows, the boundary of the layer rises while the lower part of the resonance separatrix, on the contrary, falls. They reconnect at the critical value of h , $h_{cr}^{(l)} \equiv h_{cr}^{(l)}(\omega_f)$, determined by Eq. (125), which may be considered as the absorption of the resonance by the chaotic layer. If h grows further, then the GSS curve and the resonance separatrix intersect. As a result, the trajectory starting from the state of angle (183) and action (180), for odd spikes, or from the saddle “ s ”, for even spikes, is *encompassed* by the resonance separatrix. So, it no longer forms the outer boundary of the layer. Rather it forms the inner boundary i.e. the boundary of the main island of stability inside the layer, repeated periodically in $\tilde{\psi}$ with a period 2π (cf. analogous islands in the upper layer in Fig. 13). Unless the lower chaotic layer reconnects with the upper one, the *outer* boundary of the lower layer is formed by the upper part of the *resonance separatrix*. The relevant initial angle $\tilde{\psi}(0)$ on the GSS curve corresponds to the intersection of the GSS curve with the resonance separatrix (cf. the analogous situation for the upper layer in Fig. 13).

7.2 Upper chaotic layer

The upper chaotic layer may be treated analogously²⁶ to the lower layer. We present here only the results.

Similarly to the lower-layer case, one may consider the ranges of relatively small h (namely, smaller than $h_{cr}^{(u)} \equiv h_{cr}^{(u)}(\omega_f)$ determined by Eq. (126)) and relatively large h (i.e. $h > h_{cr}^{(u)}$). In the former range, the formation of the boundary occurs in a manner which is, in a sense, opposite to that for the lower-layer case. For even spikes, the lower outer boundary is formed by *tangency* while, for odd spikes, it is formed by the lower part of the *separatrix* generated by the saddle “ \tilde{s} ”, analogous to the saddle “ s ” in the lower-layer case²⁷.

So, for even spikes, the angle of tangency $\tilde{\psi}_t^{(u)}$ is determined by:

$$\begin{aligned} & \left[|\varepsilon^{(up)}| \cos(\tilde{\psi}_t^{(u)}) \left(1 - \frac{\omega_f}{n\omega(E)} - h \frac{dq_n(E)}{dE} \cos(\tilde{\psi}_t^{(u)}) \right) - q_n(E) \sin(\tilde{\psi}_t^{(u)}) \right]_{E=E_t^{(u)}} \\ & = 0, \\ & E_t^{(u)} \equiv E_b^{(2)} - h |\varepsilon^{(up)}| \sin(\tilde{\psi}_t^{(u)}) \quad \tilde{\psi}_t^{(u)} \in [0, \pi], \\ & n \equiv 2j - 1, \quad j = 2, 4, 6, \dots, \quad \tilde{\psi}(0) = \tilde{\psi}_t^{(u)}, \end{aligned} \quad (202)$$

and $\tilde{\psi}_t^{(u)}$ determines the tangency energy:

$$E_t^{(u)} = E_b^{(2)} - h |\varepsilon^{(up)}| \sin(\tilde{\psi}_t^{(u)}), \quad (203)$$

where the quantity $\varepsilon^{(up)}$ is described by the formula

$$\varepsilon^{(up)}(\omega_f) = 2 \int_0^\infty dt \dot{q}_s^{(up)}(t) \cos(\omega_f t), \quad (204)$$

where $\dot{q}_s^{(up)}(t)$ is the time dependence of the velocity along the separatrix associated with the upper barrier and the instant $t = 0$ is chosen so that $q_s^{(up)}(t = 0)$ is equal to the coordinate of the lower barrier while $\dot{q}_s^{(up)} > 0$ for $t \in [0, \infty[$. The dependence $|\varepsilon^{(up)}(\omega_f)|$ in Eq. (204) is shown for $\Phi = 0.2$ in Fig. 21(b).

The asymptotic form of Eq. (204) is

²⁶ For any AC-driven spatially periodic Hamiltonian system, the *upper* energy boundary of the layer associated with the unbounded separatrix diverges in the adiabatic limit $\omega_f \rightarrow 0$ [42]. However, this divergence is not relevant for the present problem for the following reasons. The lower chaotic layer relates to the *bounded* separatrix while, for the upper (unbounded) layer, it is the *lower* boundary of the layer which is relevant for the onset of global chaos in between the separatrices. Moreover, even for the upper boundary of the upper layer, the divergence is not yet manifested for the driving parameters (h, ω_f) in the vicinity of the spikes minima (cf. [42]).

²⁷ This tangency may exist for a *moderately* small Φ . The boundary is then formed by the tangent trajectory rather than by the separatrix: see an example in Fig. 14(c).

$$\varepsilon^{(up)} \equiv \varepsilon^{(up)}(\omega_f) = 2\pi \cos\left(\frac{\pi\omega_f}{4\omega_m}\right). \quad (205)$$

For $\omega_f = \omega_s^{(j)} \approx (2j-1)\omega_m$, Eq. (204) reduces to

$$\begin{aligned} \varepsilon^{(up)}(\omega_s^{(j)}) &\approx 2\pi \cos\left((2j-1)\frac{\pi}{4}\right) = \sqrt{2}\pi(-1)^{\lfloor \frac{2j+1}{4} \rfloor}, \\ j &= 1, 2, 3, \dots, \quad \Phi \rightarrow 0. \end{aligned} \quad (206)$$

The lowest-order solution of (202) is given in Eq. (121), so that $E_t^{(u)}$ is approximated by Eq. (122). The maximal energy on the lower boundary of the layer corresponds to $\tilde{\psi}(t) = \pi$ if $j = 2, 6, 10, \dots$ or 0 if $j = 4, 8, 12, \dots$ and is determined by Eq. (123). The asymptotic value of the minimal deviation from the upper barrier of the energy at the boundary, $\delta_{\min}^{(u)}$, is given in Eq. (124).

For odd spikes, the boundary is formed by the lower part of the separatrix generated by the saddle “ s ”. The angle of the saddle is given in Eq. (117) while the deviation of its energy from the barrier is approximated in lowest-order by Eq. (118).

As h grows, the boundary of the layer falls while the upper part of the upper resonance separatrix rises. They reconnect at $h = h_{cr}^{(u)} \equiv h_{cr}^{(u)}(\omega_f)$, as determined by Eq. (126), which may be considered as the absorption of the resonance by the layer.

For larger h , the boundary of the layer is formed by the lower part of the upper resonance separatrix (Fig. 13), unless the latter intersects the lower GSS curve (in which case, $h_{cr}^{(u)}$ marks the onset of global chaos).

References

1. Abdullaev S.S.: Construction of Mappings for Hamiltonian Systems and Their Applications. Springer, Berlin, Heidelberg (2006).
2. Abramovitz M., Stegun I.: Handbook of Mathematical Functions. Dover, New York (1970).
3. Andronov A.A., Vitt A.A., Khaikin S.E.: Theory of Oscillators. Pergamon, Oxford (1966).
4. Arnold V.I.: Instability of dynamical systems with several degrees of freedom. Sov. Math. Dokl. **5**, 581–585 (1964).
5. Bogolyubov N.N., Mitropolsky Yu.A.: Asymptotic Methods in the Theory of Nonlinear Oscillators. Gordon and Breach, New York (1961).
6. Carmona H.A. et al.: Two dimensional electrons in a lateral magnetic superlattice. Phys. Rev. Lett. **74**, 3009–3012 (1995).
7. Chernikov A.A. et al.: Minimal chaos and stochastic webs. Nature **326**, 559–563 (1987).
8. Chernikov A.A. et al.: Some peculiarities of stochastic layer and stochastic web formation. Phys. Lett. A **122**, 39–46 (1987).
9. Chernikov A.A. et al.: Strong changing of adiabatic invariants, KAM-tori and web-tori. Phys. Lett. A **129**, 377–380 (1988).
10. Chirikov B.V.: A universal instability of many-dimensional oscillator systems. Phys. Rep. **52**, 263–379 (1979).
11. del-Castillo-Negrete D., Greene J.M., Morrison P.J.: Area-preserving non-twist maps: periodic orbits and transition to chaos. Physica D **61**, 1–23 (1996).

12. Dullin H.R., Meiss J.D., Sterling D.: Generic twistless bifurcations. *Nonlinearity* **13**, 203–224 (2000).
13. Dykman M.I., Soskin S.M., Krivoglaz M.A.: Spectral distribution of a nonlinear oscillator performing Brownian motion in a double-well potential. *Physica A* **133**, 53–73 (1985).
14. Elskens Y. and Escande D.F.: Slowly pulsating separatrices sweep homoclinic tangles where islands must be small: an extension of classical adiabatic theory. *Nonlinearity* **4**, 615–667 (1991).
15. Fromhold T.M. et al.: Effects of stochastic webs on chaotic electron transport in semiconductor superlattices. *Phys. Rev. Lett.* **87**, 046803-1–046803-4 (2001).
16. Fromhold T.M. et al.: Chaotic electron diffusion through stochastic webs enhances current flow in superlattices. *Nature* **428**, 726–730 (2004).
17. Gelfreich V., private communication.
18. Gelfreich V.G., Lazutkin V.F.: Splitting of separatrices: perturbation theory and exponential smallness. *Russian Math. Surveys* **56**, 499–558 (2001).
19. Howard J.E. and Hohn S.M.: Stochasticity and reconnection in Hamiltonian systems. *Phys. Rev. A* **29**, 418–421 (1984).
20. Howard J.E. and Humpherys J.: Non-monotonic twist maps. *Physica D* **80**, 256–276 (1995).
21. Landau L.D. and Lifshitz E.M.: *Mechanics*. Pergamon, London (1976).
22. Leonel E.D.: Corrugated Waveguide under Scaling Investigation. *Phys. Rev. Lett.* **98**, 114102-1–114102-4 (2007).
23. Lichtenberg A.J. and Leiberman M.A.: *Regular and Stochastic Motion*. Springer, New York (1992).
24. Luo A.C.J.: Nonlinear dynamics theory of stochastic layers in Hamiltonian systems. *Appl. Mech. Rev.* **57**, 161–172 (2004).
25. Luo A.C.J., Gu K., Han R.P.S.: Resonant-Separatrix Webs in Stochastic Layers of the Twin-Well Duffing Oscillator. *Nonlinear Dyn.* **19**, 37–48 (1999).
26. Morozov A.D.: Degenerate resonances in Hamiltonian systems with 3/2 degrees of freedom. *Chaos* **12**, 539–548 (2002).
27. Neishtadt A.I.: Change in adiabatic invariant at a separatrix. *Sov. J. Plasma Phys.* **12**, 568–573 (1986).
28. Neishtadt A.I., Sidorenko V.V., and Treschev D.V.: Stable periodic motions in the problem on passage through a separatrix. *Chaos* **7**, 2–11 (1997).
29. Piftankin G.N., Treschev D.V.: Separatrix maps in Hamiltonian systems. *Russian Math. Surveys* **62**, 219–322 (2007).
30. Prants S.V., Budyansky M.V., Uleysky M.Yu., Zaslavsky G.M.: Chaotic mixing and transport in a meandering jet flow. *Chaos* **16**, 033117-1–033117-8 (2006).
31. Rom-Kedar V.: Transport rates of a class of two-dimensional maps and flows. *Physica D* **43**, 229–268 (1990).
32. Rom-Kedar V.: Homoclinic tangles – classification and applications. *Nonlinearity* **7**, 441–473 (1994).
33. Schmelcher P. and Shepelyansky D.L.: Chaotic and ballistic dynamics for two-dimensional electrons in periodic magnetic fields. *Phys. Rev. B* **49**, 7418–7423 (1994).
34. Shevchenko I.I.: Marginal resonances and intermittent Behaviour in the motion in the vicinity of a separatrix. *Phys. Scr.* **57**, 185–191 (1998).
35. Shevchenko I.I.: The width of a chaotic layer. *Phys. Lett. A* **372**, 808–816 (2008).
36. Schmidt G.J.O.: Deterministic diffusion and magnetotransport in periodically modulated magnetic fields. *Phys. Rev. B* **47**, 13007–13010 (1993).
37. Soskin S.M., unpublished.
38. Soskin S.M. and Mannella R.: New Approach To The Treatment Of Separatrix Chaos. In: *Proceedings of the ICNF-2009*. In press.
39. Soskin S.M., Mannella R.: Maximal width of the separatrix chaotic layer. Submitted to *Phys. Rev. E*.
40. Soskin S.M., Mannella R., Arrayás M. and Silchenko A.N.: Strong enhancement of noise-induced escape by transient chaos. *Phys. Rev. E* **63**, 051111-1–051111-6 (2001).

41. Soskin S.M., Mannella R. and McClintock P.V.E.: Zero-Dispersion Phenomena in oscillatory systems. *Phys. Rep.* **373**, 247–409 (2003).
42. Soskin S.M., Yevtushenko O.M., Mannella R.: Divergence of the Chaotic Layer Width and Strong Acceleration of the Spatial Chaotic Transport in Periodic Systems Driven by an Adiabatic ac Force. *Phys. Rev. Lett.* **95**, 224101-1–224101-4 (2005).
43. Soskin S.M., Mannella R., Yevtushenko O.M.: Matching of separatrix map and resonant dynamics, with application to global chaos onset between separatrices. *Phys. Rev. E* **77**, 036221-1–036221-29 (2008).
44. Soskin S.M., Mannella R., Yevtushenko O.M.: Separatrix chaos: new approach to the theoretical treatment. In: Chandre C., Leoncini X., and Zaslavsky G. (eds.) *Chaos, Complexity and Transport: Theory and Applications (Proceedings of the CCT-07)*, pp. 119-128. World Scientific, Singapore, (2008).
45. Soskin S.M., Yevtushenko O.M., Mannella R.: Adiabatic divergence of the chaotic layer width and acceleration of chaotic and noise-induced transport. *Commun. Nonlinear Sci. Numer. Simulat.* In press, doi:10.1016/j.cnsns.2008.06.025.
46. Soskin S.M., Khovanov I.A., Mannella R., McClintock P.V.E.: Enlargement of a low-dimensional stochastic web. In: *Proceedings of the ICNF-2009*. In press.
47. Vecheslavov V.V.: Chaotic layer of a pendulum under low-and medium-frequency perturbations. *Tech. Phys.* **49**, 521–525 (2004).
48. Ye P.D. et al.: Electrons in a periodic magnetic field induced by a regular array of micromagnets. *Phys. Rev. Lett.* **74**, 3013-3016 (1995).
49. Yevtushenko O.M. and Richter K.: Effect of an ac electric field on chaotic electronic transport in a magnetic superlattice. *Phys. Rev. B* **57**, 14839–14842 (1998).
50. Yevtushenko O.M. and Richter K.: AC-driven anomalous stochastic diffusion and chaotic transport in magnetic superlattices. *Physica E* **4**, 256–276 (1999).
51. Zaslavsky G.M.: *Physics of Chaos in Hamiltonian systems*, 2nd edn. Imperial Colledge Press, London (2007).
52. Zaslavsky G.M.: *Hamiltonian Chaos and Fractional Dynamics*. Oxford University Press, Oxford (2008).
53. Zaslavsky G.M. and Filonenko N.N.: Stochastic instability of trapped particles and conditions of application of the quasi-linear approximation. *Sov. Phys. JETP* **27**, 851–857 (1968).
54. Zaslavsky G.M. et al.: Stochastic web and diffusion of particles in a magnetic field. *Sov. Phys. JETP* **64**, 294–303 (1986).
55. Zaslavsky G.M., Sagdeev R.D., Usikov D.A. and Chernikov A.A.: *Weak Chaos and Quasi-Regular Patterns*. Cambridge University Press, Cambridge (1991).